INSTITUTO POLITÉCNICO NACIONAL

CENTRO INTERDISCIPLINARIO DE INVESTIGACIÓN PARA EL DESARROLLO INTEGRAL REGIONAL
UNIDAD OAXACA

Doctorado en Ciencias en Conservación y Aprovechamiento de Recursos Naturales
Línea investigación: Ingeniería

EFECTO DE LA CORROSIÓN POR IÓN CLORURO EN LAS PROPIEDADES MECÁNICAS DE ACERO DE REFUERZO EMBEBIDO EN CONCRETOS TERNARIOS CP-CV-CBC

EFFECT OF CHLORIDE-ION CORROSION ON THE MECHANICAL PROPERTIES OF REINFORCING STEEL EMBEDDED IN TERNARY CONCRETE PC-FA-UtSCBA

Tesis para obtener el grado de:

Doctor en Ciencias

PRESENTA:

M. en C. Víctor Alberto Franco Luján

DIRECTORES DE TESIS:

Dr. Pedro Montes García (CIIDIR Oaxaca)
Dr. José Manuel Mendoza Rangel (UANL)

Santa Cruz Xoxocotlán agosto 2020

SIP-13-BIS

INSTITUTO POLITÉCNICO NACIONAL
SECRETARIA DE INVESTIGACIÓN Y POSGRADO

ACTA DE REGISTRO DE TEMA DE TESIS
Y DESIGNACIÓN DE DIRECTORES DE TESIS

México, D.F. a 27 de Noviembre del 2017

El Colegio de Profesores de Estudios de Posgrado e Investigación de CIIDIR-OAXACA en su sesión ORDINARIA No. 10ª celebrada el día 13 del mes de Noviembre del 2017 conoció la solicitud presentada por el(la) alumno(a):

FRANCO	LUJÁN	VÍCTOR ALBERTO
Apellido paterno	Apellido materno	Nombre (s)

Con registro: A 1 6 0 2 3 8

Aspirante de: **DOCTORADO EN CIENCIAS EN CONSERVACIÓN Y APROVECHAMIENTO DE RECURSOS NATURALES**

Se designa al aspirante el tema de tesis titulado:
Efecto de la corrosión por ion cloruro en las propiedades mecánicas de acero de refuerzo embebido en concretos ternarios CP-CV-CBC

De manera general el tema abarcará los siguientes aspectos:
Estudiar el efecto que tiene la corrosión por ion cloruro en las propiedades mecánicas de acero de refuerzo embebido en concretos con ceniza volante (CV) y ceniza de bagazo de caña (CBC).

2.- Se designan como Directores de Tesis a los Profesores:
Dr. Pedro Montes García y Dr. José Manuel Mendoza Rangel

3.- El trabajo de investigación base para el desarrollo de la tesina será elaborado por el alumno en:
CENTRO INTERDISCIPLINARIO DE INVESTIGACIÓN PARA EL DESARROLLO INTEGRAL REGIONAL (CIIDIR-OAXACA)

que cuenta con los recursos e infraestructura necesarios.

4.- El interesado deberá asistir a los seminarios desarrollados en el área de adscripción del trabajo desde la fecha en que se suscribe la presente hasta la aceptación de la tesis por la Comisión Revisora correspondiente.

Directores de Tesis

Dr. Pedro Montes García

Dr. José Manuel Mendoza Rangel

Aspirante

Franco Luján Víctor Albero

Presidente del Colegio

Dr. Belmonte Jiménez Salvador Isidro

CENTRO INTERDISCIPLINARIO DE INVESTIGACIÓN PARA EL DESARROLLO INTEGRAL REGIONAL CIIDIR UNIDAD OAXACA IPN

SIP-14
REP 2017

INSTITUTO POLITÉCNICO NACIONAL

SECRETARÍA DE INVESTIGACIÓN Y POSGRADO

ACTA DE REVISIÓN DE TESIS

En la Ciudad de Oaxaca siendo las 11:00 horas del día 18 del mes de julio del 2020 se reunieron los miembros de la Comisión Revisora de la Tesis, designada por el Colegio de Profesores de Posgrado de: CIIDIR UNIDAD OAXACA para examinar la tesis titulada:

Efecto de la corrosión por ion cloruro en las propiedades mecánicas de acero de refuerzo embebido en concretos ternarios CP-CV-CBC

del (la) alumno (a):

Apellido Paterno:	Franco	Apellido Materno:	Luján	Nombre (s):	Víctor Alberto

Número de registro: A 1 6 0 2 3 8

Aspirante del Programa Académico de Posgrado: Doctorado en Ciencias en Conservación y Aprovechamiento de Recursos Naturales

Una vez que se realizó un análisis de similitud de texto, utilizando el software antiplagio, se encontró que el trabajo de tesis tiene 19 % de similitud. **Se adjunta reporte de software utilizado.**

Después que esta Comisión revisó exhaustivamente el contenido, estructura, intención y ubicación de los textos de la tesis identificados como coincidentes con otros documentos, concluyó que en el presente trabajo **SI** ☐ **NO** ☒ **SE CONSTITUYE UN POSIBLE PLAGIO.**

JUSTIFICACIÓN DE LA CONCLUSIÓN:

El 19% de similitud en la tesis reportado por el software Turnitin es bajo. Además, considerar que de ese porcentaje el 7% corresponde al artículo de investigación ya publicado y que fue resultado del proyecto doctoral; mientras que el 12% restante corresponde a diversas fuentes debidamente referenciadas, y al diseño experimental y metodología. Éstos últimos son los mismos para tres de los cuatro artículos científicos que conforman esta tesis.

****Es responsabilidad del alumno como autor de la tesis la verificación antiplagio, y del Director o Directores de tesis el análisis del % de similitud para establecer el riesgo o la existencia de un posible plagio.**

Finalmente y posterior a la lectura, revisión individual, así como el análisis e intercambio de opiniones, los miembros de la Comisión manifestaron **APROBAR** ☒ **SUSPENDER** ☐ **NO APROBAR** ☐ la tesis por **UNANIMIDAD** ☒ o **MAYORÍA** ☐ en virtud de los motivos siguientes:

La tesis satisface los requerimientos señalados por las disposiciones reglamentarias vigentes

COMISIÓN REVISORA DE TESIS

Dr. Pedro Montes García Director de Tesis Nombre completo y firma	Dr. Juan Rodríguez Ramírez Nombre completo y firma	Dr. Víctor Guillermo Jiménez Quero Nombre completo y firma
Dr. José Manuel Mendoza Rangel 2° Director de Tesis (en su caso) Nombre completo y firma	Dr. Miguel Chávez Gutiérrez Nombre completo y firma	Dr. Salvador isidro Belmonte Jiménez Nombre completo y firma **PRESIDENTE DEL COLEGIO DE PROFESORES**

INSTITUTO POLITÉCNICO NACIONAL

SECRETARÍA DE INVESTIGACIÓN Y POSGRADO

CARTA CESION DE DERECHOS

En la Ciudad de Oaxaca el día 30 del mes julio del año 2020, el (la) que suscribe Víctor Alberto Franco Luján alumno (a) del Programa de Doctorado en Ciencias en Conservación y Aprovechamiento de Recursos Naturales con número de registro A160238, adscrito al Centro Interdisciplinario de Investigación para el Desarrollo Integral Regional, Unidad Oaxaca, manifiesta que es autor (a) intelectual del presente trabajo de Tesis bajo la dirección de los Dres. Pedro Montes García y José Manuel Mendoza Rangel y cede los derechos del trabajo titulado: **Efecto de la corrosión por ion cloruro en las propiedades mecánicas de acero refuerzo embebido en concretos ternarios CP-CV-CBC,** al Instituto Politécnico Nacional para su difusión, con fines académicos y de investigación.

Los usuarios de la información no deben reproducir el contenido textual, gráficas o datos del trabajo sin el permiso expreso del autor y/o director del trabajo. Este puede ser obtenido escribiendo a la siguiente dirección electrónica francolujan_89@hotmail.com. Si el permiso se otorga, el usuario deberá dar el agradecimiento correspondiente y citar la fuente del mismo.

Víctor Alberto Franco Luján
Nombre y firma

RESUMEN

La corrosión por iones cloruro (Cl^-) es una de las principales causas del deterioro de las estructuras de concreto reforzado y el uso de materiales cementantes suplementarios, como sustitución parcial del cemento Portland (PC), es una opción viable para retrasar su ocurrencia. El uso de ceniza de bagazo de caña de azúcar sin tratatamiento (UtSCBA) ha contribuido a producir concretos ternarios reforzados con propiedades de durabilidad superiores a aquellos con solo PC. Sin embargo, los resultados se basan únicamente en resultados de técnicas no destructivas y la condición real del acero embebido en estos concretos aun no se ha reportado. Con base en lo anterior, el objetivo de esta tesis fue evaluar el efecto de la corrosión inducida por Cl^- en las propiedades mecánicas del acero de refuerzo embebido en concretos ternarios que contienen cenizas volantes (FA) más UtSCBA. Para este propósito, se plantearon las siguientes hipótesis: (I) la adición de UtSCBA en concretos con FA no afecta las propiedades físicas, mecánicas y ultrasónicas a largo plazo de los concretos ternarios manufacturados, (II) el acero embebido en concretos FA+UtSCBA experimenta probabilidades y densidades de corrosión similares a aquel embebido en concreto con solo PC, (III) el uso de UtSCBA en concretos con FA no afecta la capacidad de ligar Cl^- de concretos ternarios y (IV) la corrosión inducida por Cl^- no afecta las propiedades mecánicas del acero embebido en los concretos FA+UtSCBA. Los resultados muestran que la adición de UtSCBA no afectó negativamente las propiedades físicas, mecánicas y ultrasónicas de los concretos ternarios. Además, la combinación FA+UtSCBA produjo concretos con una menor difusividad de Cl^-; por lo tanto, el acero de refuerzo embebido en estos concretos mostró menor probabilidad y velocidad de corrosión. La adición de UtSCBA creó concretos con mayor resistividad eléctrica, así como una mayor capacidad de ligar Cl^-. En consecuencia, las varillas de acero de los concretos con UtSCBA mostraron menores pérdidas de masa debido a la corrosión, mientras que sus esfuerzos de fluencia y último no se vieron afectados negativamente. Con respecto a las cargas a la fractura y ductilidades, el acero embebido en los concretos ternarios fue afectado en menor grado en comparación con el acero embebido en el concreto con solo CP. Los resultados evidencian la viabilidad del uso de la UtSCBA para producir concretos ternarios reforzados con un mejor desempeño contra la corrosión inducida por Cl^-.

ABSTRACT

Chloride (Cl^-)-induced corrosion is one of the main causes of the deterioration of reinforced concrete structures and the use of the supplementary cementitious materials, as partial substitution of the Portland cement (PC), is a viable option to delay it. The use of untreated sugarcane bagasse ash (UtSCBA) has shown that reinforced ternary concretes have superior durability properties than those manufactured with only PC. However, such results are based solely on non-destructive testing and the real condition of the rebars embedded in these concretes has not been reported yet. Based on he above, the objective of this thesis was to evaluate the effect of Cl^--induced corrosion on the mechanical properties of reinforcing steel embedded in ternary concretes containing fly ash (FA) plus UtSCBA. For this purpose, four hypotheses were tested: (I) the addition of UtSCBA in concretes with FA does not affect the long-term physical, mechanical and ultrasonic properties of the manufactured ternary concretes, (II) the reinforcing steel embedded in the concretes with FA+UtSCBA experience similar corrosion probabilities and corrosion rates than those embedded in concretes with only PC, (III) the use of UtSCBA in concretes with FA does not affect the chloride binding capacity of the ternary concretes, and (IV) the Cl^--induced corrosion does not affect the mechanical properties of the reinforcing steel embedded in concretes with FA+UtSCBA. The results show that the addition of UtSCBA did not negatively affect the physical, mechanical, and ultrasonic properties of the ternary concretes. Moreover, the combination FA+UtSCBA produced concretes with low chloride diffusivities; hence, the reinforcing steel showed lower probabilities and rates of corrosion. The pozzolanic reaction of the UtSCBA created concretes with higher electrical resistivities and higher chloride binding capacities. In consequence, steel bars embedded in the ternary concretes showed lower mass losses due to the corrosion, while their yield and ultimate strengths were not negatively affected. Finally, the fracture loads and ductilities were affected in a lesser degree than those embedded in the concrete control. The results evidence the viability of the UtSCBA to produce reinforced ternary concretes with a better performance against Cl^--induced corrosion.

ACKNOWLEDGEMENTS

Firstly, I am grateful to the Instituto Politécnico Nacional (IPN) and CIIDIR-Oaxaca for giving me the opportunity to study a doctoral program and provide the financial support and facilities for the successful development of the present research.

To the laboratory staff of the Instituto de Ingeniería Civil of the Universidad Autónoma de Nuevo León (UANL), for the support provided during the academic stays.

To the Consejo Nacional de Ciencia y Tecnologia (CONACyT) for the scholarship granted to me to carry out my doctoral studies. To the Secretaría de Investigación y Posgrado from IPN for the scholarship granted to me, as a part of its institutional program for research students (BEIFI).

To my supervisors, Dr. Pedro Montes García and Dr. José Manuel Mendoza Rangel for guiding me during my doctoral studies, and at the same time giving me full support when writing the research manuscripts, which are the backbone of this thesis.

To the evaluation's committee conformed by Dr. Juan Rodríguez Ramírez, Dr. Miguel Chávez Gutiérrez, Dr. Pedro Montes García, Dr. José Manuel Mendoza Rangel and Dr. Víctor Guillermo Jiménez Quero, for the helpful recommendations and suggestions to improve the quality of this thesis.

To my student partners Dr. Marco Antonio Maldonado Garcia, M.Sc. Gladis Gomez Luna, Eng. Daniela López Martínez, and Che. David Irvin Valdivieso Méndez for their valuable help in the laboratory.

Finally, I want to thank my professors and the staff from the CIIDIR-Oaxaca and UANL for their knowledge and academic support during my doctoral project.

DEDICATION

To my mother:

Estela Lujan Hernandez[†]

The woman that gave all for her children

To my father

Victor Franco Rangel, B. Eng.

For his invaluable support, advice, and love.

To my sister

Melissa Nataly Franco Lujan, B. Eng.

For always being there for me

To Nancy Rubi

For her affection and love

To the rest of my family

TABLE OF CONTENT

Abbreviations and acronyms

ACI	America Concrete Institute		I_{corr}	Corrosion current intensity	Amp
AD	Absolute density,	g/cm^3	i_{corr}	Corrosion current density	$\mu A/cm^2$
ASTM	American Society for Testing and Materials		LOI	Loss on ignition	%
Aft	Tricalcium aluminate trisulfate hydrate		LPR	Lineal Polarization Resistance	Ω-cm^2
Afm	Calcium monosulfoaluminate hydrate		NaCl	Sodium chloride	
αt	Temporal attenuation	dB/s	OUS	Original uncorroded surface	cm^2
αs	Spatial attenuation	dB/cm	Pb	Chloride binding capacity	%
BD	Bulk density	g/cm^3	PC	Portland Cement	
C	Mixture control		PSC	Percentage of surface corrosion	%
$CaCO_3$	Calcium carbonate		Pt-SCBA	Post-treated sugarcane bagasse ash	
$Ca(OH)_2$	Calcium hydroxide		PV	Percentage of voids	%
CH	Portlandite		RCS	Reinforced concrete structure	
Cl^-	Chloride ion		Rebar	Reinforcing steel	
Cm	Mass after the exposure to Cl^-	g	SP	Superplasticizer	
CO_2	Carbon dioxide		R	Coefficient of correlation	
CPC	Compound Portland Cement		R^2	Coefficient of determination	
CS	Compressive strength	MPa	RML	Real mass loss	%
C-A-S-H	Calcium aluminate silicate hydrates		SAC	Surface area of corrosion	cm^2
C-S-H	Calcium silicate hydrate		SCMs	Supplementary cementitious materials	
D_C	Chloride-ion diffusion coefficient	m^2/s	SCBA	Sugarcane bagasse ash	
EM	Elasticity Modulus	MPa	TIC	Total integrated corrosion	C
E_{corr}	Corrosion potential	mV	t_{dp}	Time of depassivation	days
ER	Electrical resistivity	KΩ-cm	TML	Theoretical mass loss	%
ε_f	Fracture strain		T0	Mixture binary	
ε_y	Yield strain		T1	Mixture ternary one	
$\mathcal{E}$	Energy content		T2	Mixture ternary two	
F	Faraday constant	C/mol	SEM	Scanning Electron Microscopy	
FA	Fly ash		Um	Uncorroded mass	g
Fl	Fracture load	KN	UPV	Ultrasonic pulse velocity	m/s
Fs	Friedel's salt		UtSCBA	Untreated sugarcane bagasse ash	
FTIR	Fourier transform infrared spectroscopy		μ	Ductility	
f_U	Ultimate strength	MPa	VI	Visual inspection	
f_Y	Yield strength	MPa	XRD	X-ray diffraction	
HRWR	High-range water-reducer				

INTRODUCTION

The use of supplementary cementitious materials (SCMs) as a partial substitution of the Portland cement (PC) to delay corrosion of reinforcing steel in concrete has been the subject matter of a very large number of research articles [1-3].

In the last 20 years, sugarcane bagasse ash (SCBA) has been characterized and studied as PC partial replacement [4-7]. These studies have shown that the SCBA, when is post-treated (Pt-SCBA), does not cause negative effects on the mechanical and durability properties of PC-based materials. On the other hand, when SCBA is no post-treated or post-treated using a low-energy demand method serious workability problem have arisen.

Recently, a long-term project on the effect ‘‘practically as received” SCBA (UtSCBA) on the rheological, microstructural, mechanical and durability properties of mortars and concretes is been conducted [8-11]. In spite of the encouraging results on the performance of the UtSCBA as a SCM, there are still many uncertainties, for example, the effect of the addition of UtSCBA on the long-term properties of FA-concrete, and on the corrosion protection of steel reinforcement embedded in these concretes.

In this regard, this thesis presents a series of manuscripts focused on the durability performance of ternary concretes containing FA plus UtSCBA, specifically on the effect of Cl^--induced corrosion on the mechanical properties of rebars embedded in such ternary concretes.

In CHAPTER ONE, the problem statement, justification, state of the art, aim of the research, hypotheses, experimental design and the specimen making are presented. In CHAPTER TWO, the concepts and theoretical models related to the study of the properties of PC-based materials and the effect of Cl^--induced corrosion on the mechanical properties of reinforcing steel embedded in UtSCBA-ternary concretes are referenced. In CHAPTER THREE the effect of the addition of the UtSCBA on the long-term physical, mechanical, and ultrasonic properties of the ternary concretes is reported. In CHAPTER FOUR the long-term

electrochemical monitoring of the rebars embedded in the concretes FA+UtSCBA exposed to Cl^- were analyzed. Moreover, in this chapter the Cl^- profiles, diffusion coefficients, microstructural characterization of the cementitious matrices of the ternary concretes are also analyzed. In CHAPTER FIVE the results of the autopsy performed on the UtSCBA-ternary-concrete specimens, in order to elucidate the protection mechanisms against corrosion provided by UtSCBA, are addressed. In CHAPTER SIX the real conditions of the extracted rebars from the autopsy, and the effect of corrosion on their mechanical properties are investigated. Finally, the results are discussed, conclusions drawn, and recommendations proposed.

References

[1] N. Chousidis, E. Rakanta, I. Ioannou, G. Batis, Mechanical properties and durability performan ce of reinforced concrete containing fly ash, Constr. Build. Mater. 101 (2015) 810–817.

[2] M.A. Baltazar Zamora, D.M. Bastidas, G. Santiago Hurtado, J.M. Mendoza Rangel, C. Gaona Tiburcio, J.M. Bastidas, F. Almeraya Calderón, Effect of silica fume and fly ash admixtures on the corrosion behavior of AISI 304 embedded in concrete exposed in 3.5% NaCl solution, Materials (Basel). 12 (2019) 1–13.

[3] W. Yodsudjai, P. Vanrak, P. Suwanvitaya, A. Jutasiriwong, Corrosion behavior of reinforcement in concrete with different compositions, J. Sustain. Cem. Mater. (2020) 1–20.

[4] J.. Martirena Hernandez, B. Middendorf, M. Gehrke, H. Budelmann, Use of wastes of the suga r industrytas pozzolanatin lime-pozzolana binders: studytof the reaction, Cem. Concr. Res.28 (1998) 1525–1536.

[5] G.C. Cordeiro, R.D. Toledo Filho, L.M. Tavares, E.M.R. Fairbairn, Pozzolanic activity and fill er effect of sugar cane bagasse ash in Portland cement and lime mortars, Cem. Concr. Comp os. 30 (2008) 410–418.

[6] G.C. Cordeiro, O.A. Paiva, R.D. Toledo Filho, E.M.R. Fairbairn, L.M. Tavares, Long Term C ompressive Behaviortof Concretes with Sugarcane Bagasse Ash as a Supplementary Cement itious Material, J. Test. Eval 46 (2018) 20160316.

[7] P. Chindaprasirt, W. Kroehong, N. Damrongwiriyanupap, W. Suriyo, C. Jaturapitakkul, Mecha nical properties, chloride resistance and microstructure of Portland fly ash cement concrete containing high volume bagasse ash, J. Build. Eng. 31 (2020) 101415.

[8] V.G. Jiménez Quero, F.M. León Martínez, P. Montes García, C. Gaona Tiburcio, J.G. Chacón Nava, Influence of sugarcane bagasse ash and fly ash on the rheological behavior of cement pastes and mortars, Constr. Build. Mater. 40 (2013) 691–701.

[9] J.C. Arenas Piedrahita, P. Montes García, J.M. Mendoza Rangel, H.Z. López Calvo, P.L. Vald ez Tamez, J. Martínez Reyes, Mechanical and durability properties of mortars prepared with untreated sugarcane bagasse ash and untreated fly ash, Constr. Build. Mater. 105 (2016) 69–81.

[10] V. Ríos Parada, V.G. Jiménez Quero, P.L. Valdez Tamez, P. Montes García, Characterization and use of an untreated Mexican sugarcane bagasse ash as supplementary material for the p reparation of ternary concretes, Constr. Build. Mater. 157 (2017) 83–95.
[11] M.A. Maldonado García, U.I. Hernández Toledo, P. Montes García, P.L. Valdez Tamez, The influence of untreated sugarcane bagasse ash on the microstructural and mechanical properti es of mortars, Mater. Constr. 68 (2018) 1–13.

CHAPTER ONE

Problem statement

Cl^--induced corrosion is one of the main causes of the deterioration of reinforced concrete structures (RCS). When a certain chloride ion (Cl^-) threshold is reached at the concrete/reinforcing steel interface of the RCS the reinforcement, otherwise protected in an alkaline environment, is depassivated and the corrosion process begins [1-3]. Once corrosion starts, corrosion products are generated and pile up at the vicinity of the reinforcing steel (rebar). Such products have a larger volume than the rebar; therefore, internal tensile stresses are imposed on the surrounding concrete, causing cracking, delamination and spalling of the concrete cover [4]. Cl^--induced corrosion is a serious issue because in addition to the need of more raw materials for the production of more cement, the increased CO_2 emmisions associated with this process, and the high costs of repair and rehabilitation of the damaged RCS, the deterioration can cause accidents with the loss of human life due to unexpected collapse [3].

A method to delay the Cl^- ingress, and therefore the rebar corrosion, is the use of suplemenaty cementitious materilas (SCMs) as PC partial substitutes. Fly Ash (FA) is the most widely used SCM for the manufacturing of PC-based materials [5]. The use of FA has contributed retarding the Cl^- penetration and hence the corrosion in reinforced concretes [6-7]. Nonetheless, the availability of FA is being compromised due to environmental regulations about its use [8]. Therefore, studies on the use of other SCMs as an alternative to FA are most required.

In this regard, the use of UtSCBA as a SCM has shown the reduction of the Cl^- diffusivity in mortars [9]. As a result, reinforced mortar slabs exposed to Cl^- presented less negative corrosion potentials, which indicates a lower corrosion probability [10]. In the case of concrete, Jimenez-Quero, [11] and Rios-Parada, [12] manufactured reinforced concretes where PC was partially substituted by the combination FA+UtSCBA. When these ternary

concretes were exposed to a NaCl solution the reinforcing steel presented lower corrosion probability and lower corrosion rates than those reinforced concretes with only PC.

Research results on the influence of the addition of UtSCBA on the corrosion performance of the ternary concretes were based solely on the results from non-destructive electrochemical measurements. In consequence, the real corrosion conditions of rebars embedded in these concretes after long-term exposed to Cl^- and the effect of corrosion on the mechanical properties of the rebars have not been reported yet. All in all, studies addressing these important subjects are highly needed.

Justification

This thesis attempts to fill a gap in knowledge. It addresses the study of the effect of Cl^--induced corrosion on the mechanical properties of reinforcing steel embedded in concretes containing FA+UtSCBA. Furthermore, the protection mechanism upon the use of UtSCBA in concrete is investigated. This research is relevant because scientific knowledge was obtained from long-term non-destructive and destructive studies, which are scarce in the literature. Moreover, such knowledge was useful to elucidate the protection mechanisms against Cl^--induced corrosion provided by UtSCBA. Furthermore, the physical evidence of the damage quantified by destructive standardized testing was shown. The research also has a direct impact on the increase in the safety of building occupants, as the use of UtSCBA may help to prevent the corrosion damage of the reinforcing steel which otherwise might cause the sudden failure and collapse of reinforced concrete structures. Moreover, this investigation contributes to the manufacturing of ecological concretes including agro-industrial waste as SCM, and at the same time to reducing considerable amounts of CO_2 emissions generated during the PC production.

State of the Art

Portland cement is the most widely used construction material around the world [13-14], and its manufacture demands excessive energy consumption, which leads to generating

significant levels of CO_2 emissions to the atmosphere [14]. In order to mitigate this problem, the partial substitution of PC by SCMs is a viable option. Such an alternative has been implemented through the standardization of PC with the addition of SCM from industrial sectors; for example, FA, ground blast furnace slag, and silica fume [15]. In addition to ecological benefits, the use of these SCMs produces PC-based materials with mechanical and durability properties superiors than those elaborated with only PC [16-18].

Since Diamond first reported data from two Danish fly ashes in 1981, this material has been the most used SCM to produce pastes, mortars, and concretes [19, 20]. Nevertheless, the availability of FA is limited in countries like Mexico; moreover, the recent regulatory uncertainties regarding the use of coal further reduce its use [8]. As an alternative to the use of FA, SCMs from agro-industrial wastes have been investigated in recent years, specifically the SCBA. When the SCBA is post-treated, it contributes to produce PC-based materials with similar or superior physical, mechanical, and durability properties than those manufactured with only PC [21-24].

Given that the post-treatments demand high amount of energy and generate a considerable amount of CO_2 emissions, the beneficial ecological impact upon the use of SCBA as a SCM is diminished. In this perspective, Jimenez-Quero et al. [25] reported that sieving through a No. 200 (75 µm) ASTM mesh for four minutes is one of the post-treatments with the lowest-energy consumption to obtain a SCBA with adequate pozzolanic properties. In the same article, the authors showed that 10% and 20% of sieved SCBA lead to workability problems of pastes and mortars; however, this inconvenience was overcome with the addition of 20%FA.

Later, Arenas-Piedrahita et al. [9] used the same four-minute sieved ash to investigate its effect on the mechanical and durability properties of mortars. In this article the authors named the ash as UtSCBA, and from now on the use of this term refers to that specific ash. The results showed that the partial replacement of PC by 10% and 20%UtSCBA did not negatively affect the 90-day CS of UtSCBA-mortars. Furthermore, UtSCBA produced mortars with higher electrical resistivity values that the mortars manufactured with only PC.

In the same manner, UtSCBA-mortars presented a better performance against permeability to Cl^-.

The use of UtSCBA also has shown to improve the microstructural properties of mortars when the PC was replaced by 10% and 20% UtSCBA. This beneficial effect increased the long-term CS of UtSCBA-mortars [26]. The authors reported that the use of 10% and 20% UtSCBA as PC replacement significantly reduced the Cl^- diffusivity through the cementitious matrix of the UtSCBA-mortars [10]. Moreover, reinforced mortars slabs elaborated with 10% and 20% of UtSCBA and exposed to wet-dry cycles of 12h each in a 3% NaCl solution experienced lower corrosion activity.

The combinations of 70%PC+20%FA+10%UtSCBA and 60%PC+20%FA+20%UtSCBA in the preparation of ternary concretes proposed by Jimenez-Quero et al. [25] was also employed by Rios-Parada et al. [27] to investigate its effect on the fresh state and mechanical properties of the concretes. In this study, the results indicate that the UtSCBA leads to reduce the workability and volumetric weight; however, the air content and temperature in the fresh state were not negatively affected. In the case of mechanical properties, the combination FA+UtSCBA slightly decreased the CS of the UtSCBA-ternary concretes; however, after 90 days the strength and elastic moduli of these concretes were not negatively affected.

Regarding the durability properties of UtSCBA-ternary concretes, Jimenez-Quero, [11] and Rios-Parada, [12] in their Doctoral and Master thesis, respectively, manufactured reinforced concrete prisms with 100%PC, 80%PC+20%FA, 70%PC+20%FA+10%UtSCBA, and 60%+20%FA+20%UtSCBA. After 28 days of curing the prisms were exposed to a 3% NaCl solution. The corrosion activity from the reinforced prisms was monitored by corrosion potentials (E_{corr}) and corrosion densities (i_{corr}) during 700 days by [11] and continuing by [12] until 1000 days. During this period, rebars embedded in the UtSCBA-ternary concretes showed both less-negative E_{corr} values and lower i_{corr} values than those from the mixtures with 100%PC and 80%PC+20%FA. This indicates that reinforcing steel embedded in the UtSCBA-ternary concretes presents an apparently better performance against corrosion induced by Cl^-.

In summary, the studies regarding the use of UtSCBA as a Portland cement partial substitute report no negative effects on the rheological, microstructural, and mechanical properties of mortars and concretes. Likewise, the use of UtSCBA produces PC-based materials with less permeability and Cl^- diffusivity, as well as, a higher electrical resistivity. In spite of the interesting findings so far, the real corrosion condition of the reinforcing steel and the effect of this corrosion on the mechanical properties of the steel reinforcement is still uncertain. Therefore, a comprehensive program aiming this research need is highly recommended.

In the current literature, several articles have reported on the effect of Cl^--induced corrosion on the mechanical properties of reinforcing steel in reinforced concretes [28-32]; however, most of the studies are short-term and/or have been carried out under accelerated conditions where the induced corrosion promoted excessive damage to the reinforcing steel. In consequence, corrosion is overestimated and the corrosion mechanisms responsible for corrosion occurring or corrosion inhibition are difficult to elucidate.

A thorough examination of the existent literature reveals that the studies on effect of the addition of UtSCBA on the long-term properties of FA-concretes are pertinent. It also shows that studies on the effect of Cl^--induced corrosion on the mechanical properties of reinforcing steel in these concretes has not been reported yet. Literature also recommends that such studies must be carried out under controlled non-accelerated conditions in order to be reliable and to ease the elucidation of the corrosion mechanism responsible for the apparent better performance of the addition of UtSCBA against corrosion.

Aim of the research

The main objective of the present Doctoral thesis was to evaluate the effect of Cl^- induced corrosion on the mechanical properties of reinforcing steel embedded in ternary concretes containing FA plus UtSCBA. For this purpose, four specific objectives emerged.

1. To characterize the long-term physical, mechanical, and ultrasonic properties of the ternary concretes manufactured with the combination of PC+FA+UtSCBA.

2. To monitor the long-term Cl^--induced corrosion of reinforcing steel embedded in ternary concretes PC+FA+UtSCBA exposed to a NaCl solution using electrochemical tests.

3. To estimate the chloride binding capacity of the cementitious matrix of the ternary concretes PC+FA+UtSCBA after the long-term exposure to a NaCl solution.

4. To analyze the effect of Cl^--induced corrosion on the mass loss, yield strength, ultimate strength, fracture load and ductility of reinforcing steel embedded in the ternary concretes PC+FA+UtSCBA.

Hypotheses

Considering the specific objectives mentioned earlier the following hypotheses were tested:

1. The addition of 10% and 20% of UtSCBA in concretes with FA does not affect the long-term physical, mechanical and ultrasonic properties of the manufactured ternary concretes.

2. The reinforcing steel embedded in the ternary concretes PC+FA+UtSCBA experience similar corrosion probabilities and corrosion rates than those embedded in concretes with only PC when they are long-term exposed to a NaCl solution.

3. The use of 10%UtSCBA and 20%UtSCBA in concretes with FA does not affect the chloride binding capacity of the ternary concretes.

4. The Cl^--induced corrosion does not affect the mechanical properties of the reinforcing steel embedded in ternary concretes PC+FA+UtSCBA.

Experimental program

Earlier studies carried out by Jimenez-Quero, [11] and Rios-Parada, [12], as a part of a long-term project, monitored the corrosive activity of rebars embedded in concretes with

FA+UtSCBA and exposed to Cl^- during 700 and 1000 days, respectively. As a follow-up of this project and in order to evaluate the influence of Cl^--induced corrosion on the mechanical properties of the reinforcing steel embedded in ternary concretes containing FA and UtSCBA, a four-level factor experimental design was developed. Four concrete mixtures were designed in accordance with the American Concrete Institute absolute volume method [33]. Table 1 shows details of the nomenclature adopted for each mixture and the ingredient proportions. A total of 15 cylinders (Ø100 mm x 200 mm) and three reinforced prisms (100 mm 150 mm x 300 mm), for each mixture, were fabricated with the different concrete mixtures for the different phases of this research project. After casting the cylindrical specimens were cured by immersion in a $Ca(OH)_2$ saturated solution until the date of testing. Similarly, the prismatic specimens were cured for 28 days and thereafter immersed in a NaCl solution for continuous monitoring and further evaluation.

Table 1. Details of the experimental design

Factor	Levels	Description
Type of mixture	C	100%CPC
	T0	80%CPC+20%FA
	T1	70%CPC+20%FA+10%UtSCBA
	T2	60%CPC+20%FA+20%UtSCBA

The experimental program of this thesis was divided into four phases. In Phase I, a long-term characterization of the physical, mechanical and ultrasonic properties of the UtSCBA-ternary concretes was conducted.

In Phase II, the Cl^--ion diffusion coefficients (D_{CS}) of the UtSCBA-ternary concretes at 28 and 90 days of age were obtained. The microstructures and mineral phases of the concretes at 2500 days of age were characterized by scanning electron microscopy (SEM) and X-ray diffraction (XRD). Then, the corrosion condition of the reinforced UtSCBA-ternary concretes exposed to the NaCl solution was evaluated by corrosion potentials (E_{corr}) using the half-cell technique and by corrosion current densities (I_{corr}) using the linear polarization resistance (LPR) technique. The D_{CS} at 28 days and the LPR test results helped to estimate

the time for depassivation of the steel reinforcement and the theoretical mass loss of the rebars.

Phase III of the experimental program consisted of carrying out electrical resistivity tests to all prismatic specimens for 3000 days. In this phase, one-out of three reinforced prisms from each mixture, the ones with the highest corrosion activity observed from the previous phase, were selected to be autopsied. Prior to the autopsy, corrosion potential maps were obtained from these prisms. Reinforcing bars embedded in the prisms along with samples of the corrosion products at the interface concrete/steel reinforcement were retrieved and kept in safe dry conditions. Corrosion potentials maps, corrosion products and corroded steel reinforcing bars were studied altogether in the following Phase IV. During the autopsy of the prisms, several small-scale concrete specimens were also obtained. In this third phase, microstructural and mineralogical characterizations of these small-scale specimens were carried out by SEM and XRD, respectively. Moreover, PVs, CSs, D_Cs, and chloride binding capacities of the UtSCBA-ternary concretes were also estimated using the small-scale concrete specimens.

In Phase IV the corrosion potential maps, corrosion products and reinforcing bars retrieved from the concrete prisms in Phase III were fully analyzed and characterized. Then, the damage by the Cl^--induced corrosion on the rebars was evaluated by inspection visual. The rusted and rust-free zones of the concrete/reinforcing steel interface were assessed by an elemental mapping by SEM/EDS. The corrosion products were identified using XDR and Fourier-transform infrared spectroscopy. The real mass losses, yield strengths, ultimate strengths, fracture loads, and ductilities of the steel reinforcing bars were obtained. Table 2 shows a summary of the experimental phases and all the tests that comprise each phase.

Table 2. Details of the phases and tests performed in this research.

Phase I: Long-term characterization of physical, mechanical and ultrasonic properties	**Phase II: Corrosion monitoring**	**Phase III: Study of the Cl^- binding capacity of UtSCBA**	**Phase IV: Study of the effect of corrosion on the mechanical properties of reinforcing steel**
- BD	- D_C	- ER	- E_{corr}
- AD	- SEM	- SEM	- VI
- PV	- XRD	- XRD	- SEM
- CS	- E_{corr}	- PV	- XRD
- UVP	- i_{corr}	- CS	- FTIR
- α_t	- t_{dp}	- D_C	- RML
- α_S	- TML	- P_b	- f_Y
- ε			- f_U
			- Fl
			- μ

BD: *bulk density*, **AD**: *absolute density*, **PV**: *percentage of voids*, **CS**: *compressive strength*, **UPV**: *ultrasonic pulse velocity*, $\boldsymbol{\alpha_t}$: *temporal attenuation*, $\boldsymbol{\alpha_S}$: *spatial attenuation*, $\boldsymbol{\varepsilon}$: *waveform energy*, **Dc**: *chloride-ion diffusion coefficient*, **SEM**: *scanning electron microscopy*, **XRD**: *X-ray diffraction*, $\mathbf{E_{corr}}$: *corrosion potential*, $\mathbf{i_{corr}}$: *corrosion density*, $\mathbf{t_{dp}}$: *time of depassivation*, **TML**: *theoretical mass loss*, **ER**: *electrical resistivity*, $\mathbf{P_b}$: *chloride binding capacity*, **VI**: *visual inspection*, **FTIR**: *Fourier-transform infrared spectroscopy*, **RML**: *real mass loss*, $\mathbf{f_Y}$: *yield stress*, $\mathbf{f_U}$: *ultimate stress*, **Fl**: *fracture load*, $\boldsymbol{\mu}$: *ductility*.

References

[1] C. Andrade, P. Merino, X.R. Nóvoa, M.C. Pérez, S. Soler, Passivation of Reinforcing Steel in Concrete, Mater. Sci. Forum. 192–194 (1995) 891–898.

[2] T. Pan, A.C.T. Van Duin, Passivation of steel surface: An atomistic modeling approach aided with X-ray analyses, Mater. Lett. 65 (2011) 3223–3226.

[3] C. Andrade, Correction to: Propagation of reinforcement corrosion: principles, testing and mod elling, Mater. Struct. 53 (2019) 1.

[4] B. Šavija, E. Schlangen, Chloride ingress in cracked concrete a literature review BT - Advances in Modeling Concrete Service Life, in: C. Andrade, J. Gulikers (Eds.), Springer Ne therlands, Dordrecht, 2012: pp. 133–142.

[5] T. Hemalatha, A. Ramaswamy, A review on fly ash characteristics Towards promoting high vo lume utilization in developing sustainable concrete, J. Clean. Prod. 147 (2017) 546–559.

[6] Y.S. Choi, J.G. Kim, K.M. Lee, Corrosion behavior of steel bar embedded in fly ash concrete, Corros. Sci. 48 (2006) 1733–1745.

[7] N. Chousidis, E. Rakanta, I. Ioannou, G. Batis, Mechanical properties and durability performan ce of reinforced concrete containing fly ash, Constr. Build. Mater. 101 (2015) 810–817.

[8] A.P. Gursel, H. Maryman, C. Ostertag, A life cycle approach to environmental, mechanical, an d durability properties of “green” concrete mixes with rice husk ash, J. Clean. Prod. 112 (20 16) 823–836.
[9] J.C. Arenas Piedrahita, P. Montes García, J.M. Mendoza Rangel, H.Z. López Calvo, P.L. Valde z Tamez, J. Martínez Reyes, Mechanical and durability properties of mortars prepared with untreated sugarcane bagasse ash and untreated fly ash, Constr. Build. Mater. 105 (2016) 69–81.
[10] M.A. Maldonado García, U.I. Hernández Toledo, P. Montes García, P.L. Valdez Tamez, Long term corrosion risk of thin cement composites containing untreated sugarcane bagasse ash, J . Mater. Civ. Eng. 31 (2019) 1–13.
[11] V.G. Jiménez Quero, Efecto de la ceniza de bagazo de caña y ceniza volante en la trabajabilid ad, propiedades mecánicas y durabilidad de concretos ternarios, centro de investigación en materiales avanzados, PhD thesis, CIMAV, México, 2013. (In Spanish).
[12] V. Ríos Parada, Análisis de las propiedades mecánicas, microestructurales y de durabilidad de concretos ternarios con ceniza de bagazo de caña. Master thesis, IPN CIIDIR Oaxaca, Méxi co, 2013. (In Spanish).
[13] M.C.G. Juenger, R. Siddique, Recent advances in understanding the role of supplementary ce mentitious materials in concrete, Cem. Concr. Res. 78 (2015) 71–80.
[14] K.L. Scrivener, V.M. John, E.M. Gartner, Eco-efficient cements: Potential economically viable solutions for a low-CO2 cement-based materials industry, Cem. Concr. Res. 114 (2018) 2–26.
[15] ASTM C595/C595M 20, Standard Specification for Blended Hydraulic Cements, ASTM Inter national, West Conshohocken, PA, 2020.
[16] M.C.G. Juenger, R. Siddique, Recent advances in understanding the role of supplementary ce mentitious materials in concrete, Cem. Concr. Res. 78 (2015) 71–80.
[17] S. Cheng, Z. Shui, R. Yu, T. Sun, X. Zhang, Multiple influences of internal curing and supple mentary cementitious materials on the shrinkage and microstructure development of reefs ag gregate concrete, Constr. Build. Mater. 155 (2017) 522–530.
[18] M.C.G. Juenger, R. Snellings, S.A. Bernal, Supplementary cementitious materials: New sources, characterization, and performance insights, Cem. Concr. Res. 122 (2019) 257–273.
[19] Q. Zeng, K. Li, T. Fen chong, P. Dangla, Determination of cement hydration and pozzolanic r eaction extents for fly ash cement pastes, Constr. Build. Mater. 27 (2012) 560–569.
[20] S.K. Ghosh, V. Kumar, Circular Economy and Fly Ash Management, Springer, 2020.
[21] Q. Xu, T. Ji, S.J. Gao, Z. Yang, N. Wu, Characteristics and applications of sugar cane bagasse ash waste in cementitious materials, Materials (Basel). 12 (2018) 1–19.
[22] G.C. Cordeiro, O.A. Paiva, R.D. Toledo Filho, E.M.R. Fairbairn, L.M. Tavares, Long Term C ompressive Behavior of Concretes with Sugarcane Bagasse Ash as a Supplementary Cement itious Material, J. Test. Eval. 46 (2018) 20160316.
[23] O.T. Maza-Ignacio, V.G. Jiménez-Quero, J. Guerrero-Paz, P. Montes-García, Recycling untreated sugarcane bagasse ash and industrial wastes for the preparation of resistant, lightweight and ecological fired bricks, Constr. Build. Mater. 234 (2020).
[24] P. Chindaprasirt, W. Kroehong, N. Damrongwiriyanupap, W. Suriyo, C. Jaturapitakkul, Mechanical properties, chloride resistance and microstructure of Portland fly ash cement concrete containing high volume bagasse ash, J. Build. Eng. 31 (2020) 101415.

[25] V.G. Jiménez Quero, F.M. León Martínez, P. Montes García, C. Gaona Tiburcio, J.G. Chacón Nava, Influence of sugar cane bagasse ash and fly ash on the rheological behavior of cemen t pastes and mortars, Constr. Build. Mater. 40 (2013) 691–701.
[26] M.A. Maldonado García, U.I. Hernández Toledo, P. Montes García, P.L. Valdez Tamez, The i nfluence of untreated sugarcane bagasse ash on the microstructural and mechanical propertie s of mortars, Mater. Constr. 68 (2018) 1–13.
[27] V. Ríos Parada, V.G. Jiménez Quero, P.L. Valdez Tamez, P. Montes García, Characterization and use of an untreated Mexican sugarcane bagasse ash as supplementary material for the pr eparation of ternary concretes, Constr. Build. Mater. 157 (2017) 83–95.
[28] I. Fernandez, J.M. Bairán, A.R. Marí, Corrosion effects on the mechanical properties of reinfo rcing steel bars. Fatigue and σ ε behavior, Constr. Build. Mater. 101 (2015) 772–783.
[29] Y.C. Ou, Y.T.T. Susanto, H. Roh, Tensile behavior of naturally and artificially corroded steel bars, Constr. Build. Mater. 103 (2016) 93–104.
[30] S. Imperatore, Z. Rinaldi, C. Drago, Degradation relationships for the mechanical properties of corroded steel rebars, Constr. Build. Mater. 148 (2017) 219–230.
[31] W. Zhu, R. François, C.S. Poon, J.G. Dai, Influences of corrosion degree and corrosion morph ology on the ductility of steel reinforcement, Constr. Build. Mater. 148 (2017) 297–306.
[32] I. Fernandez, C.G. Berrocal, Mechanical Properties of 30-Year-Old Naturally Corroded Steel Reinforcing Bars, Int. J. Concr. Struct. Mater. 13 (2019) 9.
[33] A.C.I.C. 211, Standard Practice for Selecting Proportions for Normal, Heavyweight, and Mass Concrete:(ACI 211.1-91), in: American Concrete Institute, 1991.

CHAPTER TWO

Conceptual and Theoretical framework

1. The corrosion phenomenon in the steel reinforcement-concrete matrix system

Corrosion is defined as the destruction or deterioration of materials due to their reaction with the surrounding environment [1]. In this context, the cementitious matrix of the reinforced concretes usually has a pH higher than 13.5 which provides an alkaline media, and in consequence a passivating film around the reinforcing steel is formed [2]. However, the passivation can be destroyed, and corrosion can start. In general, there are two main factors that can cause the corrosion of steel in reinforced concrete: a) the carbonation of the concrete matrix and b) the ingress of chloride ions (Cl^-) [3].

Corrosion can be caused by Cl^- when these ions penetrate through interconnected pores in the cementitious matrix of the reinforced concrete. Once a certain amount of Cl^- ions reach the interface concrete/reinforcing steel the passivating film is destroyed, and the corrosion process starts [3]. Fig. 1 illustrates the corrosion mechanism of the reinforcing steel embedded in concrete. Few factors are necessary for corrosion to start and be mantained. First, the corrosion needs both anodic and cathodic zones which are located at the steel surface. The reinforcing steel surface serves at the same time as an electrical conductor. Moreover, an electrolyte is also needed, where the pore solution in the cementitious matrix fulfills this function. At the anodic zone, the Fe is dissolved into Fe ions which precipitate into the pore solution, ($Fe \rightarrow Fe^{2+} + 2e^-$) and the lost electrons react with oxygen and water present in the cathodic zone to create hydroxyl ions ($2e^- + H_2O + ½O \rightarrow 2OH^-$). Next, the Fe ions ($Fe^{+2}$) in the pore solution react with the hydroxyl ions to produce ferrous hydroxide ($Fe^{2+} + 2OH^- \rightarrow Fe(OH)_2$), which is further oxidizes to create other corrosion products such as ferric hydroxide ($4Fe(OH)_2 + O_2 + 2H_2O \rightarrow 4Fe(OH)_3$).

Despite the corrosion activity occurs at the reinforcing steel surface, the roles of the concrete/reinforcing steel interface and the concrete matrix are of primal importance for corrosion to start, be maintained, or be stifled. Most of the species needed for the corrosion process, moisture, and oxygen are provided by the concrete matrix. For this reason, the understanding of its properties can greatly help to elucidate the mechanisms involved in the corrosion phenomenon.

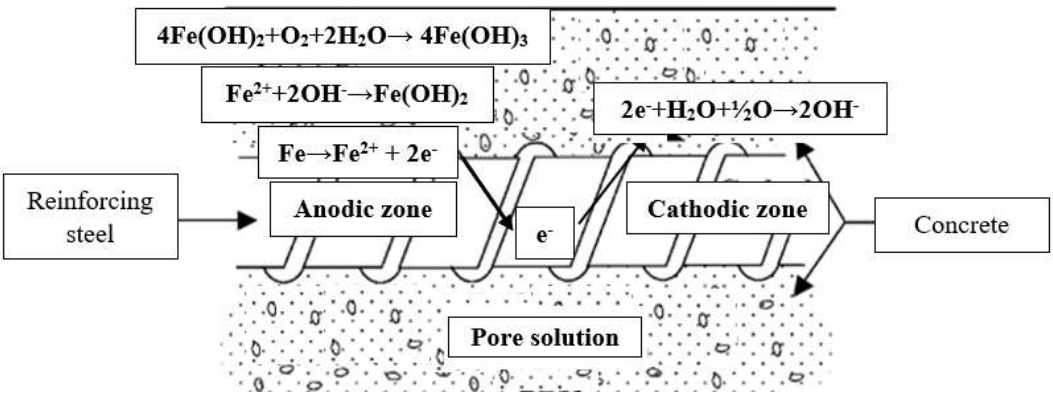

Fig 1. Schematic representation of the corrosion process of reinforcing steel embedded in concrete. Adapted from Ahmad [2]

2. The concrete matrix

Hydraulic concrete is a material made of a binder which is formed mostly by the chemical reaction between the Portland cement (PC) and water. Despite the main ingredient of hydraulic concrete is PC, chemical and mineralogical admixtures, which are nowadays widely used to modify certain properties of concrete have become also very important. Moreover, fine and coarse aggregates are also embedded in order to create a matrix similar to a rock [4]. In this context, the concrete is a key component in building construction owing to its advantages; for example, low cost, appropriate mechanical properties and adequate durability, high heat storage capacity, high chemical inertia, and ease of being molded into different sizes and shapes [5].

2.1 Portland cement, the main ingredient of concrete

The PC is manufactured by feeding crushed, ground, and screened raw mix into a rotary kiln, which heats the mixture to a temperature of about 1300–1450 °C. Next, the clinker is cooled and crushed to a fine powder; finally, a small amount of gypsum is added, and the resulting product is the commercial Portland cement [6].

2.2 Contextual overview of the cement

The cement was discovered 175 years ago, since then, it has been the binder material more widely used by the construction industry [7]. The cement is the base material for building infrastructure; for example, bridges and dams, skyscrapers, roads and railways, high-rise apartments, and single-family homes [8].

In the last 65 years the amount of cement produced increased approximately 34-fold [8]. In 1950 the cement-based materials represented about 7% of the total global materials, whereas, in 2005, it represented 30% of the total global materials use including fossil fuels [9]. This growth rate is much higher than other commodities such as steel, and it is estimated that the demand for cement will increase by about 6 billion tons by 2050 [8]. Despite the advantages of the use of the cement, its manufacture consumes a great deal of energy and releases a large quantity of CO_2. An estimate of between 0.8 and 1.0 tons of CO_2 are generated for 1 ton of manufactured cement. In general, the cement industry emits over 6% of total man-made CO_2 emissions [5].

The manufacture of Portland cement is a fairly simple process; however, the final product is a complex material from which a great deal of research articles has been published. Some aspects of its manufacture, components, hydration and properties have been investigated; however, many uncertainties still remain.

2.3 Components of the Portland cement

Portland cement is not a simple material because is a mixture of several compounds where the following five are at least 90% of it [4]:

(I) Tricalcium silicate (C_3S) (45-60% by mass of PC): This component can be considered as the main component of the clinker; moreover, it provides high initial strength to the concrete.

(II) Dicalcium silicate (C_2S) (5-30% by mass of PC): This component provides low resistance in the first days because it hydrates and hardens slowly; however, contributes to the increase in resistance after one week.

(III) Tricalcium aluminate (C_3A) (6-15% by mass of PC): This compound reduces the burning temperature of the clinker and facilitates the combination of gypsum and silica. C_3A contributes slightly to the development of early resistance; however, it can bind chlorides, which may reduce the risk of corrosion of the reinforcing steel.

(IV) Tetracalcium ferroaluminate (C_4AF) (6-8% by mass of PC): This compound controls the reactions inside the rotary kiln when the clinker is manufactured.

(V) Gypsum (3-5% by mass of PC): This compound is added to the clinker before grinding in order to control the rate of hydration of C_3A and C_4AF.

2.4 Portland cement hydration

The hydration of the Portland cement is defined as the combination of all the simultaneous and physical-chemical reactions between the PC particles, water, and other additives. The hydration of the PC is complex and to understand the chemical processes of such hydration is necessary to study the hydration of each of its components separately.

2.4.1 Hydration of the C_3S and C_2S

Hydration of C_3S and C_2S create two products: (I) calcium silicate hydrate (C-S-H) and (ii) calcium hydroxide ($Ca(OH)_2$). Both calcium silicates have a similar hydration process, distinguishing themselves by the amount of $Ca(OH)_2$ formed and the heat of hydration released. Therefore, this section focuses only on the C_3S hydration process, where the Fig. 2 shows a typical exothermic heat flow curve of C_3S hydration, identifying 5 stages [10].

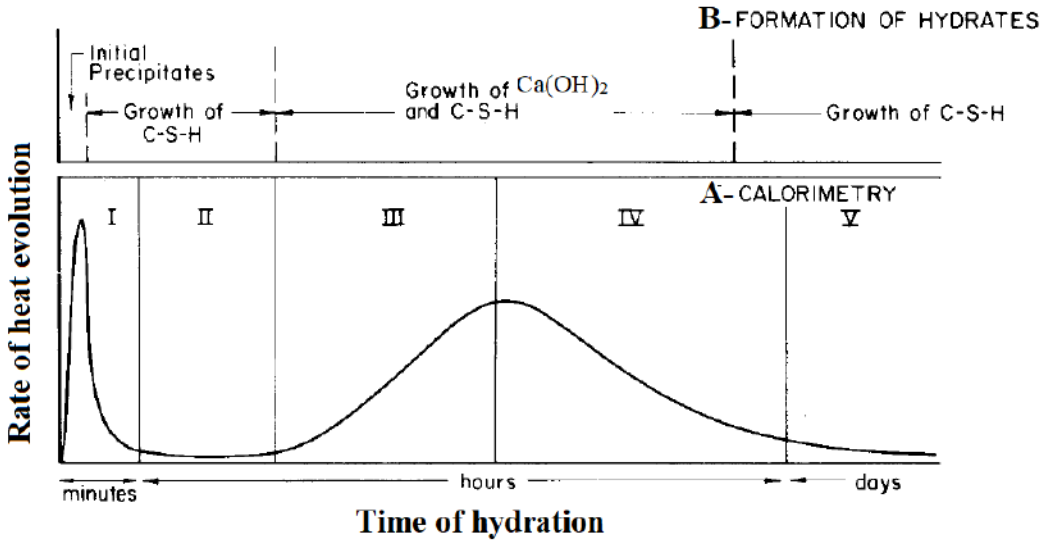

Fig. 2. A typical exothermic heat flow curve of C_3S hydration
Adapted from Ramachandran [10]

Stage 1 Pre-induction: in the first stage, as soon as C_3S mixes with water, it releases silicate ions, $H_2SiO_4^{2-}$, (OH) ions, and Ca^{2+} ions in the solution.

$$C_3S + 3H_2O \rightarrow 3Ca^{2+} + 4(OH) + H_2SiO_4^{2-} \qquad \text{Eq.1}$$

Next, the solution is oversaturated with respect to the C-S-H, which precipitates according the follow reaction.

$$3Ca^{2+} + 2(OH)^{-} + 2H_2SiO_4^{2-} + 2H_2O \rightarrow Ca_3H_2Si_2O_7(OH)_2.3H_2O \qquad \text{Eq. 2}$$

Stage 2 Induction: in this state, the water consumption and the amount of hydrates formed are very small, which explains why the concrete is workable. The induction period can be explained by the theory of the physical barrier to diffusion, which is based on the formation of a C-S-H film around the C_3S particle (Fig. 3) where $Ca(OH)_2$ must leave. This film slows down the reaction rate because water must penetrate through such film and in countercurrent to $Ca(OH)_2$.

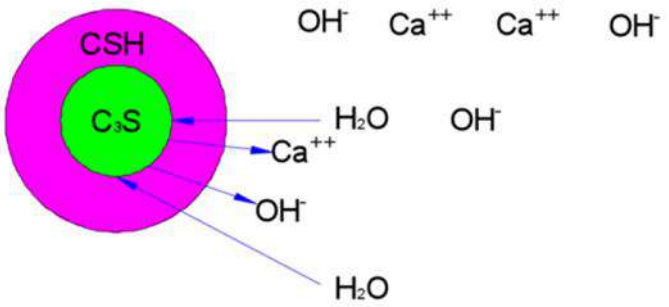

Fig. 3. Schematic representation of a C_3A particle surrounded by a C-S-H film

Stage 3 Acceleration: in this state, the initial setting of the concrete begins. The C_3S begins to hydrate rapidly again since the $Ca(OH)_2$ begins to crystallize out of the C-S-H film (Fig. 4) consequently, the diffusion of water towards the nucleus of the C_3S particle increases.

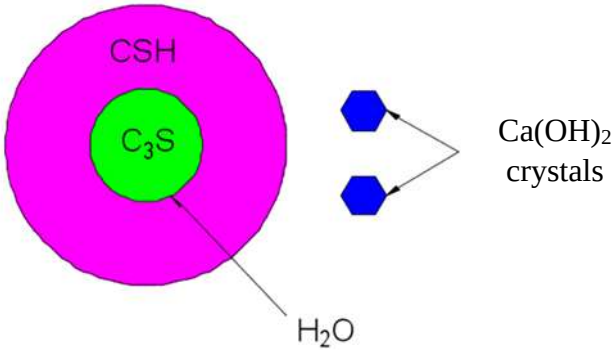

Fig. 4. Schematic representation of the crystallization of $Ca(OH)_2$

Stage 4 Deceleration: due to C_3S hydration, the thickness of the C-S-H film continues to increase and movement through such film determines the rate of the reaction, and hydration is controlled by the rate of diffusion into the C-S-H film. Diffusion-controlled reactions are generally quite slow, and the rate decreases as the thickness of the diffusion barrier increases.

Stage 5 Diffusion: in this stage, diffusion is so slow that the rate of hydration is controlled only by the rate of diffusion. As the thickness of the C-S-H film continues to grow (Fig. 5), the diffusion rate continues to decrease until there is no more C_3S to hydrate.

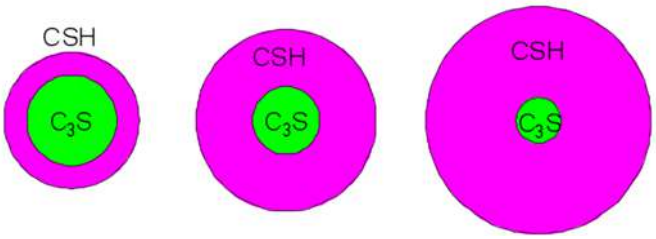

Fig. 5. Schematic representation of the growth of the C-S-H film surrounding a C_3S particle

2.4.2 Hydration of the C_3A, C_4AF, and Gypsum

The hydration processes of C_3A and C_4AF in the presence of gypsum are similar; however, the reactions of C_4AF are slower than C_3A. Therefore, this section focuses on describing the hydration process of C_3A in the presence of gypsum, which is divided into four stages [10].

Stage I: in this stage, C_3A and gypsum dissolve rapidly in water, according to the reactions:

$$Ca_3Al_2O_6 + 2H_2O \rightarrow 3Ca^+ + 2AlO_2^- + 4(OH)^- \quad \text{Eq. 3}$$

$$CaSO_4.2H_2O \rightarrow Ca^{2+} + SO_4^{2-} + 2H_2O \quad \text{Eq. 4}$$

These reactions generate a great amount of heat and the ions formed combine instantly to form ettringite crystals

$$29H_2O + 6Ca^+ + 2AlO_2^- + 3SO_2^{2-} + 4(OH)^- \rightarrow [Ca_2Al(OH)_6].Ca_2(SO_4)_3.25H_2O \quad \text{Eq. 5}$$

or

$$C_3A + 3C\bar{S}H_2 + 26H \rightarrow C_6A\bar{S}_3H_{32} \quad \text{Eq. 6}$$

During this first stage, an ettringite film is formed that covers and protects the surface of the C_3A particles, preventing the diffusion of SO_4^{2-}, $(OH)^-$, and Ca^{2+} ions.

Stage II: this stage is characterized by slow reactions, however, the creation of ettringite continues. The duration of this stage depends on the amount of gypsum available in the

mixture. The reaction rate is retarded due to the ettringite film, since SO_4^{2-} and Ca^{2+} ions must pass through of this film by diffusion before they can react to form more ettringite. C_3A hydration is delayed while ettringite forms a diffusion barrier around the C_3A particles (Fig. 6).

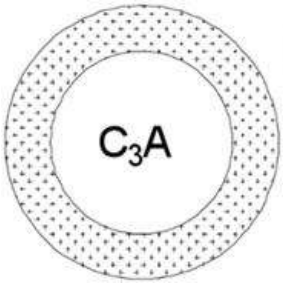

Fig. 6. Schematic representation of ettringite covering a C_3A particle

Stage III: after 10-24 hours, the gypsum has been completely depleted, this decreases the concentration of sulfate and calcium ions. The above causes that the solution saturates with respect to ettringite, which dissolves according to the following reaction:

$$29H_2O + 6Ca^+ + 2AlO_2^- + 3SO_4^{2-} + 4(OH)^- \rightarrow [Ca_2Al(OH)_6]_2.Ca_2(SO_4)_3.25H_2O \quad \text{Eq. 7}$$

The above reaction creates a source of sulfate ions, which with the aluminate that is still present, forms a new compound, the calcium monosulfoaluminate hydrate according to the reaction:

$$19H_2O + 4Ca^+ + 2AlO_2^- + SO_2^{2-} + 4(OH)^- \rightarrow [Ca_2Al(OH)_6]_2.Ca(SO_4)_3.15H_2O \quad \text{Eq. 8}$$

or

$$2C_3A + C_6A\bar{S}_3H_{32} + 4H \rightarrow C_4A\bar{S}H_{12} \quad \text{Eq. 9}$$

When ettringite begins to convert to monosulfate, the hydration rate of C_3A begins to increase again, because the protective barrier breaks down during conversion from ettringite to monosulfate (Fig. 7).

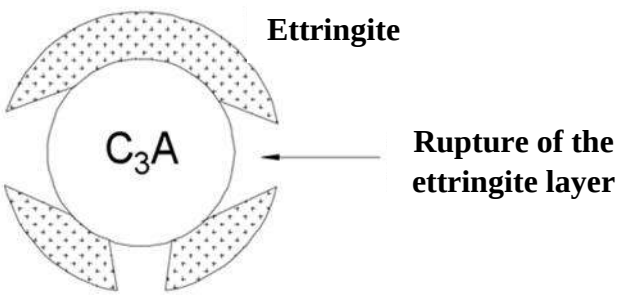

Fig. 7. Schematic representation of the rupture of the ettringite layer that surrounds the C_3A particle

Stage IV: During this period, the ettringite formed is completely transformed on monosulfoaluminate through long-term reactions

$$C_6A\bar{S}_3H_{32} + 2C_3A + 4H \rightarrow 3C_4A\bar{S}H_{12} \qquad \text{Eq. 10}$$

Subsequently, the monosulfoaluminate reacts slowly with excess aluminate and ferro-aluminate creating a complex hydrated product, which contains aluminate, ferrate, sulfate, calcium, and hydroxyl ions.

The rate and the mechanism of hydration of the main compounds of Portland cement can be modified by the incorporation of additives, these changes induce the corresponding changes to the fresh and hardened state properties of concrete.

2.5 Chemical admixtures and Supplementary Cementitious Materials (SCMs)

There is a very large variety of additives used in the concrete industry; however, those reacting with the concrete ingredients, especially with Portland cement, have a greater effect on the final properties of concrete. These additives can be classified into two large groups, the so-called chemical admixtures and the fairly-new mineral admixtures.

On one hand, chemical admixtures are materials different than water, hydraulic cement, and reinforcing fibers that are used as an ingredient in concrete [11]. Chemical admixtures are added to the mixture before, during, or after the mixing. Nowadays, the admixtures can be

used to reduce costs or to modify certain properties of concrete to adapt them to different working conditions. Chemical admixtures can modify the properties of concrete as follows:

- Increase the workability without increasing o decreasing the water content,
- Increase the compressive strength at an early age,
- Increase the resistance to severe exposure conditions,
- Decrease concrete permeability,
- Increase the adhesion between the concrete and reinforcing steel, and
- Inhibit the corrosion of reinforcing steel embedded in concrete.

On the other hand, mineral admixtures, also known as supplementary cementitious materials (SCMs), are soluble siliceous, aluminosiliceous, or calcium aluminosiliceous powders, commonly used as partial substitute of the clinker in cement or of Portland cement in cement-based composites [12]. SCMs are also known as pozzolans because by themselves have few or no cementitious properties; however, when they are finely divided, and in the presence of moisture, chemically react with $Ca(OH)_2$ to create compounds with cementitious properties [13].

The use of SCMs, in addition to reducing cost during concretes production, allows improving the performance of the cement and cement-based materials. In the ecological context, the partial replacement of PC by SCMs significantly decreases the cement consumption reducing accordingly the CO_2 emissions produced during the concrete manufacture [14].

3. Influence of SCM on the concrete matrix

Several studies have shown that the partial substitution of PC by SCMs significantly influences the workability, mechanical properties and durability of cement-based materials. Some SCMs have detrimental effects on the concrete workability. In some cases, the water demand for a concrete mixture increases because of the small particle sizes of the SCMs. In other cases, high internal porosity of the SCMs increases the water demand through water absorption [15-17]. On the other hand, it has been reported than the addition of some SCMs,

specifically FA, significantly improves the rheological properties of cement-based materials [18, 19].

Regarding the effect of the SCMs on the mechanical properties of cement-based materials, it is known that their use of some of them reduces their compressive strengths at and early age [20]. This effect is the result of the dilution of PC; however; a beneficial effect is experienced at a long-term age. This improvement is caused by the reaction between the SCMs and $Ca(OH)_2$ produced during the hydration of PC after 28 days [20]. More details about this reaction are presented in the following sections.

In the case of durability, the cementitious compounds produced by the reaction of the SCMs with $Ca(OH)_2$ reduce the porosity and permeability of the cement-based materials [21]. As a result, many durability properties are improved, for example, the sorptivity, permeability, and diffusivity of Cl^- and CO_2 are lowered [14]; in consequence the corrosion phenomenon is also positively altered.

3.1 Types of the SCMs

SCMs can be classified as natural and artificial. Natural SCMs are present in nature but its availability is limited because it can be found in only few specific regions [8]. Other examples of natural SCMs are calcined clays, vegetable ashes, and zeolites [5]. The extraction, manufacture, and transportation of these natural SCMs alter ecosystems and also cause pollution.

On the other hand, artificial SCMs are obtained from the industry as waste. A substantial amount of wastes is produced globally as by-products from the industrial and agricultural sectors [22]. Typical industrial SCMs are fly ash, blast furnace slag, and silica fume [8] whereas agro-industrial SCMs are rice husk ash, palm oil fuel ash, sugarcane bagasse ash, wood waste ash, and bamboo leaf ash [22].

As mentioned earlier, the SCMs, also known as pozzolans, partially replace PC leaving weak spots in the concrete matrix because SCMs are generally less dense and less reactive than PC. In order to compensate this weakness most of the SCMs react at a later age with $Ca(OH)_2$ produced from the hydration reaction of PC. For this reason, it is crucial to understand the pozzolanic reaction which is explained in some detail next.

3.2 Pozzolanic Reaction

The reaction between materials with pozzolanic properties, $Ca(OH)_2$ from the cement hydration and water is known as the pozzolanic reaction [4]. The products created during the pozzolanic reaction are similar to the C-S-H produced during the hydration of the PC and other compounds known as calcium aluminate silicate hydrates (C-A-S-H) [21].

Similarly, to the hydration of cement particles, the pozzolanic reaction is also a complex phenomenon. An intesting approach to explain the pozzolanic reaction is considering only the reaction mechanisms of C_3S and C_3A with the pozzolan particles.

The hydration mechanism of a C_3S-pozzolan system is schematically represented in Fig. 8. Ca^{++} ions dissolved from C_3S are captured by the pozzolana grains and those are adsorbed on the surfaces. On contact with water, Na^+ and K^+ from the pozzolanic grains are dissolved, resulting in a Si and Al rich amorphous film. Next, the film is broken and SiO_4^{4-} and AlO diffuse to meet Ca^+. The condition of precipitation being satisfied, C-S-H and Ca-Al hydrate precipitate on the surface of the outer hydrates of C_3S. The solution near the outer surfaces of the destroyed film becomes poorer in Na^+ and K^+ than on the inside, and Ca^{2+} is adsorbed on the film, resulting in the precipitation of C-S-H and Ca-Al hydrate.

The hydration mechanism of C_3A-pozzolana system is also schematically represented in Fig. 9. In contact with water, a rich film of amorphous Al is formed around the C_3A grain, while Ca^{++} and SO^{-}_4 ions are released into the solution. On the other hand, the pozzolana grain releases Na^+ and K^+ ions, and a film rich in Al and Si is formed around it. Next, the

film around the pozzolan grain is destroyed and AlO_2^- and SiO_4^{4+} ions are released, while Ca^{++} ions are absorbed to form C-S-H and mono-Ca-Al hydrates.

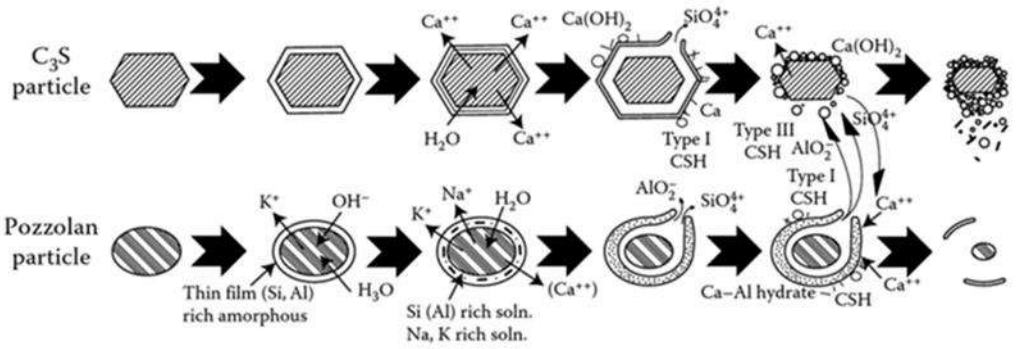

Fig. 8. Schematic representation of the hydration mechanism in the C_3S-pozzolan system [23]

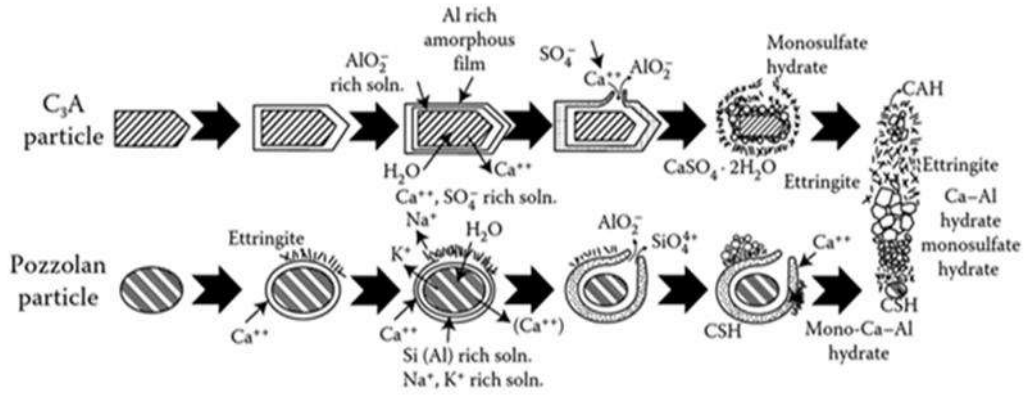

Fig. 9. Schematic representation of the hydration mechanism in the C_3A-pozzolan system [24]

The hardened paste of cement-SCMs has a lower $Ca(OH)_2$ content and a higher C-S-H content compared to paste obtained with only PC. It is important to mention that the amount of PC replaced by SCMs must be adjusted to the amount of $Ca(OH)_2$ produced in the hydration of the PC. This is necessary because the excess of SCMs will not react and therefore, it will behave like an inert addition [4].

3.3 Binary and ternary concretes

In order to improve the workability, as well as the mechanical and durability properties of the cement-based materials one or more SCM can be used as PC partial replacement. When

the PC is partially substituted by one SCM, binary concretes are produced [25]. The addition of one SCM can enhance some properties of the material but hinder other properties. One option to overcome this disadvantage is the the addition of a second SCM, this results in the advent of ternary concretes [26].

4. Physical and mechanical properties of the concrete matrix

A concrete matrix contains several types of solid phases; the most relevant properties of such solid phases are the density, porosity, and compressive strength [4]. These properties can be determined using destructive testing and their relationships further investigated. Another manner to non-destructively estimate these properties and their corresponding relationships is by the response to the propagation of ultrasonic guided waves through the concrete matrix [27]. These important subjects are revised next.

4.1 Density and porosity

Density is a fundamental property of materials, which relates the nature of its constituents and the existence of voids or pores between them. Density is defined as unit mass per unit volume. Bulk and absolute densities are useful for the characterization of materials; the first involves the pores present in the material which are filled by air, whereas, the absolute density involves only the amount of matter present in the material. Both densities of concrete can be determined by the ASTM C 642-13 standard [28].

The porosity of a material is defined as the volume of voids present divided by the total volume of such material [29]. This physical property has a main role on the compressive strength and modulus of elasticity of concrete [30]. The pores in the concrete matrix are classified according to their size. In this context, three kinds of pores are identified; micropores, mesopores and macropores, with sizes ranging between 1 nm to 100 nm, 100 nm to 10 µm, and 100 µm to 1 cm, respectively [31]. The porosity of a concrete can be characterized by mercury intrusion porosimetry, which provides also information about the pore-size distribution of a concrete [32]. Nevertheless, the ASTM C 642-13 standard [28]

gives a simpler procedure to obtain the total porosity of concretes by relating the absolute and bulk densities of the material.

4.2 Compressive strength

The compressive strength (CS) is used as a measure to judge the quality of concrete [33]. The CS is also the backbone of the design and proportioning methods of concrete mixtures. This property is obtained from casted and cured concrete specimens in accordance with the ASTM C39/C39M-20 standard [34]. The test consists in applying a uniaxial compression load to concrete specimens using a universal machine until failure occurs. The CS of the concrete specimens is determined by dividing the load applied during the test by its cross-sectional area. The CS of a concrete depends on many factors, for example, porosity, type and interaction between aggregates, moisture in the specimen, as well as, form and size of the specimens [35].

4.3 Response to ultrasonic guided waves

The ultrasonic guided waves are mechanical waves with a frequency larger than 20 kHz which propagates in a media by an external force causing the displacement of a particle apart from its equilibrium position. This displacement induces the displacement of the neighboring particles, leading to a chain reaction that allows the propagation of the wave [36]. Three types of ultrasonic waves can be used to characterize a material, namely, compressional waves (also called longitudinal or P-waves), shear waves (also called transverse or S-waves) and surface waves [37]. An ultrasonic wave is generated by two piezoelectric transducers, transmitter and receiver, connected to a signal transmitter-receiver equipment. This equipment emits electrical pulses, which are transformed into pressure pulses by the emitting transducer, transmitting them into the sample. Subsequently, the pressure pulses are sensed in the receiving transducer, which transforms them into electrical pulses that are registered in the transmitter-receiver equipment. The equipment can be connected to an oscilloscope which digitizes the signal and it can be further processed. One of the outcomes from the test is the time the wave travels through the specimen, also called transit time (t_v) (see Fig. 10a).

Once the t_v is estimated, the ultrasonic pulse velocity (UPV) can be calculated by dividing the length of the specimen by t_v.

Despite the UPV is useful to predict certain properties of a porous matrix, at the end it is a unidirectional test and predictions are not very accurate. To overcome this limitation the digitization of the signal allows its manipulation to obtain other ultrasonic parameters, such as spatial attenuation (α_S), temporal attenuation (α_t), and energy content in the signal.

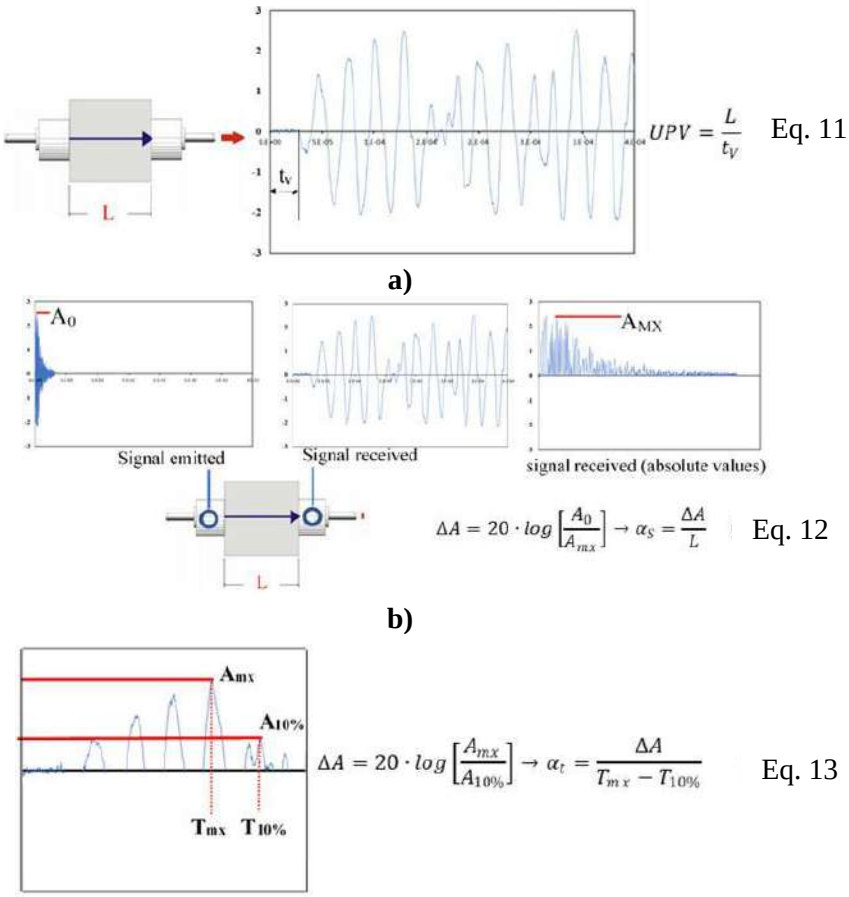

Fig 10. Schematic representation of a P-wave and how the ultrasonic parameters are calculated Adapted from Martinez-Martinez et al. [36]

The α_S can be calculated using the maximum amplitude of the ultrasonic signal emitted by the emitting transducer (A_0), the maximum amplitude of the signal received at the receiving transducer (A_{mx}), and the length of the specimen (L) (see the equation in Fig. 10b). The α_t

can be calculated using the maximum amplitude of the signal received by the receiving transducer (A_{mx}), the value of 10% of the maximum amplitude ($A_{10\%}$), the time in which the maximum amplitude is recorded (T_{mx}) and the time in which $A_{10\%}$ is last registered ($T_{10\%}$) (see the equation in Fig. 10c). Finally, the energy content in the signal is the integrated area under the signal [36]. The ultrasonic parameters can also be estimated from the S-wave and can help to more accurately estimate the porosity and compressive strength of a porous matrix, for example concrete [38].

5. Durability properties of the concrete matrix

Durability is one of the most important properties of reinforced concrete structures (RCS) because is associated with their service life after they are exposed to certain conditions or environments [2]. Durability means that an RCS will maintain its required strength and serviceability during the specified or traditionally expected service life [39]. The most studied durability properties of concrete and reinforced concrete are initial surface absorption, water absorption, sorptivity, alkali–silica reaction, resistance against sulfate attack, chloride diffusivity, chloride binding and resistance against corrosion induced by chlorides and carbonation [14].

5.1 Resistance to chloride diffusion

The chloride ingress into concrete is a complex phenomenon involving multiple mechanisms such as convection, capillarity suction, and diffusivity [40]. In this context, diffusion is the flow or movement of ions or molecules from one area with a higher concentration to another with a lower concentration to produce a homogeneous composition [41]. In the case of concretes, diffusion is the primary mechanism of chloride transport and it can be studied by the Fick´s second law (Eq. 14)

$$\frac{\partial C}{\partial t} = D_c \frac{\partial^2 C}{\partial X^2} \qquad \text{Eq. 14}$$

where D_C = diffusion coefficient, t = diffusion time, C = chloride concentration in the concrete, and x = distance at which chloride concentration is measured.

Under the assumptions of (1) homogeneous concrete, (2) constant chloride concentration at the exposure surface, and (3) constant diffusion coefficient [42], an error function solution to the Fick's second law is usually used as follows:

$$C(x,t) = C_s\left[1 - erf\left(\frac{x}{2\sqrt{D_c t}}\right)\right] \quad \text{Eq. 15}$$

where D_C = diffusion coefficient (m^2/s); t = time of exposure (s), $C(x, t)$ = chloride concentration at depth x after time t ($\%/m^3$), C_S = surface chloride concentration ($\%/m^3$), and *erf* is the error function. D_C and Cs are calculated based on a chloride concentration profile obtained from a concrete sample exposed at a chloride surce (Fig. 11).

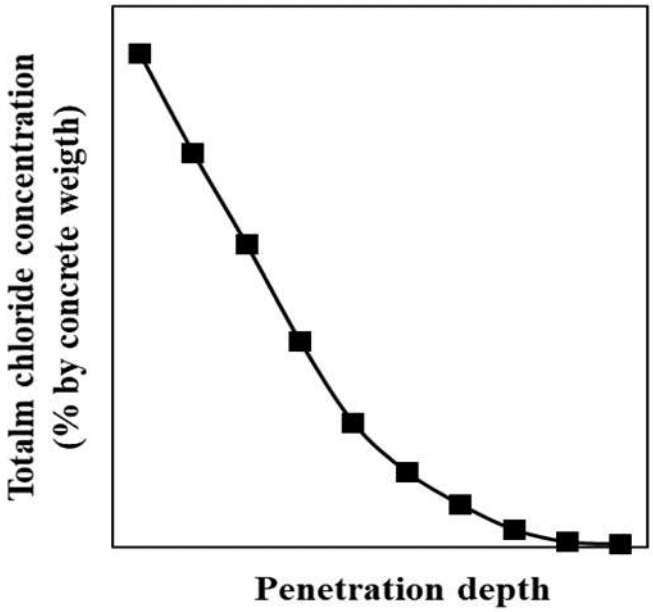

Fig. 11. Typical Chloride centration profile obtained of a concrete sample

The chlorides that have penetrated concrete can exist as either in the pore solution (free chlorides) or capture by the hydration products, which are known as bound chlorides [43]. In this context, it is important to mention that the concentration profile for calculating Dc and

Cs is obtained of total chloride concentration i.e. free plus bound chlorides. D_C is the parameter widely used to determine the penetration rate of chlorides through the cementitious matrix of concrete [44]. The rate or resistance to the Cl^- diffusion into concrete can be influenced by many factors for example total porosity, pore-size distribution, connectivity, tortuosity, and, chloride binding capacity of the concrete matrix.

5.2 Chloride binding capacity

In this perspective, the chloride binding capacity (P_b) of a concrete matrix must be considered as a relevant factor to evaluate their durability performance. It is known that the Pb of concrete depends on two main mechanisms: (I) chemical reactions and (II) physical adsorption [45]. The chemical reaction is through the formation of Friedel's salt ($C_3A{\cdot}CaCl_2{\cdot}10H_2O$) by the reactions between Cl^- and the Aft and Afm phases from concretes. However, some studies report that the alumina from SCMs can also chemically react with the Cl^- to form Friedel's salt [46]. The second mechanism involves the physical interaction of Cl^- with the C-S-H by three types of interaction: both electrostatic and Van der Waals forces, Cl^- adsorption into the C–S–H interlayer spaces, and Cl^- intimately bound in the C–S–H lattice [47].

The chloride binding capacity of concrete systems has been estimated by some using the Langmuir isotherms which indicate a non-linear relationship between free and bound chlorides [48, 49]. The conventional Langmuir isotherm can represent the adsorption phenomenon for a gas-solid system; however, the solution-solid system should be represented by the modified Langmuir isotherm. In addition, the Langmuir isotherms require the following assumptions: uniform surface, monolayer adsorption, one molecule per site, adsorbed molecules do not interact with each other and adsorption occurs by collisions with a vacant site, conditions that are very difficult to fulfil in a concrete matrix system. Finally, the Langmuir isotherms have been used mostly to estimate P_b values at early ages. Other approaches for the estimation of P_b of a concrete matrix are the use of linear models such as the Freundlich adsorption isotherms where an empirical equation defines a linear relationship between the absorbate and the absorbant, or the use of a linear relationship between free and

total chlorides from long-term experiments [50, 51]. At the end, the decision of using a linear or non-linear model is up to the trend showed by the data.

6. Mechanical properties of the reinforcing steel embedded in a concrete matrix

The mechanical properties are important in the design of RCS because the operation and performance depend on their ability to resist deformations under the stresses to which are subjected. The mechanical properties of RCS are mostly dictated by the properties of the steel reinforcement because it greatly contributes to defining the behavior of the whole system when subjected to mechanical stresses. The most important mechanical properties of the reinforcing steel can be calculated based on the stress-strain diagram from a tensile test.

The tensile test on a steel bar consists of applying a uniaxial load with a gradual increase until the breakage of the bar is achieved. Tensile tests provide information on the strength and ductility of materials under uniaxial stresses [52]. Fig. 12 shows the typical stress-strain diagram obtained from a tensile test of a steel rebar. The diagram depicts the elastic, yield, strain hardening, and descending or necking effect zones. The design parameters of the reinforcing steel, such as modulus of elasticity (E), yield strength (f_Y), ultimate strength (f_U), fracture strength (f_f), as well as the respective yield strain (ε_Y), ultimate strain (ε_U), and fracture strain (ε_f) are illustrated. Most of the parameters will change when the chemical composition of the steel also changes. For example, the increase in the carbon content increases the strengths accordingly but decreases the achievable strains. The exception to this behavior is the value of E which will remain constant despite of the increase in carbon content of the steel. The yield strenth indicates the maximum stress that the material can handle without experiencing plastic deformation; which occurs when a material is deformed to the point where it cannot return to its original axial dimension. The ultimate strength corresponds to that obtained when the maximum load is applied to the material, whereas, the fracture load is where the breakage of the bar occurs [53]. As mentioned before, for each stress of interest there is an associated strain; however, the strain or rather the relationship between strains is of particular relevance. For example, the ratio between ε_f and ε_Y brings about and important parameter called ductility.

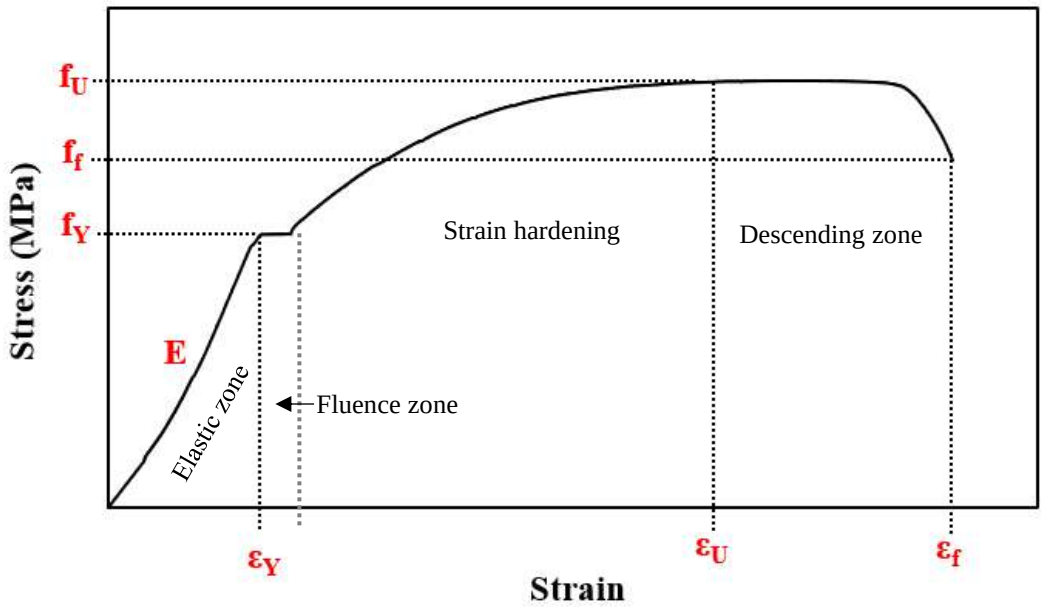

Fig. 12. Typical diagram stress-strain of a steel bar

Ductility is defined as the ability of a material to change its shape without fracture [53]. It is of critical importance for engineering materials for both the manufacturability and performance of the RCSs. The ductility of steel rebar can be determined by the Eq. 16 proposed by Bruneau et al. [54].

$$\mu = \frac{\varepsilon_f}{\varepsilon_Y} \qquad \text{Eq. 16}$$

where μ is the ductility of the rebar, while ε_f and ε_Y are the fracture and yield strains, respectively.

Ductility of a metal is an important property, but the loss of ductility is doubtless of paramount importance because downsizing this property can lead to the sudden collapse of a reinforced concrete element or of an entire RCS. The failure or collapse of RCS has not only serious economic and/or ecological impacts but also threats for human life preservation.

7. Cl^--induced corrosion of steel reinforcement embedded in a concrete matrix: causes and monitoring

One of the factors that cause deterioration of the reinforced concrete durability is the presence of a Cl^- in a high enough amount to cause the depassivation of the reinforcing steel. Two theories regarding the mechanism by which the Cl^- destroys the passivating film are proposed. The first theory suggests that Cl^- replace the oxygen atoms in the passivating film, which increases the conductivity and solubility of such layer. This replacement causes differences in the electrochemical potential, deteriorating the passivating film and therefore corrosion occurs [55]. The second theory suggests that the passivating film has defects and pores, where Cl^- penetrate such film forming anodic zones on the reinforcing steel surface, which are surrounded by large cathodic areas, and therefore corrosion occurs [56].

Based on the fact that corrosion is an electrochemical phenomenon the technique of corrosion potentials measurements (E_{corr}) allows evaluating the probability or risk of corrosion of the embedded reinforcing steel in concrete. This technique has been widely used over the years to monitor the risk of corrosion of reinforcing steel in concrete structures [57]. Results of corrosion potential can be interpreted in accordance with the ASTM C 876-15 standard [58].

Another technique to monitor corrosion is the called linear polarization resistance (LPR) which assumes that the polarization curve close to the corrosion potential is linear [59]. A small current is applied to polarize the reinforcing steel, which allows monitoring the amount of current required to achieve a defined variation in potential [60]. LPR measurement is normally performed with a three electrodes system. A stable electrode (reference electrode) measures both the corrosion potential and the overpotential between the reinforcing steel (working electrode) and the auxiliary electrode (counter electrode) [61]. The slope created by the graph of potential and current is the resistance to polarization, with which the total corrosion current is calculated [62]. Subsequently, the corrosion density (i_{corr}) is obtained by dividing the total corrosion current (I_{corr}) by the corroded area of the reinforcing steel. Results from this thecnique can be interpreted in accordance with the recommendations provided by Bromfield [63] (Table 1).

Table 1. Corrosion condition based on the corrosion density values [63]

Condition	Corrosion density (μA/cm^2)
Pasive	< 0.1
Low to moderate corrosion	0.1 to 0.5
Moderate to high corrosion	0.5 to 1.0
High corrosion rate	> 1.0

The electrical resistivity (ER) is another interesting and robust technique used to characterize a concrete matrix. It can be considered a durability test because correlates well with the diffusion coefficients, corrosion portentials and corrosion current density of a reinforced concrete system [64]. The ER of concrete is measured using the Wenner four-point probe principle. The test consists of applying an electric current to the two outer points of the Wenner probe [65] (Fig. 13).

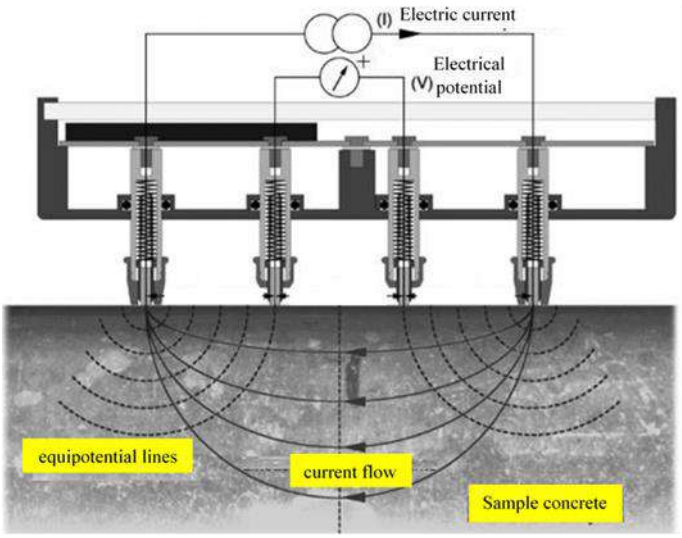

Fig. 13. Electrical resistivity test to a concrete specimen using the Wenner four-point probe Adaptated from Arenas-Piedrahita [66]

Subsequently, the electrical potential produced is measured with the interior points of the probe. The ER is measured to determine the protection provided by the concrete to the reinforcing steel. The ER mainly depends on the degree of saturation of the concrete, pore network, the type of cement, the water/cement ratio, and the quality of the aggregates [67].

8. Strategies to improve the durability of reinforced concrete structures exposed to chlorides

Cl^- induced corrosion can be slowed-down using first principles. A wide variety of methods, such as the use of corrosion inhibitors, galvanized steel, epoxy coatings, and cathodic protection, or the combination of some of them, have been used to improve the durability of reinforced concrete structures [68]. However, some methods like epoxy coatings can delay only for few years the corrosion [69], or the combination corrosion inhibitors and superplasticizers can decrease the compressive strength of concrete between 10 and 20% [70]. For this reason, more robust methods are the subject of on-going research.

As it was stated in previous sections, another alternative to improve the durability properties of reinforced concrete is through the incorporation of SCMs in the concrete mixture. Fly ash, which is one of the most popular SCM, reacts with the hydration products from PC to create secondary C-S-Hs. The porosity and permeability of the cementitious matrix are decreased, and in consequence, the diffusion of aggressive agents such as Cl^- can diminish. Nevertheless, the level of replacement of cement by fly ash cannot be considerably increased to respond to the raising concerns on the sustainability of the use of PC. For this reason, alternative SCM materials have to be investigated for this purpose. The combination of fly ash and UtSCBA to create ternary concretes is an interesting approach; however, comprehensive studies on their workability, mechanical properties, and durability are needed. This doctoral project fills that gap investigating the latter.

References

[1] M.G. Fontana, Corrosion engineering, Tata McGraw-Hill Education, 2005.

[2] S. Ahmad, Reinforcement corrosion in concrete structures , its monitoring and service life predi ction—a review, Cem. Concr. Compos. 25 (2003) 459–471.

[3] U. Angst, B. Elsener, C.K. Larsen, Ø. Vennesland, Critical chloride content in reinforced concr ete—A review, Cem. Concr. Res. 39 (2009) 1122–1138.

[4] L. Bertolini, B. Elsener, P. Pedeferri, E. Redaelli, R. Polder, Corrosion of steel in concrete, Wil ey Online Library, 2013.

[5] M. Valipour, M. Yekkalar, M. Shekarchi, S. Panahi, Environmental assessment of green concre te containing natural zeolite on the global warming index in marine environments, J. Clean . Prod. 65 (2014) 418–423.
[6] A. Horvath, CONSTRUCTION MATERIALS AND THE ENVIRONMENT, Annu. Rev. Envir on. Resour. 29 (2004) 181–204.
[7] M.C.G. Juenger, F. Winnefeld, J.L. Provis, J.H. Ideker, Advances in alternative cementitious bi nders, Cem. Concr. Res. 41 (2011) 1232–1243.
[8] K.L. Scrivener, V.M. John, E.M. Gartner, Eco efficient cements: Potential economically viable solutions for a low CO_2 cement based materials industry, Cem. Concr. Res. 114 (2018) 2–26.
[9] J.K. Steinberger, F. Krausmann, N. Eisenmenger, Global patterns of materials use: A socioecon omic and geophysical analysis, Ecol. Econ. 69 (2010) 1148–1158.
[10] V.S. Ramachandran, J.J. Beaudoin, Handbook of analytical techniques in concrete science and technology: principles, techniques and applications, Elsevier, 2000.
[11] ACI Committee 116, ACI 116R 00. Cement and concrete terminology. American Concrete In stitute; 2000.
[12] M.C.G. Juenger, R. Snellings, S.A. Bernal, Supplementary cementitious materials: New sourc es, characterization, and performance insights, Cem. Concr. Res. 122 (2019) 257–273.
[13] ASTM C125 20, Standard Terminology Relating to Concrete and Concrete Aggregates, AST M International, West Conshohocken, PA, 2020.
[14] M.C.G. Juenger, R. Siddique, Recent advances in understanding the role of supplementary ce mentitious materials in concrete, Cem. Concr. Res. 78 (2015) 71–80.
[15] R. Walker, S. Pavía, Physical properties and reactivity of pozzolans, and their influence on the properties of lime–pozzolan pastes, Mater. Struct. 44 (2011) 1139–1150,
[16] G. Quercia, A. Lazaro, J.W. Geus, H.J.H. Brouwers, Characterization ofmorphology and textu re of several amorphous nano silica particles used in concrete, Cem. Concr. Compos. 44 (2 013) 77–92,
[17] D. Kong, Y. Su, X. Du, Y. Yang, S. Wei, S.P. Shah, Influence of nano silica agglomeration o n fresh properties of cement pastes, Constr. Build. Mater. 43 (2013) 557–562,
[18] D. Ravina, P.K. Mehta, Properties of fresh concrete containing large amounts of fly ash, Cem. Concr. Res. 16 (1986) 227–238.
[19] V.G. Jiménez Quero, F.M. León Martínez, P. Montes García, C. Gaona Tiburcio, J.G. Chacón Nava, Influence of sugar cane bagasse ash and fly ash on the rheological behavior of ceme nt pastes and mortars, Constr. Build. Mater. 40 (2013) 691–701.
[20] H.E. Elyamany, A.E.M. Abd Elmoaty, B. Mohamed, Effect of filler types on physical, mecha nical and microstructure of self compacting concrete and Flow able concrete, Alexandria E ng. J. 53 (2014) 295–307.
[21] B. Lothenbach, K. Scrivener, R.D. Hooton, Supplementary cementitious materials, Cem. Conc r. Res. 41 (2011) 1244–1256.
[22] E. Aprianti, P. Shafigh, S. Bahri, J.N. Farahani, Supplementary cementitious materials origin f rom agricultural wastes A review, Constr. Build. Mater. 74 (2015) 176–187.
[23] K. Ogawa, H. Uchikawa, K. Takemoto, I. Yasui, The mechanism of the hydration in the syste m C_3S-pozzolana, Cem. Concr. Res. 10 (1980) 683–696.

[24] H. Uchikawa, S. Uchida, Influence of pozzolana on the hydration of C_3A, in: Proc. 7th Int. Co ngr. Chem. Cem. Sub-Theme IV, Paris, Fr., 1980: pp. 24–29.
[25] H. Binici, The effect of fineness on the properties of the blended cements incorporating groun d granulated blast furnace slag and ground basaltic pumice, Constr. Build. Mater. 21 (2007) 1122–1128.
[26] T.K. Erdem, Ö. Kırca, Use of binary and ternary blends in high strength concrete, Constr. Bui ld. Mater. 22 (2008) 1477–1483.
[27] J. Krautkrämer, H. Krautkrämer, Ultrasonic Testing by Determination of Material Properties BT Ultrasonic Testing of Materials, in: J. Krautkrämer, H. Krautkrämer (Eds.), Springer B erlin Heidelberg, Berlin, Heidelberg, 1990: pp. 528–550.
[28] ASTM C 642 13, Standard Test Method for Density, Absorption, and Voids in Hardened Con crete, ASTM International, West Conshohocken, PA, 2013.
[29] J.R. Nimmo, Porosity and pore size distribution, Encycl. Soils Environ. 3 (2004) 295–303.
[30] X. Chen, S. Wu, J. Zhou, Influence of porosity on compressive and tensile strength of cement mortar, Constr. Build. Mater. 40 (2013) 869–874.
[31] G. Fuyuan, Z. Dawei, S. Evdon, U. Tamon, Empirical Estimation of Pore Size Distribution in Cement, Mortar, and Concrete, J. Mater. Civ. Eng. 26 (2014) 4014023.
[32] H. Ma, Mercury intrusion porosimetry in concrete technology: tips in measurement, pore struc ture parameter acquisition and application, J. Porous Mater. 21 (2014) 207–215.
[33] E.I. Al Sahawneh, Size effect and strength correction factors for normal weight concrete speci mens under uniaxial compression stress, Contemp. Eng. Sci. 6 (2013) 57–68.
[34] ASTM C39 / C39M 20, Standard Test Method for Compressive Strength of Cylindrical Concr ete Specimens, ASTM International, West Conshohocken, PA, 2020
[35] J.R. del Viso, J.R. Carmona, G. Ruiz, Shape and size effects on the compressive strength of hi gh-strength concrete, Cem. Concr. Res. 38 (2008) 386–395.
[36] J. Martínez Martínez, D. Benavente, M.A. García del Cura, Spatial attenuation: The most sens itive ultrasonic parameter for detecting petrographic features and decay processes in carbon ate rocks, Eng. Geol. 119 (2011) 84–95.
[37] V.M. Malhotra, N.J. Carino, Handbook on nondestructive testing of concrete, CRC press, 200 3.
[38] Z. Lafhaj, M. Goueygou, A. Djerbi, M. Kaczmarek, Correlation between porosity, permeabili ty and ultrasonic parameters of mortar with variable water / cement ratio and water content , Cem. Concr. Res. 36 (2006) 625–633.
[39] A. Neville, Consideration of durability of concrete structures: Past, present, and future, Mater. Struct. 34 (2001) 114–118.
[40] J. Bernal, M. Fenaux, A. Moragues, E. Reyes, J.C. Gálvez, Study of chloride penetration in co ncretes exposed to high mountain weather conditions with presence of deicing salts, Constr . Build. Mater. 127 (2016) 971–983.
[41] H. Song, C. Lee, K.Y. Ann, Factors influencing chloride transport in concrete structures expos ed to marine environments, Cem. Concr. Compos. 30 (2008) 113–121.
[42] K. Audenaert, Q. Yuan, G. De Schutter, On the time dependency of the chloride migration coefficient in concrete, Constr. Build. Mater. 24 (2010) 396–402.

[43] Z. Yang, S. Sui, L. Wang, T. Feng, Y. Gao, S. Mu, L. Tang, J. Jiang, Improving the chloride binding capacity of cement paste by adding nano-Al_2O_3: The cases of blended cement pastes, Constr. Build. Mater. 232 (2020) 117219.
[44] N.T. Nordtest, Concrete, hardened: Accelerated chloride penetration, Nord. NT Build. 443 (1995).
[45] R. Luo, Y. Cai, C. Wang, X. Huang, Study of chloride binding and diffusion in GGBS concret e, Cem. Concr. Res. 33 (2003) 1–7.
[46] M. Thomas, Chloride thresholds in marine concrete, Cem. Concr. Res. 26 (2019) 513–519.
[47] C. Arya, Y. Xu, Effect of cement type on chloride binding and corrosion of steel in concrete, Cem. Concr. Res. 25 (1995) 893–902.
[48] H. Hirao, K. Yamada, H. Takahashi, H. Zibara, Chloride binding of cement estimated by bind ing isotherms of hydrates, J. Adv. Concr. Technol. 3 (2005) 77–84.
[49] Y. Lee, M. Kim, Z. Chen, H. Lee, S. Lim, Chloride Binding Capacity of Portland Cement Pas te Blended with Synthesized CA_2 ($CaO{\cdot}_2Al_2O_3$), Adv. Mater. Sci. Eng. 2018 (2018) 54189 30.
[50] T. Cheewaket, C. Jaturapitakkul, W. Chalee, Long term performance of chloride binding capa city in fly ash concrete in a marine environment, Constr. Build. Mater. 24 (2010) 1352–1357.
[51] W. Chalee, T. Sasakul, P. Suwanmaneechot, C. Jaturapitakkul, Utilization of rice husk bark as h to improve the corrosion resistance of concrete under 5 year exposure in a marine enviro nment, Cem. Concr. Compos. 37 (2013) 47–53.
[52] ASTM E8 / E8Mt 6ae1, Standard Test Methods for Tension Testing of Metallic Materials, A STM International, West Conshohocken, PA, 2016.
[53] F.P. Beer, E.R. Johnston, J.T. DeWolf, D.F. Mazurek, Mecánica de materiales, Mc Graw Hill, 2010.
[54] M. Bruneau, C. M. Uang, R. Sabelli, Ductilite Desing of Steel Structures, Second, McGrawHi ll, 2011.
[55] E. Moreno Fernández, A. Cobo Escamilla, M. Fernández Cánovas, Ductility of reinforcing ste el with different degrees of corrosion and the 'equivalent steel' criterion, Mater. Construcci ón. 57 (2007) 5–18.
[56] Y. Liu, Modeling the Time to Corrosion Cracking of the Cover Concrete in Chloride Contami nated Reinforced Concrete Structures, 1996, Doctoral thesis, Virginia Polytechnic Institute and State University, Virginia, USA.
[57] R.R. Hussain, Underwater half cell corrosion potential bench mark measurements of corrodin g steel in concrete influenced by a variety of material science and environmental engineeri ng variables, Meas. J. Int. Meas. Confed. 44 (2011) 274–280.
[58] ASTM C876 15, Standard Test Method for Corrosion Potentials of Uncoated Reinforcing Stee l in Concrete, ASTM International, West Conshohocken, PA, 2015.
[59] V. Matsagar, Advances in structural engineering, Springer, 2015.
[60] K. Hornbostel, C.K. Larsen, M.R. Geiker, Relationship between concrete resistivity and corro sion rate - A literature review, Cem. Concr. Compos. 39 (2013) 60–72.
[61] S.G. Millard, D. Law, J.H. Bungey, J. Cairns, Environmental influences on linear polarisation corrosion rate measurement in reinforced concrete, NDT E Int. 34 (2001) 409–417.

[62] ASTM G59-97(2014), Standard Test Method for Conducting Potentiodynamic Polarization Resistance Measurements, ASTM International, West Conshohocken, PA, 2014.
[63] J.P. Broomfield, Corrosion of steel in concrete: understanding, investigation and repair, CRC Press, 2003.
[64] K. Hornbostel, C.K. Larsen, M.R. Geiker, Relationship between concrete resistivity and corro sion rate - A literature review, Cem. Concr. Compos. 39 (2013) 60–72.
[65] A. TP95, Standard Method of Test for Surface Resistivity Indication of Concrete's Ability to Resist Chloride Ion Penetration, Am. Assoc. State Highw. Transp. Off. AASHTO, Washington, DC. (2011).
[66] J.C. Arenas Piedrahita, Correlación entre propiedades mecánicas y de durabilidad de morteros que contienen ceniza de bagazo de caña, Master thesis, IPN CIIDIR Oaxaca, México. (In Spanish).
[67] S.C. Kranc, A.A. Sagüés, Polarization current distribution and electrochemical impedance res ponse of reinforced concrete when using guard ring electrodes, Electrochim. Acta. 38 (199 3) 2055–2061.
[68] E. Rakanta, T. Zafeiropoulou, G. Batis, Corrosion protection of steel with DMEA based organ ic inhibitor, Constr. Build. Mater. 44 (2013) 507–513.
[69] P. Montes, T.W. Bremner, I. Kondratova, Eighteen year performance of epoxy coated rebar in a tunnel structure subjected to a very aggressive chloride contaminated environment, Corr osion. 60 (2004) 974–981.
[70] B. Sangoju, B.H. Bharatkumar, R. Gettu, P. Srinivasan, K. Ramanjaneyulu, N.R. Iyer, Influen ce of PCE SP and calcium nitrite inhibitor on mechanical and durability parameters of con crete, J. Sci. Ind. Res. 74 (2015) 82–87.

CHAPTER THREE

Long-term physical, mechanicals, and ultrasonic properties of ternary concretes containing FA and UtSCBA

Víctor Alberto Franco-Luján, Marco Antonio Maldonado-García, José Manuel Mendoza-Rangel, Pedro Montes-García.

2020.

Manuscript to be sent to Journal of Materials in Civil Engineering (JCR, Q1, IF=1.984)

Long-term physical, mechanical and ultrasonic properties of ternary concretes containing FA and UtSCBA

Víctor Alberto Franco-Luján [a], Marco Antonio Maldonado-García [a], José Manuel Mendoza-Rangel [b], Pedro Montes-García [c,*]

[a] Instituto Politécnico Nacional, CIIDIR-Oaxaca, Hornos 1003, Col. Noche Buena, Sta. Cruz Xoxocotlán, C.P. 71230, México.
[b] Universidad Autónoma de Nuevo León, FIC, Cd. Universitaria S/N, San Nicolás de los Garza, Nuevo León C.P. 66451, México.
[c] Instituto Politécnico Nacional, CIIDIR-Oaxaca, Grupo de Materiales y Construcción, México
* Corresponding Author. E-mail addresses: pmontes@ipn.mx, pmontesgarcia@gmail.com (P. Montes-García).

Abstract

The aim of this paper was to characterize the long-term physical, mechanical and ultrasonic properties of ternary concretes prepared with Portland Cement (PC), fly ash (FA) and untreated sugarcane bagasse ash (UtSCBA). Cylindrical specimens containing only PC, PC+FA and, PC+FA+UtSCBA were manufactured and cured in a $Ca(OH)_2$ solution for 2500 days. After curing, the bulk and absolute densities, percentage of voids, and compressive strength were determined. Furthermore, the characterization of the concretes using ultrasonic pulses was carried out. P and S wave velocities, temporal and spatial attenuations and energy contents were calculated. The results show that the addition of UtSCBA significantly reduced the absolute densities and percentages of voids of the ternary concretes with respect to control, while their compressive strengths remained similar. Results also indicate that the addition of 20%FA+20%UtSCBA produced significant changes in the ultrasonic parameters. Moreover, correlations between physical, mechanical, and ultrasonic properties were also analyzed and discussed.

Keywords: Energy content, long-term characterization, non-destructive techniques, ternary concretes, ultrasonic attenuation, ultrasonic pulse velocity.

1. Introduction

In recent years the supplementary cementitious materials (SCMs) have been used as Portland cement (PC) partial replacement in order to improve the microstructural, mechanical, and durability properties of PC-based materials. Moreover, the SCMs are useful to reduce the emissions of carbon dioxide associated with the manufacture of the PC [1]. The most used SCM for the manufacture of concrete is doubtless fly ash (FA); however, nowadays the production of FA has been negatively affected by the reduction of coal combustion. On the contrary, the demand for PC is continuously increasing, as an estimate of about 6 Gt of PC is projected to be consumed by 2050 [2]. Therefore, the development of new SCMs has been carried out to support the demand of PC and fulfill the decline of FA production [1]. In this sense, agro-industrial waste such as sugarcane bagasse ash (SCBA) has been investigated.

In the last 10 years or so, SCBA, a by-product obtained from the bagasse combustion in sugar mills, has been characterized and used as a PC partial replacement. A research project dealing with the use of ‘‘practically as received” SCBA (termed UtSCBA), which was only sieved through the 75 μm sieve, on the workability, microstructure mechanical and durability properties of mortars and concretes is been conducted. Studies about of the compressive strength (CS) of mortars report that the addition 10 and 20%UtSCBA decrease their CS at 7 and 14 days of age [3]. However, the pozzolanic reaction of the amorphous silica and alumina in the UtSCBA with the $Ca(OH)_2$ generated from the PC hydration produces secondary C-S-H. This reaction improves the microstructure of the UtSCBA-mortars and hence their 28-day

CS is similar to the strength of mortars with only PC. Moreover, the CS keeps increasing until 600 days of age [4].

The studies early mentioned shown that the use of UtSCBA does not negatively affect the long-term CS of mortars, however, both studies reported workability problems with the addition of UtSCBA. As a solution to this inconvenience Jimenez-Quero et al. [5] reported that the addition of 20%FA in mortars with 10 and 20%UtSCBA significantly improved their flow properties, fulfilling the requirement of the ASTM C311/C311M-08 [6] standard. In another research Rios-Parada et al. [7] used the combinations 20%FA+10UtSCBA and 20%FA+20%UtSCBA to evaluate effect of the addition of UtSCBA on their CS. The results indicate that the addition of UtSCBA in order to manufacture ternary concretes reduces their CS at 7, 28, and 56 days when compared with the control concrete. Nonetheless, the pozzolanic reaction of UtSCBA identified by X-ray diffraction was beneficial at 90 and 120 days, producing concretes with CS similar to the strength of the concrete with only PC. In addition to the CS, density and porosity are important in PC-based materials due to their role in the relation between mechanical and durability properties [8]. The ultrasonic pulse velocity (UPV) is another technique of common use to evaluate the properties of PC-based materials. UPV can be advantageous because it is a non-destructive technique, but its reliability is questionable. Nevertheless, the propagation of both the compression ultrasonic wave (P-wave) and the shear ultrasonic wave (S-wave) can provide parameters such as attenuation and energy content of the signal for the non-destructive characterization of PC-based materials [9]. Posteriorly, these parameters can be correlated with strength and porosity for a more comprehensive study of the properties of the PC-based materials [10, 11]. Several studies have demonstrated that P-waves and S-waves can be used to predict the CS and the

elastic and shear modulus of concretes [12, 13]. Other studies indicate that P- and S-waves attenuation can be correlated with other properties such as permeability or porosity of materials elaborated with PC [14]. In this context, the aim of this study is to characterize the physical, mechanical properties and ultrasonic parameters of concretes where the PC was partially substituted by FA and FA+UtSCBA. The bulk and absolute densities, percentage of voids, CS and ultrasonic parameters from both P-wave and S-wave were investigated for this purpose. Moreover, the relationships between properties and ultrasonic parameters were also analyzed.

2. Materials and methods

2.1 Experiment design

To characterize the physical and mechanical properties, and the ultrasonic parameters of the UtSCBA-ternary concretes an experimental design consisting of one factor with four levels and 11 quantitative response variables was implemented (Table 1).

Table 1. Details of the experiment design.

Factor	Levels	Description	Response variables
Type of mixture	Control (C)	100%PC	Bulk density (BD) Absolute density (AD) Percentage of voids (PV) Compressive strength (CS) P-wave velocity (V_P) S-wave velocity (V_S) P-wave spatial attenuation (α_{sp}) S-wave spatial attenuation (α_{ss}) P-wave temporal attenuation (α_{tp}) S-wave temporal attenuation (α_{ts}) P-wave energy content ($\mathcal{E}_P$) S-wave energy content ($\mathcal{E}_S$)
	Binary (T0)	80%PC+20%FA	
	Ternary 1 (T1)	70%PC+20%FA+10%UtSCBA	
	Ternary 2 (T2)	60%PC+20%FA+20%UtSCBA	

2.2 Description of the materials

Portland cement Holcim^{TM} (CPC-30R) readily available in the southwest of Mexico, fly ash Admix tech^{TM}, and UtSCBA were used to prepare the concrete mixtures. The PC fulfills the requirements established by the NMX-C-414-ONNCCE-2004 Mexican standard [15]. According to the ASTM C 618-19 standard [16], the FA was classified as class F pozzolan. The SCBA was collected from a sugar mill located in the community of Tezonapa, Veracruz, Mexico. Next, the SCBA was sieved through the 75 μm ASTM mesh for four minutes (UtSCBA). The densities of the PC, FA, and UtSCBA were of 2.94, 2.27, and 2.19 g/cm^3, respectively. Table 2 shows the chemical compositions of the cementitious materials used to prepare the concrete mixtures. It can be observed that the sums of the major oxides (SiO_2+Al_2O_3+Fe_2O_3) for the FA and UtSCBA were 89.55% and 88.28%, respectively; therefore, the ashes can be considered as materials with a high pozzolanic potential. On the other hand, the CPC and UtSCBA have higher LOIs than that recommended by the [16]. However, previous investigations do not report negative effects of these materials on the rheological, microstructural, and mechanical properties of PC-based materials [4, 5, 7].

Table 2. Chemical compositions of the cementitious materials (% by mass).

Material	Al_2O_3	CaO	Fe_2O_3	K_2O	MgO	MnO	Na_2O	P_2O_5	SiO_2	TiO_2	SO_3	LOI
CPC	4.87	60.03	3.57	0.85	1.50	0.08	0.52	0.19	20.67	0.58	4.95	8.40
UtSCBA	15.00	2.57	7.16	3.52	1.19	0.22	0.54	1.14	66.12	1.13	0.26	9.00
FA	20.01	4.00	5.42	0.96	0.63	0.10	0.19	0.38	64.12	1.12	0.86	2.60

LOI = Loss on ignition at 950 ºC for the CPC and at 750 ºC for the UtSCBA and FA.

Regarding the aggregates, river sand and calcareous crushed coarse aggregate were used in the concrete mixtures. The fineness modulus of the sand and the maximum size of the coarse aggregate were 2.97 mm and 19 mm, respectively. Furthermore, bi-distilled water and a high-

range water-reducer (HRWR) Plastol 4000^{TM} were used to prepare the concrete mixtures. The HRWR was used to keep the workability of the concrete mixtures containing UtSCBA.

2.3 Mix Design, preparation and casting of the concrete mixtures

The experiment includes four concrete mixtures designed in accordance with the absolute volume method from the American Concrete Institute [17]. All concrete mixtures were prepared under laboratory conditions with a 0.5 water/cementitious materials ratio. The mixture C was designed to achieve a slump target of 75±20 mm and a CS target of 25±8 MPa at 28 days. Table 3 shows the proportions of the concrete mixtures and the CS values achieved. Six cylinders of Ø100 mm x 200 mm were cast for each concrete mixture and cured in a $Ca(OH)_2$ saturated solution for 2500 days. The first set of three cylinders from each mixture was used to determine the bulk and absolute densities as well as the percentage of voids (PV) of the concretes. The second set of three cylinders was employed to carry out the ultrasonic guided wave tests and the CS tests.

Table 3. Proportions of the concrete mixtures (kg/m^3) [7].

Mixture	CPC	FA	UtSCBA	Fine aggregate	Coarse aggregate	Water	HRWR	Slump	28-day CS
C	410	--	--	727	1015	205	2.7	78	31
T0	328	82	--	727	1015	205	1.6	79	31
T1	287	82	41	727	1015	205	3.1	88	29
T2	256	82	82	727	1015	205	4.9	90	27

HRWR in ml per kg of cementitious materials, slump is in mm, and CS in MPa

2.4 Bulk and absolute densities, and percentage of voids of the concrete mixtures at 2500 days

The bulk and absolute densities and the percentage of voids were obtained according to the ASTM C 642-13 standard [18]. The bulk density was determined using concrete samples of Ø100 mm x 50±2 mm whereas absolute density was obtained from concrete fragments of approximately 20 mm x 20 mm. The absolute density test was carried out in an inert media using nitrogen gas, employing a multi-pycnometer from Quantachrome Instruments™. The concrete samples were dried in an electric oven at 110±1 °C for 24 hours before the tests. Finally, the PV of the concretes was determined according to Eq. 1 described in the ASTM C 642-13 standard [18].

$$PV = \frac{AD-BD}{AD} x100\% \quad (1)$$

where AD and BD were the absolute and bulk densities, respectively.

2.5 Compressive strength of the concrete mixtures

The CS of the concrete mixtures at 2500 days of age was obtained following the procedures of the ASTM C39/C39M-20 standard [19]. For this test, cylindrical samples described in the 2.3 section were used. The CS test was carried out on a hydraulic press Instron® model 600DX-B1-C3-G1A. Prior to the CS test, the cylinders were used to carry out the ultrasonic tests, which are described next.

2.6 Ultrasonic testing of the concrete mixtures

The ultrasonic guided waves test of the cylindrical specimens was carried out in the saturated condition. The test consisted of the induction of vibration of the specimens using ultrasonic

transducers. To do this, a pair of P-waves transducers X1021 Panametrics®, with a frequency of 50 kHz; and a pair of S-waves transducers V1548 Panametrics® with a frequency of 0.1 MHz were used. The transducers were coupled to the concrete samples in the transmission-reception mode (Fig. 1a). A flaw detector 5058PR Olympus® and a digital phosphor oscilloscope Tektronix® TDS 3014C were used for the signal generation and acquisition of data, respectively. The parameters used for the flaw detector were a rep-date of 50 Hz, damping of 200 Ω and a voltage of 200 V. No filters were used during the signal acquisition. Five signals for P- and S-waves were obtained from each cylinder, as shown in Fig. 1b. The ultrasonic pulse velocity, temporal attenuation (α_t), spatial attenuation (α_S) and waveform energy (Ɛ) for each P- and S-waves were obtained. All parameters were calculated according to tha procedure proposed by Martinez-Martinez et al. [20].

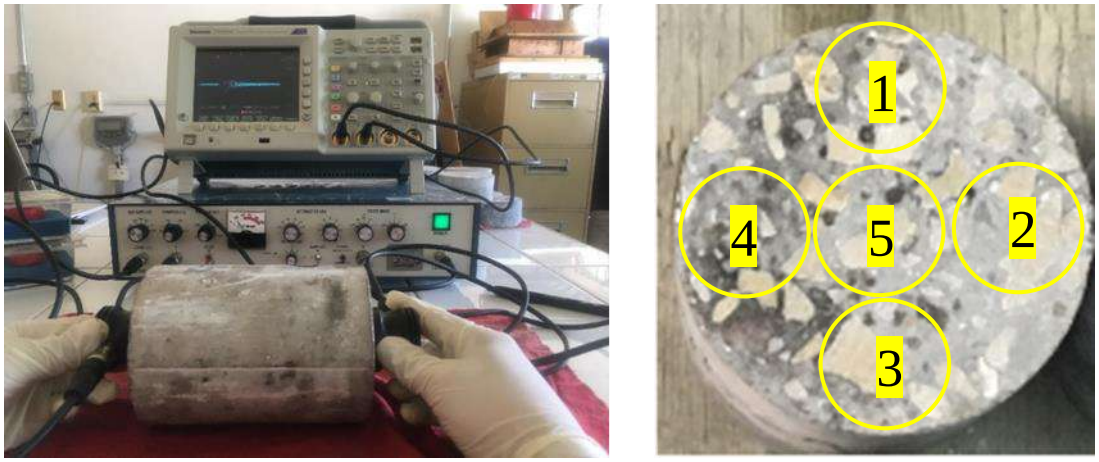

a) b)

Fig. 1. a) Equipment used for the ultrasonic testing and b) test setup of the ultrasonic measurements of the concretes at 2500 days

2.7 Statistical analysis of data

The data obtained from all tests were statistically analyzed by employing an ANOVA to determinate the significant differences. When the data did not comply with both the normality

and homogeneity of variance requirements, the nonparametric Kruskal-Wallis test was used. In all cases, SPSS® statistical software was used.

3. Results and discussion

3.1 Physical and mechanical properties of the concrete mixtures.

3.1.1 Densities and percentage of voids.

The bulk and absolute densities, and the percentages of voids (PV) of the studied concrete mixtures are shown in Fig. 2. It can be observed that the addition of FA and FA+UtSCBA appears to reduce the bulk densities in mixtures T0 and T1-T2, respectively, compared with the mixture C; however, all bulk densities are not statistically different ($p=0.096$).

With respect to the absolute densities, the results show that the partial substitution of PC by 20%FA, 20%FA+10%UtSCBA, and 20%FA+20%UtSCBA significantly reduced the absolute densities of the mixtures T0, T1, and T2, respectively, compared with the concrete C ($p<<0.005$ for T0, T1, and T2). In the case of the PVs, the partial replacement of 20%PC by FA slightly reduced the PVs of the mixture T0; nevertheless, when FA is combined with 10%UtSCBA and 20%UtSCBA, the PVs of the mixtures T1 and T2 are significantly lower than the PV of the concrete C ($p<<0.05$ and $p=0.008$ for T1 and T2, respectively). This result is apparently intriguing because T0, T1, and T2 concretes are less dense than the control concrete, as FA and UtSCBA have lower densities than cement (section 2.2). A possible explanation for this behavior is the fact that the pozzolanic reaction between the ashes and the products of the hydration of PC, which occurs at a late age, contributes to considerably densify the concrete matrix. In mixture C, a large amount of $Ca(OH)_2$ was produced which

precipitated and remained in solution, whereas, in mixtures T0, T1 and T2 the produced $Ca(OH)_2$ was depleted by the pozzolans to produce secondary C-S-H, which are less dense than the $Ca(OH)_2$ [21]. Such pozzolanic reaction was shown by X-ray diffraction tests carried out to the same mixtures at 120 days in previous research [7]. Moreover, these secondary products can add to the reduction in porosity of the concretes containing pozzolan.

Another explanation for the reduction of the porosity in the mixtures T0, T1, and, T2 is the so-called filler effect [22, 23] of the FA and UtSCBA unreacted particles as well as, carbon particles present in the UtSCBA. These particles have lower density than those from PC; however, these particles are deposited in the microstructures of concretes with FA and FA+UtSCBA obstructing pores and cracks and therefore, decreasing the porosity of such concretes.

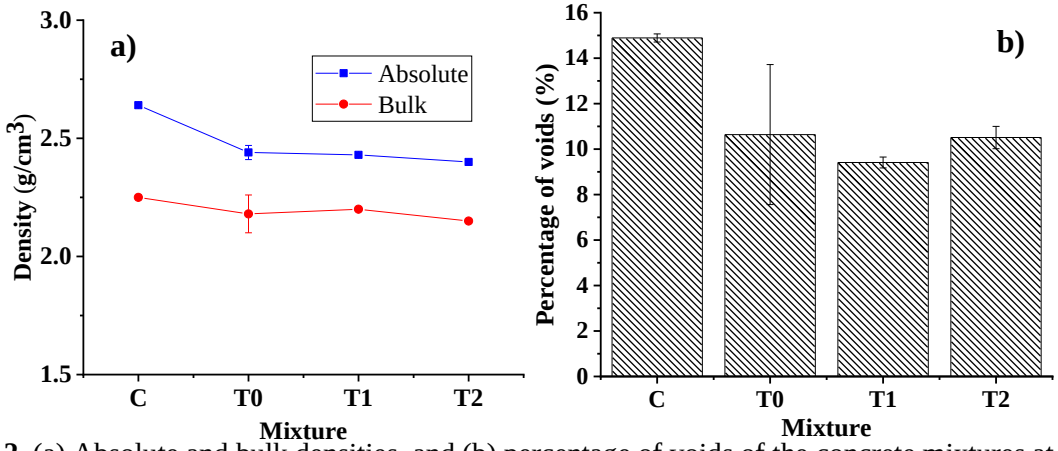

Fig. 2. (a) Absolute and bulk densities, and (b) percentage of voids of the concrete mixtures at 2500 days

3.1.2 Compressive strength

The CSs of the concrete mixtures at 2500 days of age are shown in Fig. 3. For comparison purposes, the CSs at 28, 56, 90, and 120 days, which have been already reported by Rios-

Parada et al. [7], are also shown in this figure. The results indicate that the CS of the mixture C with 100%PC significantly increased from 28 to 90 days ($p=0.046$) and after 90 days it remained essentially the same ($p=0.987$ and $p=0.995$ for the CS from 90 at 120 days and 120 to 2500 days, respectively).

In the case of mixture T0, its CSs were significantly higher than the mixture C but behaved similarly to this concrete; this means that the CS significantly increased from 28 at 90 days ($p<<0.05$), while was similar from 90 at 2500 days ($p=0.995$ and $p=0.916$ for CSs from 90-120 and 120-2500 days, respectively). With respect to UtSCBA-ternary concretes, the CSs of mixture T1 showed an apparently slight increase with age; however, the statistical analysis indicates that their CSs from 28 to 2500 days are similar ($p=0.089$, $p=0.737$, $p=0.999$, and $p=0.999$ for the CSs from 28 to 56, 56 to 90, 90 to 120, and 120 to 2500 days, respectively). For the concrete with 20%FA+20%UtSCBA, the statistical analysis shows a significant increase on its CSs from 28 to 56 days ($p=0.028$), as well as, a significant increase from 56 to 90 days can be also observed ($p=0.029$). Next, the strengths of the mixture T2 remains constant ($p=0.409$ and $p=1.000$ for CS from 90 to 120 and 120 to 2500 days, respectively).

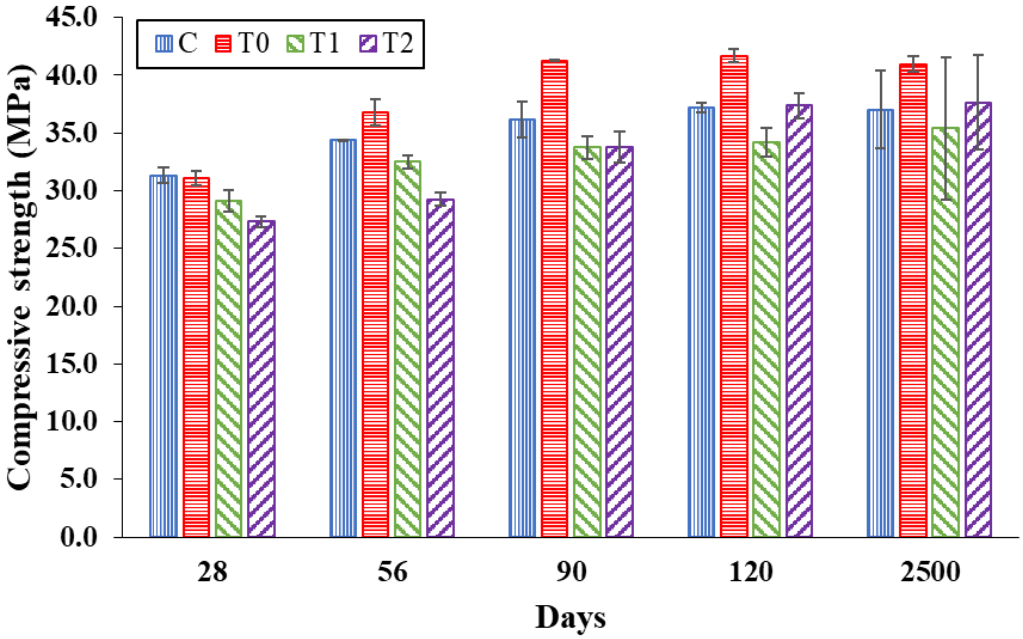

Fig. 3. Compressive strength of the studied concrete mixtures

Regarding the 2500-days CSs, the statistical analysis indicates that the strengths of all concretes were not significantly different when they are compared to mixture C ($p=0.864$, $p=0.960$, and $p=0.999$ for T0, T1, and T2, respectively). This outcome confirms that the use of 10 and 20% of UtSCBA as partial replacement of PC does not cause a reduction in their long-term CS. Similar results have also been reported by other studies where UtSCBA and ground SCBA were used as PC partial replacement in mortars [4] and concretes [24] at 600 days and 10 years, respectively.

Similarly, to the results from PV, results from CS carried out at 2500 days could be also intriguing (Fig. 4) because non-significant differences between the different concretes were already stated; however, significant differences were earlier found between the PV of the different mixtures. This appears to be contradictory because a more porous concrete matrix is expected to have a lower compressive strength. A possible explanation for this would rely

on the fact that FA and UtSCBA have lower densities than PC, and UtSCBA has, in addition to lower density, higher carbon content. The concrete matrices containing FA and UtSCBA are less porous than the matrix of mixture C due to the filler effect [22, 23] produced by both the unreacted and carbon particles, which at the end do not contribute to the increase in strength [25, 26].

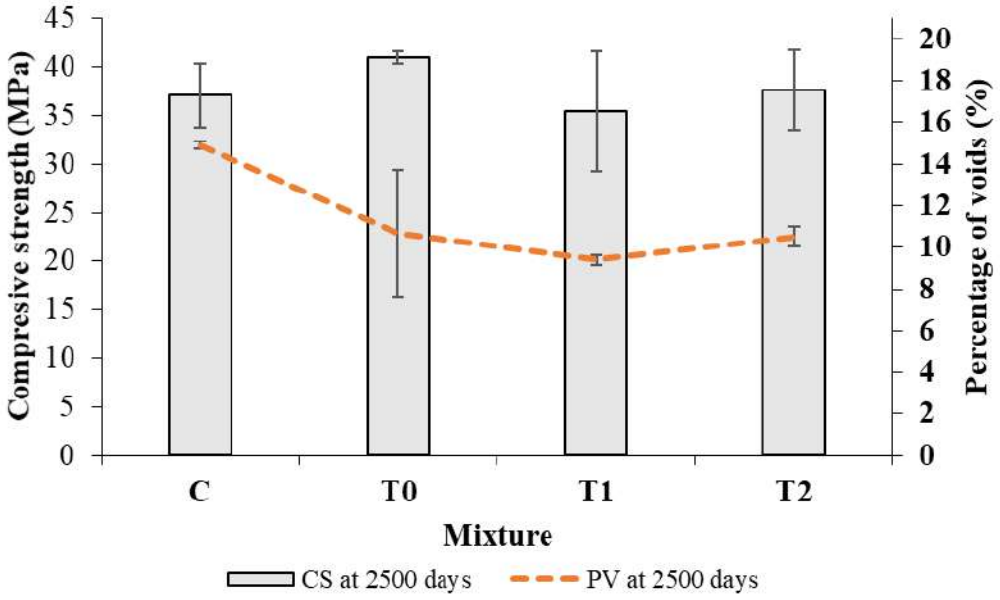

Fig. 4. Relationship between PV and CS of studied concretes at 2500 days

In conclusion, it appears that the addition of UtSCBA to the concrete mixtures makes a more complex microstructure which is less porous than the mixture C with only PC but with similar strength specifically originated by the carbon particles acting as weak spots in the former. An attempt to corroborate this assumption is presented in the following sections by analyzing the results from the ultrasonic parameters.

3.2 Ultrasonic parameters

3.2.1 P-wave and S-wave velocities

Fig. 5 shows both P-waves (V_p) and S-waves (V_S) ultrasonic pulse velocities of the concrete mixtures. The statistical analysis did not show significant differences between the V_p of the mixture C with mixtures T0 and T1 (p=0.205 and p=0.078, respectively), while the V_p of the mixtures C and T2 are statistically different (p=0.019). Despite a slight decrease of the V_p in the mixture T2, V_p of all studied concretes are higher than 4100 m/s (p<<0.05), limit value proposed for good quality concretes [27, 28].

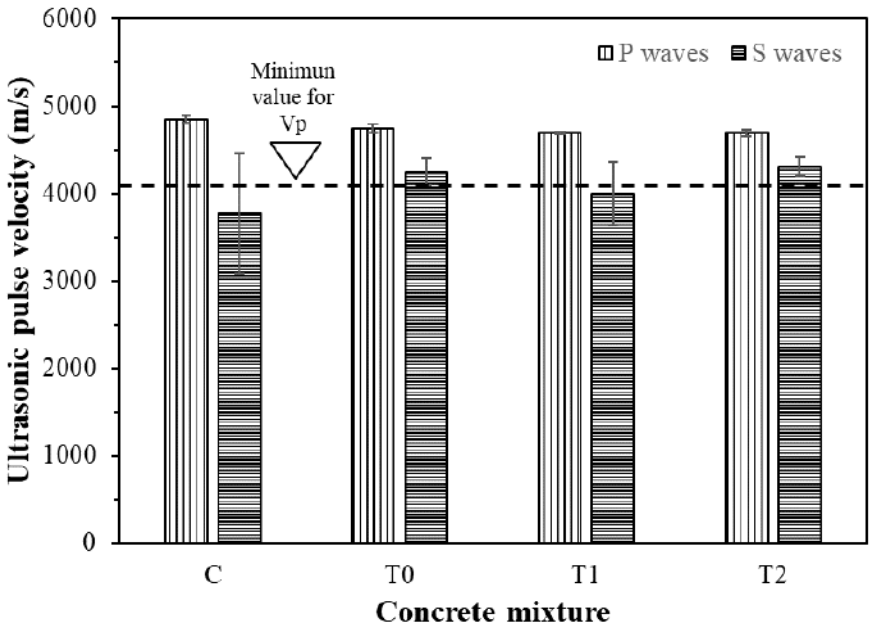

Fig. 5. P-wave and S-wave ultrasonic pulse velocities of the concrete mixtures at 2500 days

In the case of the V_S of the studied concretes, Fig 5 shows that their values are lower than the V_P values. The above can be due to that the propagation of the S-wave is perpendicular with respect to wave movement [20]. Moreover, the S-wave only propagate in solid media; therefore, its velocity is lower than the P-wave [29]. Unlike the V_P, the statistical analysis

showed the PC partial replacement by FA in T0 and FA+UtSCBA in T1 and T2 did not affect their V_S values when compared to the mixture C (p=0.414).

3.2.2 P-wave and S-wave spatial attenuation

The effect of the addition of FA and FA+UtSCBA on the spatial attenuation from P-waves and S-wave (α_{sp} and α_{ss}, respectively) of the studied concretes is illustrated in Fig. 6. In general, all concretes show similar αsp ranging from 4.22 and 4.26 dB/cm, while the statistical analysis did not show significant differences between all concretes (p=0.960).

With respect to αss, it can observe that their values are larger than αsp values, which can be due to that the propagation of S-waves is only in solid media and therefore, their attenuation is sensible to pores and cracks present in such media [30]. On the other hand, P-waves can also propagate in fluids and gases, which can occupy the discontinuities present on a solid media, and hence, the P-wave attenuations are lower than those from S-waves.

A more detailed analysis shows that the PC partial substituted by 20%FA and 20%FA+10%UtSCBA does not significantly affect the α_{ss} of the mixtures T0 and T1 with respect to mixture C (p=0.703 and p=0.999 for mixtures T0 and T1, respectively). On the contrary the addition of 20%FA+20%UtSCBA significantly reduced (p=0.010) the α_{ss} of T2 with respect to mixture C.

It is well-known that a signal will experience attenuation as a result of absorption and scatter of the medium where it propagates [31]. Therefore, concretes with a more heterogeneous microstructure will have higher attenuation. On the whole, the results of α_{sp} and α_{sp} suggest that the addition of UtSCBA in concretes with PC+FA does not negatively affect the microstructural properties of UtSCBA-ternary concretes as previous studies have reported

[7]. However; the analysis of α_{ss} indicates a higher S-wave propagation through the mixture T2, which suggests a certain improvement in their microstructure respect to mixture C.

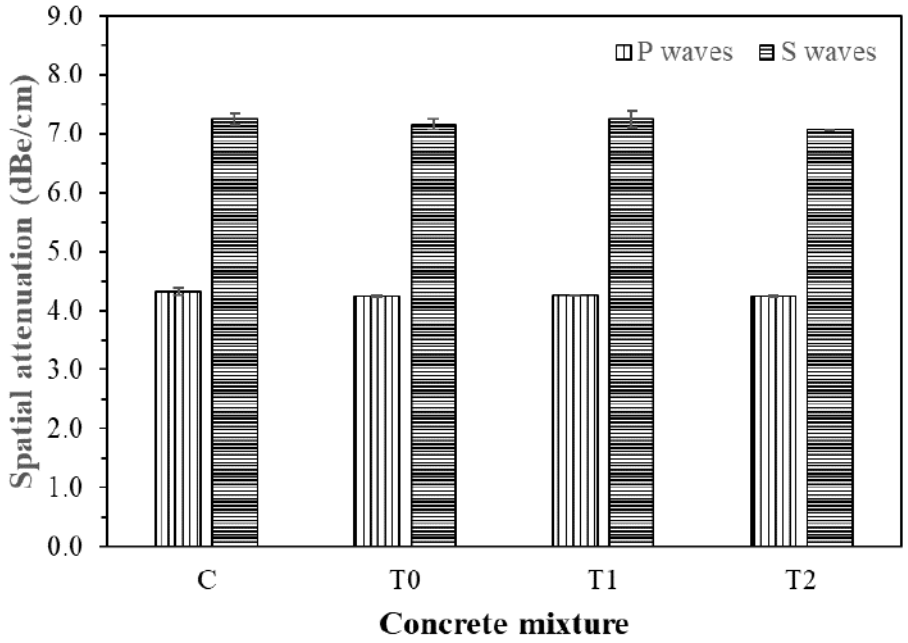

Fig. 6. P-wave and S-wave spatial attenuation of concrete mixtures at 2500 days

3.2.3 P-wave and S-wave temporal attenuation

Temporal attenuation from P-waves and S-wave (α_{tp} and α_{ts}, respectively) of the studied concretes are shown in Fig. 7. The results show that the addition of FA and FA+UtSCBA produced concretes with αtp similar to the valued of the mixture C (p=0.330).

In the case of αts, it can be observed that this ultrasonic parameter appears to decrease as the partial substitution of PC increased. However, such reduction is not significant when the PC is partially replaced by 20%FA and 20%FA+10%SCBA (p=0.110 and p=0.097, respectively). On the contrary, the addition of 20%FA+20%UtSCBA significantly decreased (p=0.001) the α_{ts} of the mixture T2 with respect to the mixture C.

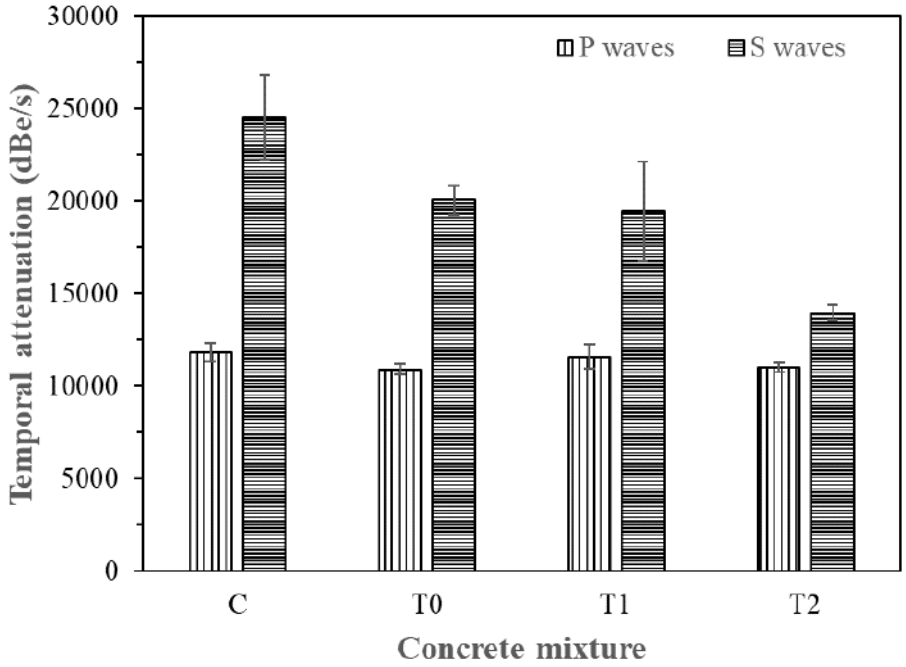

Fig. 7. P-wave and S-wave temporal attenuation of concrete mixtures at 2500 days

3.2.4 P-wave and S-wave energy

Fig. 8 shows the P-wave energy ($\mathcal{E}_p$) and S-wave energy ($\mathcal{E}_S$) of the concrete mixtures. The results indicate the addition of FA and FA+UtSCBA does not negatively affect the $\mathcal{E}_P$ of concretes T0, T1, and T2 with respect to the mixture C (p=0.402). In the case of the S-wave, the results show the mixtures T0 and T1 present $\mathcal{E}_S$ values about 480000 and 6200000, respectively; which are not significantly different with respect to the mixture C (p=0.110 and p=0.097 for T0 and T1, respectively). On the other hand, when a 20%FA+20%UtSCBA is combined with PC, the $\mathcal{E}_S$ of T2 significantly increased (p=0.001) with respect to the mixture C. The P-wave and S-wave energy agree with results from spatial attenuation; moreover, the $\mathcal{E}$s allows appreciate clearly the effect of the addition of 20%UtSCBA in concretes with FA. Valdeon et al. [32] mentioned the reduction in energy of ultrasonic waves is attributed to the pores, cracks, and heterogeneity of the materials. The above suggest that the combination

FA+UtSCBA produces concretes with similar heterogeneity and porosity than those manufactured with only PC and PC+FA, making the use of UtSCBA advisable to elaborate ternary concretes.

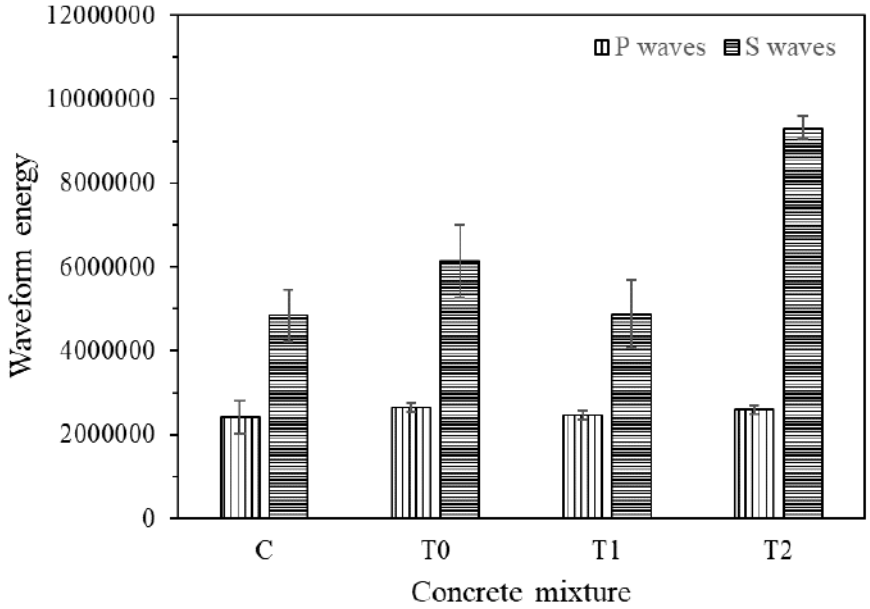

Fig. 8. P-wave and S-wave energy of concrete mixtures studied at 2500 days

3.3 Correlations

In this section, the correlations between PV and CS with the ultrasonic parameters from the studied concretes at 2500 days of age are investigated. Given that the bulk and absolute densities were used to calculate PV, only PV and CS were used for the analysis. Also, only V_P, αss, αts, and ε_S were used for the correlation analysis because were found to be significant when PC is partially replaced by FA and FA+UtSCBA.

Previous research reports that the effect of the addition of SCMs on the mechanical and durability properties of mortars cannot be represented by only one general model. For this reason, particular regression equations for mortars containing FA and UtSCBA were

proposed [3]. Based on this finding, in the present research particular regression equations to correlate the ultrasonic parameters with the PV and CS of the studied concretes are also proposed. Table 4 shows a summary of the proposed correlations between ultrasonic parameters of interest with PV and CS of the concretes under evaluation. High correlation coefficients can be observed for most of the relationships, which are discussed in detail in the following sections.

The correlations between PV and V_P of the concrete mixtures show an inverse relationship between these variables. When V_P increases the PV decreases accordingly. This tendency also has been already reported by Hernandez et al. [33]. In that study the authors mentioned that ultrasonic P-wave velocities propagating in concretes depend mainly on their porosity, i.e. in PC-based materials with reduced porosity the propagation of the P-wave will be easier. In the case of the correlations between CS and V_P, there is a directly proportional relationship between these variables; i.e. when V_P increases the CS also increases. This behaviour has also been reported by Demirboğa et al. [27], where the authors partially replaced the PC by FA, blast furnace slag (BFS), and FA+BFS in order to manufactured binary and ternary concretes.

The correlations between α_{ss} and PV indicate that when α_{ss} decreases the PV also decreases. This behavior is due to the fact that the energy loss of the wave increases in media with higher discontinuities, fissures, and pores [34, 35]. No research about the correlations α_{ss} and PV has been reported in the literature.

The correlation α_{ss}-CS shows that an increase in α_{ss} causes a decrease in CS. This trend is in accordance with the literature where it has been reported that concretes with high strength values, their S-wave spatial attenuation is low [36].

The correlation between α_{ts} and PV indicates that when α_{ts} values are large the PVs of the concretes are also high. In this case, the coefficients of correlation of the concretes C, T0, and, T1 were higher than 0.90, while the data of α_{ts} and PV of the mixture T2 presented the lower R-value of the 0.74.

Regarding the α_{ts} and CS correlation indicates that when α_{ts} increased the CS decreases accordingly. It is worth notice that the correlations between S-wave temporal attenuation with PV and CS have not been reported in the literature; however, the correlation between these parameters agrees with the relationship of α_{ss}-CS; nevertheless, the correlationsp α_{ts}-CS of the studied concrete mixture presented higher coefficients of correlation.

The $\mathcal{E}_s$ vs. PV correlations show an inverse relationship between variables. Concretes with high $\mathcal{E}_s$ values have low PVs. These results agree with the relationships of α_{ss} vs. PV and α_{ts} vs. PV for each concrete mixture. Both relationships, α_{ss} vs. PV and α_{ts} vs. PV show that the attenuations of the S-wave, which are inverse to the energetic contents [37], increase in concretes with high PV values, i.e. the energy loss of a wave increases in media with higher discontinuities, fissures, and pores [35, 36].

Table 4. Summary of proposed correlations between the significant ultrasonic parameters and PV and CS of the studied concrete mixtures

Mixture	Linear regression equation	R
C	$PV = -0.003V_P + 32.39$	0.85
T0	$PV = -0.60V_P + 299.81$	0.93
T1	$PV = -0.02V_P + 108.51$	0.94
T2	$PV = -0.008V_P + 50.41$	0.70
C	$CS = 0.06V_P - 292.6$	0.86
T0	$CS = 0.01V_P - 29.22$	0.99
T1	$CS = 0.42V_P - 1956.1$	0.74
T2	$CS = 0.09V_P - 428.71$	0.97
C	$PV = 1.73\alpha_{ss} - 2.33$	0.92
T0	$PV = 34.77\alpha_{ss} - 238.45$	0.92
T1	$PV = 1.55\alpha_{ss} - 1.89$	0.82
T2	$PV = 53.48\alpha_{ss} - 368.19$	0.94
C	$CS = -32.55\alpha_{ss} + 273.02$	0.92
T0	$CS = -8.47\alpha_{ss} + 101.72$	0.99
T1	$CS = -47.21\alpha_{ss} + 377.79$	0.98
T2	$CS = -377.61\alpha_{ss} + 2706$	0.78
C	$PV = 7.0 \times 10^{-5}\alpha_{ts} + 13.16$	0.91
T0	$PV = 3.8 \times 10^{-3}\alpha_{ts} - 65.51$	0.95
T1	$PV = 8.0 \times 10^{-5}\alpha_{ts} + 7.78$	0.92
T2	$PV = 9.0 \times 10^{-4}\alpha_{ts} - 2.55$	0.74
C	$CS = -1.3 \times 10^{-3}\alpha_{ts} + 69.61$	0.91
T0	$CS = -9.0 \times 10^{-4}\alpha_{ts} + 58.95$	0.99
T1	$CS = -2.3 \times 10^{-3}\alpha_{ts} + 80.23$	0.99
T2	$CS = -1.0 \times 10^{-2}\alpha_{ts} + 180.02$	0.95
C	$PV = -3.0 \times 10^{-7}\varepsilon_S + 16.21$	0.95
T0	$PV = -3.0 \times 10^{-6}\varepsilon_S + 28.74$	0.81
T1	$PV = -3.0 \times 10^{-7}\varepsilon_S + 10.83$	0.96
T2	$PV = -2.0 \times 10^{-6}\varepsilon_S + 26.45$	0.94
C	$CS = 5.0 \times 10^{-6}\varepsilon_S + 12.30$	0.95
T0	$CS = 8.0 \times 10^{-7}\varepsilon_S + 37.40$	0.96
T1	$CS = 8.0 \times 10^{-6}\varepsilon_S - 1.65$	0.98
T2	$CS = 1.0 \times 10^{-5}\varepsilon_S - 0.60$	0.77

The correlations show a direct proportional relationship between CS and ε_S values, which indicate that concretes with high ε_S values, their CSs are also large. Similarly, to the

correlations involving α_{ts}, no research about the correlation with the S-wave energetic content with PV, CS, or other physical and mechanical properties of concrete have been reported in the literature. In this case, the correlations between PV-$\mathcal{E}_S$ and CS-$\mathcal{E}_S$ agree with the correlations from α_{ss} and α_{ts} with the PV and CS of the studied concretes. The above is due to the energetic content is an ultrasonic parameter inverse to the attenuation of an ultrasonic wave [20].

A more comprehensive analysis of the results must consider the construction of a non-linear model to estimate the PV of the studied concretes based on all the significant ultrasonic parameters. Another model to estimate the CS of the same concretes considering only the ultrasonic parameters or the PV estimated with the first model could be built. Nevertheless, this subject is beyond the scope of this thesis.

Conclusions

Based on the analysis of results of the long-term tests the following conclusions can be drawn:

1. The addition of 10% and 20% of UtSCBA to concretes containing 20%FA significantly decreases the absolute densities of ternary concretes.
2. The addition of 10% and 20% of UtSCBA to concretes containing 20%FA produces less porous concretes but their compressive strengths are similar to concrete with only PC or with PC+20%FA.
3. The ultrasonic pulse velocity (V_P), obtained using the P-wave is the only parameter useful to detect differences between a concrete containing 20%UtSCBA and only PC.

4. The spatial attenuation, temporal attenuation and energy (α_{ss}, α_{ts} and ε_s), obtained using the S-wave can be used to detect differences between a concrete containing 20% UtSCBA and a concrete containing only Portland cement.
5. The correlations between ultrasonic parameters and concrete properties corroborate the following: when V_p increases PV decreases and CS increases; when α_{ss} increases PV increases and CS decreases; when α_{ts} increases PV increase and CS decrease; when ε_S increases PV decrease and CS increases. The correlations between α_{ts} and ε_S with PV and CS have not been reported in the literature; however, their trends agree with the correlations α_{ss}-PVs and α_{ss}-CSs.
6. The addition of 10% and 20% of UtSCBA to a concrete mixture containing 20% of FA mixtures makes a more complex concrete microstructure which cannot be properly characterized using only the V_p obtained from the transit of the P-wave through the concrete matrix. For a better characterization of these concretes the attenuation and energy parameters from the S-wave test are required.

Conflict of interest

The authors declare no conflict of interest.

Acknowledgments

The authors are grateful to the Instituto Politécnico Nacional (IPN) of Mexico for the facilities and financial support provided for this research. Further, the authors thanks to the Facultad de Ingeniería Civil of the Universidad Autónoma de Nuevo León in Mexico for the facilities during the microstructural and mechanical characterization of the concretes. Finally,

the authors are also grateful to the Consejo Nacional de Ciencia y Tecnología (CONACyT) of Mexico for the doctoral scholarships granted to Víctor Alberto Franco-Luján.

References

[1] M.C.G. Juenger, R. Snellings, S.A. Bernal, Supplementary cementitious materials: New sources, characterization, and performance insights, Cem. Concr. Res. 122 (2019) 257–273.

[2] K.L. Scrivener, V.M. John, E.M. Gartner, Eco efficient cements: Potential economically viable solutions for a low CO_2 cement based materials industry, Cem. Concr. Res. 114 (2018) 2–26.

[3] J.C. Arenas Piedrahita, P. Montes García, J.M. Mendoza Rangel, H.Z. López Calvo, P.L. Valdez Tamez, J. Martínez Reyes, Mechanical and durability properties of mortars prepared with untreated sugarcane bagasse ash and untreated fly ash, Constr. Build. Mater. 105 (2016) 69–81.

[4] M.A. Maldonado García, U.I. Hernández Toledo, P. Montes García, P.L. Valdez Tamez, The influence of untreated sugarcane bagasse ash on the microstructural and mechanical properties of mortars, Mater. Constr. 68 (2018) 1–13.

[5] V.G. Jiménez Quero, F.M. León Martínez, P. Montes García, C. Gaona Tiburcio, J.G. Chacón Nava, Influence of sugar cane bagasse ash and fly ash on the rheological behavior of cement pastes and mortars, Constr. Build. Mater. 40 (2013) 691–701.

[6] ASTM C311/C311 M18, Standard Test Methods for Sampling and Testing Fly Ash or Natural Pozzolans for Use in Portland Cement Concrete, ASTM International, West Conshohocken, PA, 2018.

[7] V. Ríos Parada, V.G. Jiménez Quero, P.L. Valdez Tamez, P. Montes García, Characterization and use of an untreated Mexican sugarcane bagasse ash as supplementary material for the preparation of ternary concretes, Constr. Build. Mater. 157 (2017) 83–95.

[8] X. Chen, S. Wu, J. Zhou, Influence of porosity on compressive and tensile strength of cement mortar, Constr. Build. Mater. 40 (2013) 869–874.

[9] S. Sharma, A. Mukherjee, Ultrasonic guided waves for monitoring the setting process of concretes with varying workabilities, Constr. Build. Mater. 72 (2014) 358–366.

[10] T.P. Philippidis, D.G. Aggelis, An acousto ultrasonic approach for the determination of water-to-cement ratio in concrete, Cem. Concr. Res. 33 (2003) 525–538.

[11] F. Benmeddour, G. Villain, O. Abraham, M. Choinska, Development of an ultrasonic experimental device to characterise concrete for structural repair, Constr. Build. Mater. 37 (2012) 934–942.

[12] R. Solís Carcaño, E.I. Moreno, Evaluation of concrete made with crushed limestone aggregate based on ultrasonic pulse velocity, Constr. Build. Mater. 22 (2008) 1225–1231.

[13] A. Jain, A. Kathuria, A. Kumar, Y. Verma, K. Murari, Combined Use of Non Destructive Tests for Assessment of Strength of Concrete in Structure, Procedia Eng. 54 (2013) 241–251.

[14] Z. Lafhaj, M. Goueygou, A. Djerbi, M. Kaczmarek, Correlation between porosity, permeabilit y and ultrasonic parameters of mortar with variable water/cement ratio and water content, Cem. Concr. Res. 36 (2006) 625–633.
[15] NMX C 414 ONNCCE 2004, Industria de la construcción cementos hidráulicos especificacion es y métodos de prueba, normas mexicanas, organismo nacional de normalización y certifi cación de la construcción y edificación, S.C., pp. 1–2 (In Spanish).
[16] ASTM C618 M19, Standard Specification for Coal Fly Ash and Raw or Calcined Natural Poz zolan for Use in Concrete, ASTM International, West Conshohocken, PA, 2019.
[17] A.C.I.C. 211, Standard Practice for Selecting Proportions for Normal, Heavyweight, and Mass Concrete:(ACI 211.1-91), in: American Concrete Institute, 1991.
[18] ASTM C642 M13, Standard Test Method for Density, Absorption, and Voids in Hardened Co ncrete, ASTM International, West Conshohocken, PA, 2013.
[19] ASTM C39/C39 M20, Standard Test Method for Compressive Strength of Cylindrical Concre te Specimens, ASTM International, West Conshohocken, PA, 2020.
[20] J. Martínez Martínez, D. Benavente, M.A. García del Cura, Spatial attenuation: The most sens itive ultrasonic parameter for detecting petrographic features and decay processes in carbon ate rocks, Eng. Geol. 119 (2011) 84–95.
[21] E. Aprianti, P. Shafigh, S. Bahri, J.N. Farahani, Supplementary cementitious materials origin f rom agricultural wastes – A review, Constr. Build. Mater. 74 (2015) 176–187.
[22] H.E. Elyamany, A.E.M. Abd Elmoaty, B. Mohamed, Effect of filler types on physical, mecha nical and microstructure of self compacting concrete and Flow able concrete, Alexandria E ng. J. 53 (2014) 295–307.
[23] G.C. Cordeiro, K.E. Kurtis, Effect of mechanical processing on sugar cane bagasse ash pozzol anicity, Cem. Concr. Res. 97 (2017) 41–49.
[24] G.C. Cordeiro, O.A. Paiva, R.D. Toledo Filho, E.M.R. Fairbairn, L.M. Tavares, Long Term C ompressive Behavior of Concretes with Sugarcane Bagasse Ash as a Supplementary Ceme ntitious Material, J. Test. Eval. 46 (2018) 20160316.
[25] P. Lawrence, M. Cyr, E. Ringot, Mineral admixtures in mortars effect of type, amount and fin eness of fine constituents on compressive strength, Cem. Concr. Res. 35 (2005) 1092–1105.
[26] M. Cyr, P. Lawrence, E. Ringot, Efficiency of mineral admixtures in mortars: Quantification o f the physical and chemical effects of fine admixtures in relation with compressive strength , Cem. Concr. Res. 36 (2006) 264–277.
[27] R. Demirboğa, İ. Türkmen, M.B. Karakoç, Relationship between ultrasonic velocity and comp ressive strength for high volume mineral admixtured concrete, Cem. Concr. Res. 34 (2004) 2329–2336.
[28] M. Shariq, J. Prasad, A. Masood, Studies in ultrasonic pulse velocity of concrete containing G GBFS, Constr. Build. Mater. 40 (2013) 944–950.
[29] G. Mavko, D. Jizba, The relation between seismic P and S wave velocity dispersion in saturated rocks, Geophysics. 59 (1994) 87–92.
[30] A. Nur, Effects of stress on velocity anisotropy in rocks with cracks, J. Geophys. Res. 76 (197 1) 2022–2034.

[31] P.A. Gaydecki, F.M. Burdekin, W. Damaj, D.G. John, The propagation and attenuation of me dium frequency ultrasonic waves in concrete: A signal analytical approach, Meas. Sci. Tec hnol. 3 (1992) 126–134.
[32] L. Valdeon, M.H. de Freitas, M.S. King, Assessment of the quality of building stones using si gnal processing procedures, Q. J. Eng. Geol. Hydrogeol. 29 (1996) 299 LP – 308.
[33] M.G. Hernández, M.A.G. Izquierdo, A. Ibáñez, J.J. Anaya, L.G. Ullate, Porosity estimation of concrete by ultrasonic NDE, Ultrasonics. 38 (2000) 531–533.
[34] J.A. Bogas, M.G. Gomes, A. Gomes, Compressive strength evaluation of structural lightweigh t concrete by non destructive ultrasonic pulse velocity method, Ultrasonics. 53 (2013) 962–972.
[35] Y. Ju, L. Sudak, H. Xie, Study on stress wave propagation in fractured rocks with fractal joint surfaces, Int. J. Solids Struct. 44 (2007) 4256–4271.
[36] F.K. Boadu, Fractured rock mass characterization parameters and seismic properties: Analytic al studies, J. Appl. Geophys. 37 (1997) 1–19.
[37] D. Benavente, J. Martínez Martínez, P. Jáuregui, M.A. Rodríguez, M.A.G. del Cura, Assessm ent of the strength of building rocks using signal processing procedures, Constr. Build. Mat er. 20 (2006) 562–568.

CHAPTER FOUR

Chloride-induced reinforcing steel corrosion in ternary concretes containing fly ash and untreated sugarcane bagasse ash

Víctor Alberto Franco-Luján, Marco Antonio Maldonado-García, José Manuel Mendoza-Rangel, Pedro Montes-García.

Article published in Construction and Building Materials (JCR, Q1, IF=4.046)
https://doi.org/10.1016/j.conbuildmat.2018.12.004.

Construction and Building Materials 198 (2019) 608–618

Contents lists available at ScienceDirect

Construction and Building Materials

journal homepage: www.elsevier.com/locate/conbuildmat

Chloride-induced reinforcing steel corrosion in ternary concretes containing fly ash and untreated sugarcane bagasse ash

Víctor Alberto Franco-Luján [a], Marco Antonio Maldonado-García [a], José Manuel Mendoza-Rangel [b], Pedro Montes-García [c,*]

[a] Instituto Politécnico Nacional, CIIDIR-Oaxaca, Hornos 1003, Col. Noche Buena, Sta. Cruz Xoxocotlán, C.P. 71230, Mexico
[b] Universidad Autónoma de Nuevo León (UANL), FIC, Cd Universitaria S/N, San Nicolás de los Garza, Nuevo León C.P. 66451, Mexico
[c] Instituto Politécnico Nacional, CIIDIR-Oaxaca, Grupo de Materiales y Construcción, Mexico

HIGHLIGHTS

- Untreated sugarcane bagasse ash (UtSCBA) was used in ternary concretes.
- Chloride diffusion of UtSCBA-ternary concretes was discussed.
- Long-term microstructure and compressive strength of UtSCBA-ternary concretes were evaluated.
- Corrosion in reinforced UtSCBA-ternary concretes was monitored and discussed.

ARTICLE INFO

Article history:
Received 20 June 2018
Received in revised form 13 November 2018
Accepted 1 December 2018

Keywords:
Untreated sugarcane bagasse ash
Ecological concretes
Corrosion
Electrochemical techniques
Long-term durability

ABSTRACT

The corrosion of reinforced ternary concretes containing fly ash (FA) and untreated sugarcane bagasse ash (UtSCBA) was evaluated. Chloride-ion diffusion at 28 and 90 days, as well as microstructural properties, percentage of voids, and compressive strength (CS) in cylinders were evaluated at 2500 days of age. Moreover, corrosion was monitored in prismatic specimens exposed to a NaCl solution by corrosion potentials and linear polarization resistance techniques. Results show that the combination of FA plus UtSCBA decreased the chloride-ion diffusion and did not affect the compressive strength (CS) of the concrete. For the studied concretes, the combination of FA plus UtSCBA appears a suitable option against chloride-induced corrosion.

1. Introduction

Chloride-induced corrosion is considered one of the major causes of damage in reinforced concrete (RC). There are several methods to prevent chloride-induced corrosion in RC such as cathodic protection, corrosion inhibitors and epoxy coatings [1]. However, these methods are either expensive or not effective.

The partial replacement of Portland cement (PC) by supplementary cementitious materials (SCM) is another viable and ecological option in preventing corrosion. SCM decrease the porosity and permeability of concrete due to the creation of cementitious compounds (CM) by pozzolanic reaction with the $Ca(OH)_2$ from the cement hydration [2].

Fly ash (FA) is an industrial waste which has been widely used in concrete as a SCM because of its positive effects on increasing the compressive strength (CS) to long-term ages and lowering permeability and chloride-ion diffusion. These benefits are attributed to the pozzolanic reaction of the FA, in addition to the filler effect of its fine particles [3]. Nonetheless, the availability of FA has declined due to the regulatory uncertainties regarding the use of coal [4]. This has led to the use of other SCM such as agricultural waste.

Sugarcane bagasse ash (SCBA) is a byproduct obtained from the bagasse combustion in sugar mills and is mainly deposited in open dumps, causing disposal problems and pollution. When the SCBA is post-treated it can be used as SCM in mortar and concrete mixtures because of its pozzolanic activity, which improves the microstructure of concrete without negative effects on its mechanical properties [5,6]. On the other hand, it has been reported that SCBA leads to significant workability issues during the mixing and placing of concrete. The different sizes and shapes of SCBA particles [7] and

* Corresponding author.
E-mail addresses: pmontes@ipn.mx, pmontesgarcia@gmail.com (P. Montes-García).

https://doi.org/10.1016/j.conbuildmat.2018.12.004
0950-0618/

its high loss on ignition (LOI) content, which is related to fibrous carbon particles, can be blamed for this negative effect [8]. This LOI can also decrease the pozzolanic activity of the SCBA and hence the CS development of concrete [9]. Re-calcination, sieving, grinding or the combination of these methods has been suggested to improve the properties of SCBA [5,10,11].

Researchers report that the addition of 10%-30% SCBA as a cement replacement (subjected to different post-treatments) reduces the permeability and chloride-ion diffusion in mortar and concrete mixtures [6,12–15]; nevertheless, most of these post-treatments require a significant amount of energy, making necessary the use of "practically as received" SCBA. From these studies, sieving appears to be the most environmentally-friendly option [16], since SCBA requires minimum post-treatment for proper pozzolanic activity.

Reviewing the literature, it appears that only one study reports on the durability of mortars containing "practically as received" SCBA. In this study the SCBA was sieved by a 75-μm ASTM mesh for only four minutes, but workability problems were experienced when 20% SCBA was added to the mortar [17]. The authors called this ash untreated sugarcane bagasse (UtSCBA) because of its low-energy demand post-treatment.

One option to diminish the disadvantages of UtSCBA as SCM in concrete is its use in combination with another pozzolanic material. To address this, a comprehensive long-term research project on the effect of the combination of UtSCBA plus FA on the workability, mechanical properties and durability of mortars and concretes is ongoing. As an outcome of this project, a first study reported a significant improvement in workability when 20% FA was added to pastes and mortars containing 10% and 20% UtSCBA [18]. The authors concluded that FA reduces the yield stress of the mortars with UtSCBA due to the spherical shape of its particles, yielding a mortar with flow properties like those required by the ASTM C311-04 standard. A second study reported that the combination of UtSCBA plus FA reduces the CS and modulus of elasticity of the ternary concretes at early ages because of the physical effect of the dilution of the CP and the high carbon content in the UtSCBA. However, after 90 days the pozzolanic reaction of UtSCBA produces ternary concretes with mechanical properties comparable with concretes prepared only with CP [19].

As a follow-up to the long-term project, the study of these concretes durability properties is highly needed. In the present research, the effect of the combination of UtSCBA plus FA against chloride-induced corrosion of steel reinforcement in ternary concretes is investigated. For this purpose, a chloride-ion diffusion test was carried out. In addition, microstructural properties, percentage of voids, and CS and electrochemical tests to long-term age were carried out. As well, the time for depassivation of the reinforcing steel was estimated.

2. Materials and methods

2.1. Description of materials

Blended Portland cement (CPC-30R), UtSCBA and Admix Tech® FA were used as cementitious materials for the concrete mixtures. The CPC fulfills the requirements established by the NMX-C-414-ONNCCE-2004 standard. The UtSCBA was collected from a sugar mill located in the community of Tezonapa, Veracruz, Mexico. It was sieved through a 75-μm ASTM mesh for four minutes. The FA is classified as class F in accordance with the ASTM C 618 standard. The chemical composition of the materials is shown in Table 1. The sum of the major oxides (SiO_2, Al_2O_3 and Fe_2O_3) for the UtSCBA and FA was 88.28% and 89.55%, respectively. The LOI content of the CPC and UtSCBA was higher than the LOI value established by the ASTM C 618. This could be attributed to the presence of calcium carbonate ($CaCO_3$) in the CPC [20] and unburned fibrous particles in the UtSCBA [7]. Despite this, both the CPC and the UtSCBA do not show negative effects on the properties of fresh and hardened state of mortars and concretes prepared with these materials [18,19].

River sand and calcareous crushed coarse aggregate were used to prepare the concrete mixtures. The volumetric weight, specific gravity and adsorption of the fine and coarse aggregates were 1596 kg/cm^3, 2.78 and 1.74%, and 1624 kg/cm^3, 2.66 and 0.47%, respectively. The fineness modulus of the sand was 2.97 and the maximum size of the coarse aggregate was 19 mm. Finally, bi-distilled water and a polycarboxilate-based superplasticizer (SP) Plastol 4000® were used in the concrete mixtures. The SP fulfills the requirements of the ASTM C 194 standard.

2.2. Mix design, casting and exposure conditions of the concrete mixtures

Four concrete mixtures containing 100% CPC (C), 80% CPC + 20% FA (T0), 70% CPC + 20% FA + 10% UtSCBA (T1) and 60% CPC + 20% FA + 20% UtSCBA (T2) were prepared. The concrete mixtures were designed in accordance with the absolute volume method from the ACI 211.1. All mixtures had a 0.5 water/cementitious materials ratio and were designed to achieve a slump value of 75 ± 20 mm (ASTM C143). The mixture C was designed to achieve a CS value of 25 MPa. The proportions of the concretes are shown in Table 2.

A total of 9 cylinders (100ϕ × 200 mm) and 3 prismatic specimens (100 × 150 × 300 mm) were cast from each concrete mixture. All specimens were demolded after 24 h and cured in a Ca$(OH)_2$-saturated solution until the time of testing.

Two sets of 3 cylinders each were cured for 28 and 90 days to obtain the chloride-ion diffusion coefficients (D_C) at those ages. These cylinders were exposed to chloride contamination following the procedures from the NT BUIL 443 standard. A third set of 3 cylinders was cured for 2500 days to determine the microstructural characterization and obtain the percentage of voids and CS of the concretes. The prismatic specimens were reinforced with two steel bars (rebar) 9.5 mm in diameter. An area of 28.4 cm^2 equivalent to a length of 260 mm was outlined in the middle section of each rebar using an epoxy coating, leaving 20 mm at the upper part of the rebar for the electrochemical testing. The thickness of the concrete cover was 45.5 mm. The prismatic specimens were cured for 28 days and thereafter immersed in a 3.5% NaCl solution, leaving 30 mm of concrete cover above the NaCl solution. The exposure period to evaluate the corrosion performance of the specimens was also 2500 days (Fig. 1). The temperature and rela-

Table 1
Chemical composition of the used cementitious materials (% by mass) [19].

Material	Al_2O_3	CaO	Fe_2O_3	K_2O	MgO	MnO	Na_2O	P_2O_5	SiO_2	TiO_2	SO_3	LOI
CPC	4.87	60.03	3.57	0.85	1.50	0.08	0.52	0.19	20.67	0.58	4.95	8.40
UtSCBA	15.00	2.57	7.16	3.52	1.19	0.22	0.54	1.14	66.12	1.13	0.26	9.00
FA	20.01	4.00	5.42	0.96	0.63	0.10	0.19	0.38	64.12	1.12	0.86	2.60

LOI = Loss on ignition at 950 °C for the CPC and 750 °C for the UtSCBA and FA.

Table 2
Proportions of the concrete mixtures (kg/m^3).

Mixture	CPC	UtSCBA	FA	Fine aggregate	Coarse aggregate	Water	SP	Slump
C	410	–	–	727	1015	205	2.7	78
T0	328	82	–	727	1015	205	1.6	79
T1	287	82	41	727	1015	205	3.1	88
T2	256	82	82	727	1015	205	4.9	90

SP = Polycarboxilate-based superplasticizer (ml per kg of cementitious materials), Slump is in mm.

Fig. 1. The exposure conditions of the reinforced prismatic specimens.

tive humidity of the testing room were recorded during that time using a HoBo® data logger device.

2.3. Chloride-ion diffusion coefficients of the concrete mixtures

After exposure to the NaCl solution, the chloride profiles of the concrete mixtures at 28 and 90 days were obtained in accordance with the NT BUILD 208 standard. For this purpose, powder samples were taken every 2 mm from the cylinders described in Section 2.2. A total of 10 samples were obtained from each cylinder for the profiles; then the profiles were used to estimate the chloride-ion diffusion coefficients (Dc) of the concrete mixtures using the Table Curve software version 5.01®.

2.4. Mineralogical and microstructural analysis of the concrete mixtures

The morphology of the concrete mixtures at 2500 days was observed using a high vacuum scanning electron microscope, (SEM) JEOL® model JSM-6510LV, equipped with an EDS microanalysis system from Oxford Instruments®. Small fragments of concrete paste (5 mm^3) were obtained by cutting small disks (1 mm in thickness) out of the cylinders described in Section 2.2. The fragments were dried in an electric oven at 40 °C for 10 min; finally, the samples were covered with a gold-paladium film using Denton Vacumm Desk IV® equipment.

The mineralogical phases of the concrete mixtures at 2500 days were identified using an Empyrean® diffractometer. The samples (1 gr) were obtained by cutting small disks (1 mm in thickness) out of the cylinders described in Section 2.2. The disks were crushed to remove large aggregate particles from the cementing paste and then the fragments were manually ground and sieved through a 75-μm ASTM mesh. The equipment uses a Cu anode and it was operated with a voltage of 45 kV and a current of 40 mA. The X-ray diffraction (XRD) tests were carried out from 5 to 70° (2-Theta) at a scanning speed of 0.5 s and increments of 0.026°. Finally, the mineral phases were identified using the software EVA version 11.0.03®.

2.5. Determination of the percentage of voids and compressive strength of the concrete mixtures

The percentage of voids of the concrete mixtures at 2500 days was determined according to the ASTM C 642 standard by means of measuring both bulk (dry) and absolute densities. The bulk density was obtained with samples of $\phi 100 \times 50 \pm 2$ mm, which were cut from the cylinders described in Section 2.2. The absolute density was measured using a multi-pycnometer from Quantachrome Instruments®. The tests were carried out in an inert media using nitrogen gas. In this case, small concrete fragments were used. The fragments were dried in an electrical oven at 110 ± 5 °C for 24 h before the tests.

The compressive strength test (CS) of the concrete mixtures at 2500 days was carried out using a hydraulic press, Instron® model 600DX-B1-C3-G1A, in accordance with the ASTM C 39 standard. Three cylinders with $100\phi \times 138$ mm from each concrete mixture were used for the tests. The cylinders were obtained after cutting the small disk used for the microstructural and percentage of voids tests. The CS results were corrected by size according to the ASTM C 42 standard.

2.6. Estimated time for depassivation of rebar embedded in concrete mixtures

The time for the depassivation (t_{dp}) of rebar in the concrete mixtures was estimated using Ficks second law. For this purpose, the D_Cs taken at 28 days, the initial chloride content, a critical Cl^- threshold value of 0.05% [21], and the concrete cover depth of the steel embedded in the prismatic specimens were used. The results were correlated with the corrosion potentials and current densities measurements obtained as described in the following section.

2.7. Electrochemical testing

The corrosion conditions of the rebar embedded in the ternary concretes were evaluated weekly by half-cell corrosion potentials (E_{corr}) and linear polarization resistance (LPR) tests. The E_{corr} were taken in accordance with the ASTM C 876 standard. An Ag/AgCl reference electrode and a high impedance multimeter Mc Miller Co LC-4® were used for this purpose. The LPR tests were carried out following the ASTM G 59–97 standard.

A potentiostat Gamry® series G300, an Ag/AgCl reference electrode and a stainless-steel bar as external counter were used for the tests. The working electrode was polarized to ±20 mV vs R_{ref} at a scan rate of 0.075 mV/s. The LPR results were processed using the Gamry Echem Analyst™ version 5.1.3 software to obtain the current densities (i_{corr}). After that, the total integrated corrosion was estimated according to the ASTM G 109 standard. Finally, the theoretical mass loss (T_{ms}) of the rebar embedded in the concrete mixtures was calculated using Faradaý's law for electrolysis considering a valence of 2.5 for the Fe^{2+} and Fe^{3+} [22].

3. Results and discussion

3.1. Chloride profiles and chloride-ion diffusion coefficients

The Cl^- concentration profiles of the concrete mixtures at 28 and 90 days are shown in Fig. 2a and b, respectively. At 28 days mixture C showed the highest concentration. The Cl^- concentration of the mixture T0 gradually decreased with respect to mixture C after approximately 5 mm of depth until it reached the critical Cl^- threshold value from 15 to 17 mm of depth. The Cl^- concentrations of mixtures T0 and T1 showed a similar behavior. Both concentrations decreased in respect to mixtures C and T0 after 3 mm of depth, and this trend remained until the last tested depth. The Cl^- concentrations of concretes containing the combination of FA plus UtSCBA decreased below the critical Cl^- threshold value from 13 to 15 mm of depth. This shows that such a combination has a positive effect on lowering the Cl^- ingress in the concrete. This positive effect could be attributed to the presence of fine particles in the concrete rather than pozzolanic reactions of the ashes which could occur after 28 days [23]. These particles reduce the connectivity between the capillary pores by the physical effects of dividing or reducing the size of the pores [19]. Another way to explain the Cl^- content reduction in the concrete mixtures containing FA plus UtSCBA is based on the chemical Cl^- binding with the alumina from the ashes [24].

At 90 days the mixture C again showed the highest Cl^- concentration along all the tested depths while the Cl^- content of the mixture T0 decreased quickly and was less than the critical Cl^- threshold value between 10 and 11 mm of depth. As at 28 days, mixtures T1 and T2 showed less Cl^- concentrations with respect to mixtures C and T0. The Cl^- concentrations of mixtures T1 and T2 decreased below the critical value between 8 and 9 mm of depth. The best performance shown by concrete mixtures containing FA plus UtSCBA could be attributed to the pozzolanic reaction of these ashes. The cementitious compounds from the pozzolanic reaction make a cementitious matrix with lesser voids, which in turn reduces the Cl^- ingress into the concrete [3]. The occurrence of the pozzolanic reaction of the used FA and UtSCBA was corroborated by Rios-Parada et al. [19]. The proposed Cl^- bonding at 28 days could be more evident at 90 days. This is observed in the profiles in which the curves of the concretes containing FA plus UtSCBA turn more concave because of the presence of a greater Cl^- content in the first tested depths. This behavior has been reported by other researchers and is attributed to the Cl^- binding capacity of the SCM [25].

Fig. 3 shows that the addition of 20% FA to the concrete reduces the 28-day D_C by approximately 46%, while the additions of 20% FA + 10% UtSCBA and 20% FA + 20% UtSCBA decrease it by 58% and 61%, respectively. These decrements support the effect of fine FA and UtSCBA particles and the possible Cl^- binding capacity of the alumina from the ashes [24]. The 90-day D_Cs of all the concretes decreased considerably with respect to the 28-day Dc. At this age, reductions of 64%, 77% and 81% were observed when compared to mixture C. The higher reduction of the D_C by increasing the initial curing time in the concretes could be attributed to the

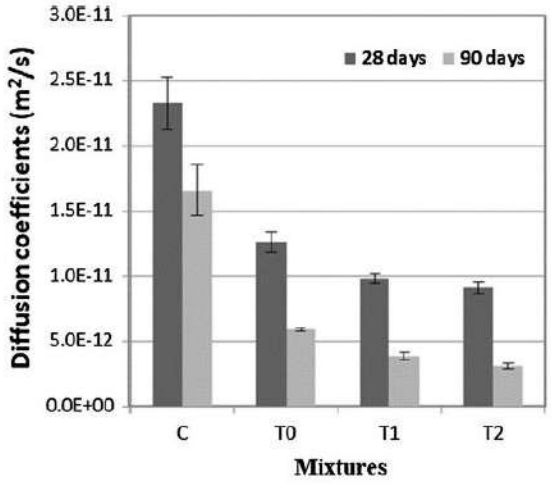

Fig. 3. Chloride diffusion coefficients of the concrete mixtures at 28 and 90 days.

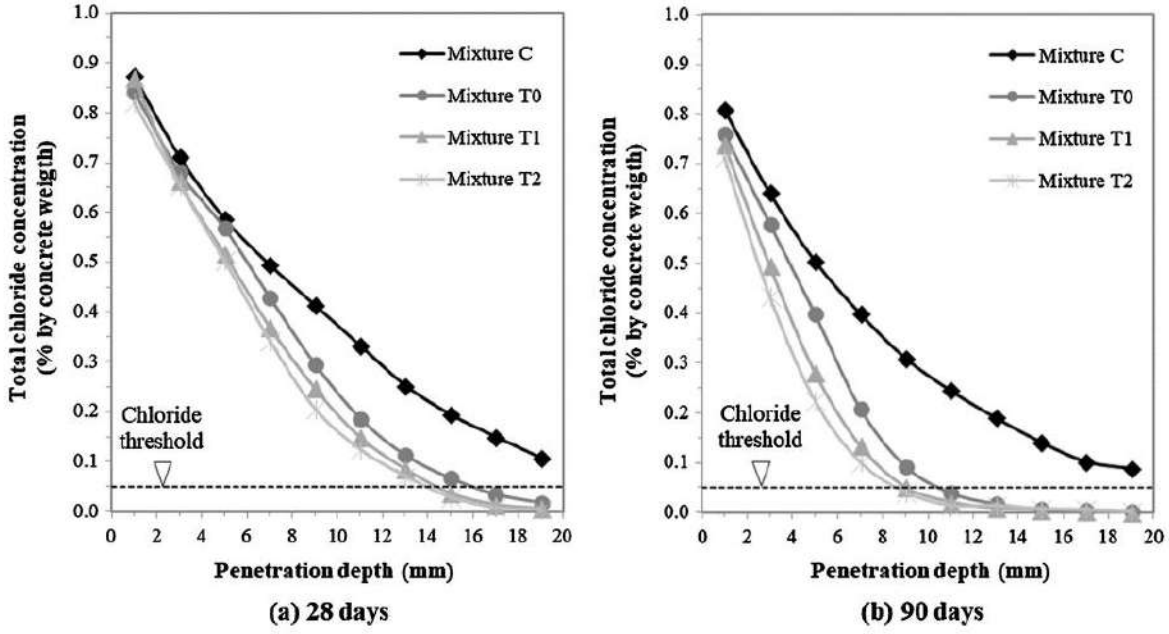

Fig. 2. Chloride concentration profiles in the concrete mixtures.

refinement of the cementitious matrix by the pozzolanic reaction of the FA and UtSCBA. The additional C-S-H from the pozzolanic reaction reduced the porosity and increased the tortuosity of the concrete [26], decreasing the ingress of Cl^- into the concrete.

3.2. Morphological and mineralogical characteristics

Details of the microstructure of the concrete mixtures at 2500 days are shown in selected micrographs in Fig. 4. Mixture C shows a cementitious matrix mainly composed of C-S-H (Fig. 4a). However, some pores (with an approximate average diameter of 10 μm) and fissures were observed. These pores contain AFt needles inside them, which contribute to enhancing the CS of the concrete. The EDS analysis indicates the presence of some cementitious compounds rich in CA, Si and C (spectrum 1). Furthermore, some anhydrous cement particles were identified (spectrum 2). The addition of FA in mixture T0 created a cementitious matrix with less voids compared to mixture C (Fig. 4b).

The combination of FA plus UtSCBA in mixtures T1 and T2 also created cementitious matrixes with less voids and with a more complex nature with respect to mixtures C and T0 (Fig. 4c and d). However, some unreacted FA and UtSCBA particles were observed. The presence of these particles has been reported in mortar and concrete mixtures at 600 and 120 days of age, respectively [19,16]. Moreover, partially reacted FA and UtSCBA particles covered with cementitious compounds from the pozzolanic reaction were also identified. In this research, the occurrence of pozzolanic reactions of the FA and UtSCBA particles at long-term ages is more evident than in previous studies. However, the presence of partially reacted FA and UtSCBA particles in mixture T2 suggests that the CH was depleted before the pozzolanic reactions ended. Spectrums 3 and 4 show the composition of selected cementitious compounds rich in Ca, C and Si (Fig. 4d). In accordance with the morphological analysis, the combination of 20% FA plus 10% UtSCBA can be suitable for preparing ternary concretes.

Fig. 5 shows the major crystalline phases identified in the concrete mixtures at 2500 days. Tobermorite (C-S-H), portlandite (CH) and ettringite (AFt) were identified as the main hydration products from CPC in mixture C (Fig. 5a). A minor phase of calcium-aluminum silicate hydrate (W) was also identified in the XRD patterns. This phase derives from the reaction between aluminates and silicates with the CH [27]. The convoluted phase of calcite (C) was detected with the C-S-H and could be attributed to the $CaCO_3$ in the CPC [20], while the phases of quartz (Q) and anorthite (A) are attributed to the sand. The addition of 20% FA in T0 increased the intensity of the C-S-H peaks with respect to mixture C (Fig. 2b); however, a small peak of CH was detected. The remaining CH in mixture T0 may be the result of the level of replacement used in this research, as a very large amount of FA (around 50%) is needed to deplete the cement hydration products [28]. The higher intensity of the C-S-H peaks in T0 is due to additional C-S-H compounds produced by the pozzolanic reaction of the FA and CH. The combination of FA plus UtSCBA in T1 slightly increased the intensity of the C-H-S peaks with respect to mixture C, while in mixture T2 the intensity of the C-S-H peaks is similar to mixture C (Fig. 5c and 5d). Furthermore, the CH phase was practically depleted in those mixtures. This indicates the occurrence of pozzolanic reactions between UtSCBA and CH to produce additional C-S-H compounds, which contribute to creating a more complex cementitious matrix, as shown in the SEM results. Because the intensity of the C-S-H peaks are comparable in mixtures C and T2, the addition of up to 20% UtSCBA apparently does not show a beneficial effect. Nevertheless, equilibrium between the C-S-H compounds from cement hydration and the C-S-H from pozzolanic reactions of the UtSCBA is suggested.

3.3. Percentage of voids and compressive strength

Results of the percentage of voids of the concrete mixtures at 2500 days are shown in Table 3. Mixture C had a percentage of voids of 14.69%. This value is slightly larger than that reported in

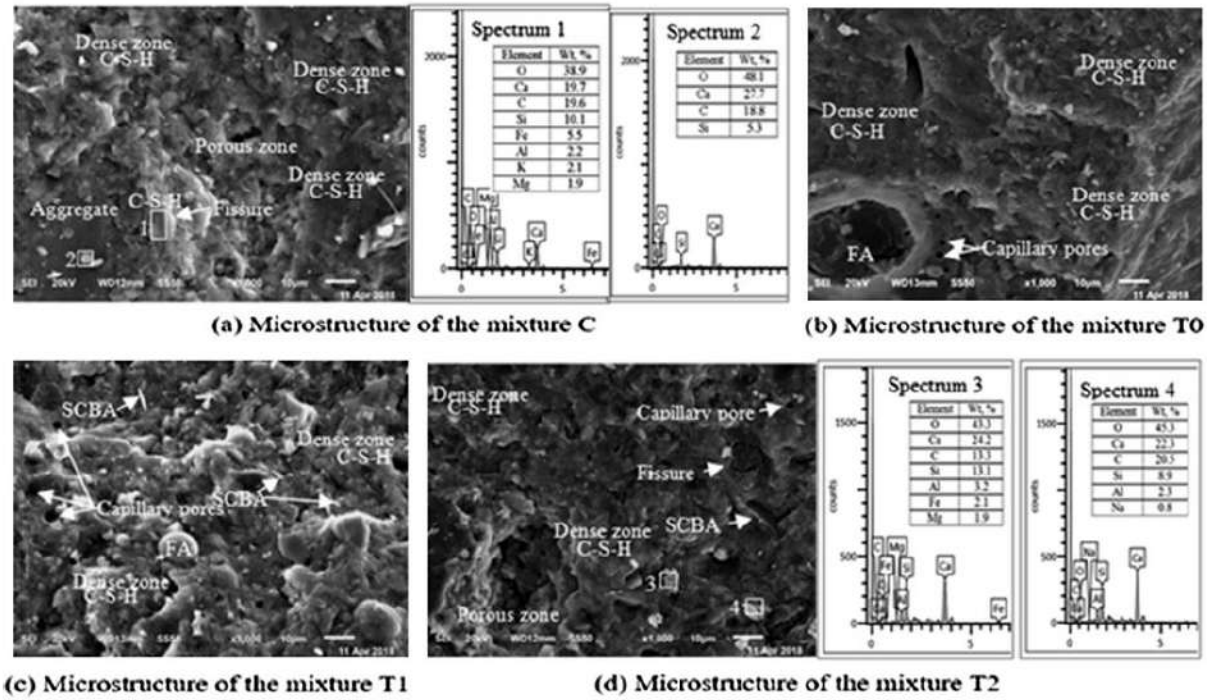

Fig. 4. Microstructure of the concrete mixtures at 2500 days.

than that containing only Portland cement, considering that only a certain percentage of this material reacts with the hydration products of cement. Thus, the unreacted material might work as filler [34,35]. In this sense, a more complex microstructure is not necessarily a better microstructure from the point of view of strength. For example, impurities embedded in the cementitious matrix would suggest a decrease in porosity; however, the long-term compressive strength of concrete containing additions could be similar in value to that of concrete with only Portland cement.

On the other hand, diffusivity and compressive strength of concretes are not directly related because the transport of chlorides depends mostly on the connectivity and binding capacity of the porous system [36]. Compressive strength, on the contrary, is influenced by the quality of the products formed during the hydration and pozzolanic reactions, as well as by the porosity of the concrete matrix. Hence, the pore discontinuities created as a result of the pozzolanic reaction have more impact on diffusivity than on compressive strength. In the present study, when practically untreated SCBA (UtSCBA) is added to the concrete mixture the resistance to the diffusion of chlorides through its porous matrix is improved, whereas the compressive strength at a long-term age is similar to concretes in which no UtSCBA was added.

3.4. Corrosion risk of the steel reinforcement

Fig. 6 shows the E_{corr} readings in the reinforced concretes taken at 2500 days. The horizontal dotted lines show the boundaries between regions of corrosion probability [37].

The temperature and relative humidity of the testing room and the t_{dp} of the rebar in the concrete mixtures (identified by the vertical dotted lines) are also presented in Fig. 6. In general, the reinforced concretes show an increment in the E_{corr} readings and fluctuations (*T0-A, B, C, D, E, F* and *G*) as time passes. From this, the fluctuations *B* to *G* could be associated with the polarization phenomenon induced by the low oxygen diffusion in the concrete as reported in the literature [38]. Because the prismatic specimens are not completely immersed in the NaCl solution, the polarization phenomenon can be caused by the increment of the relative humidity in the testing room. This increment saturates the upper section in the prismatic specimens due to the hygroscopic capacity of chlorides [39].

The temperature change in the testing room is another cause for the E_{corr} fluctuations because of the sensitivity of the electrochemical tests to environmental changes [40].

A detailed analysis of the E_{corr} readings shows that steel bars embedded in mixture C had a 10% risk of corrosion during the

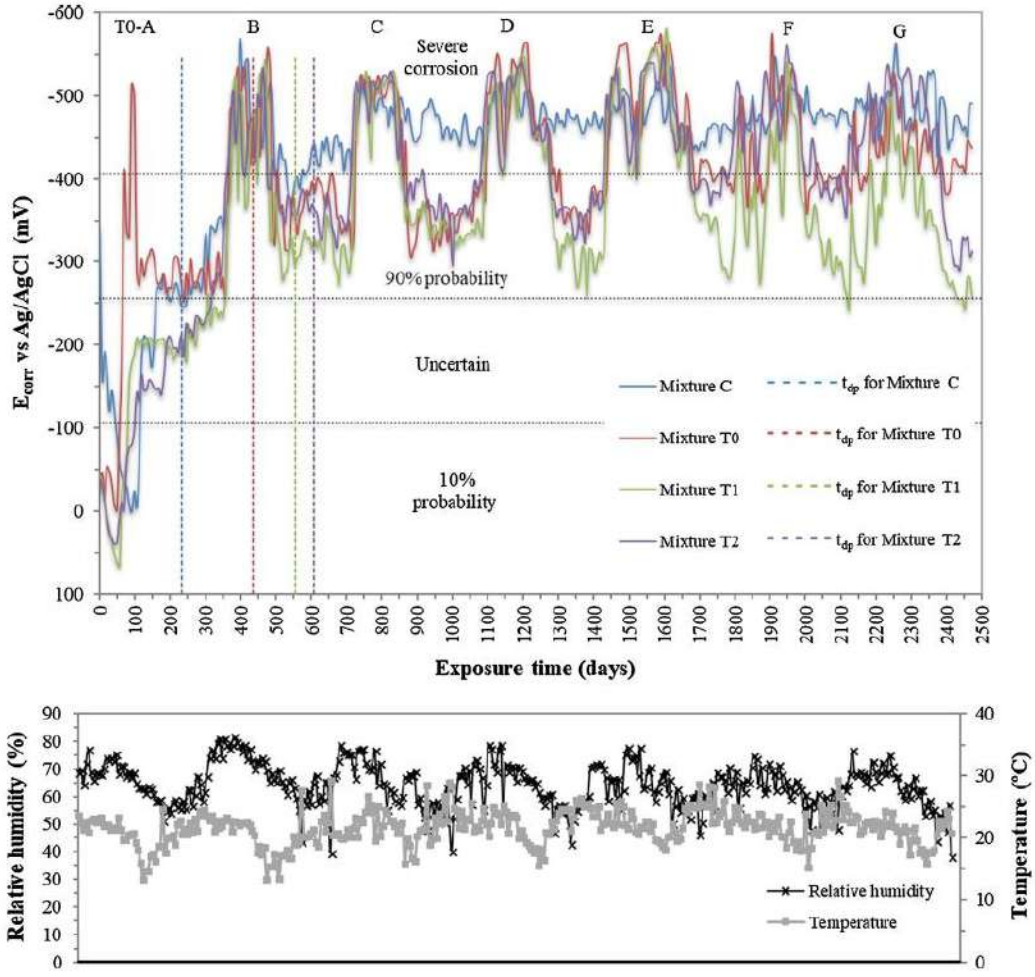

Fig. 6. Record of corrosion potentials of the concrete mixtures under investigation.

initial 120 days, then an uncertain risk of corrosion up to 270 days, followed by a sudden drop from −256 to −350 mV observed at 270 days. This drop is close in value to the t_{dp}, which was estimated to be 233 days. This behavior could indicate active corrosion of the rebar in mixture C, since −330 mV vs Ag/AgCl (−350 mV/SCE) is a criterion for steel depassivation [41,42]. Finally, the E_{corr} readings in mixture C increased rapidly to the severe corrosion condition, showing the mentioned fluctuations due to environmental changes in the testing room over the years.

The addition of 20% FA decreased the corrosion probability in mixture T0. Mixture T0 remained in the zone with a 10% corrosion probability from 0 to 50 days. After that, the corrosion probability quickly increased between days 60 and 90 (see the fluctuation *T0-A*). This fluctuation can be explained by the breakdown of the FÁs amorphous structure in the pozzolanic reaction [19], where Si^{4+} and Al^{+3} ions from the silica and alumina respectively are dissolved into the pore solution [43]. This increases the number of ions in the pore solution and therefore the corrosion probability of steel in this mixture rises. Following the fluctuation *T0-A* the E_{corr} readings were less negative, reaching values between −256 and −300 mV until day 360. Subsequently, the E_{corr} readings in mixture T0 were more negative than −330 mV over time. In this case, the fluctuations in the E_{corr} readings were more evident than in mixture C. This could be attributed to the lower percentage of voids in the concrete containing FA, which in turn produces less oxygen availability and accentuates the polarization phenomenon. The t_{dp} of the steel reinforcement in mixture T0 was estimated at 435 days, which is within the time period of fluctuation *B*. At the end of fluctuation *B* the E_{corr} values of the steel reinforcement in mixture T0 were more negative than −330 mV, which suggests that the depassivation of the rebar occurred during such a period.

The E_{corr} readings in mixture T1 had a similar behavior as those values in mixture T0 over time; however, the E_{corr} values in mixture T1 were less negative (in about 50 mV) than those values observed in mixture T0. In this case, the corrosion potentials remained in the 10% probability zone from 0 to 80 days. After that, the E_{corr} readings were in the uncertain corrosion zone from 81 to 400 days. This indicates a beneficial effect of combining FA plus UtSCBA in ternary concretes on lowering the corrosion probability at early ages. The t_{dp} in mixture T1 was estimated at 556 days, which is a longer period than in mixtures C and T0. In this case, a clear identification of the depassivation period in the mixture T1 was not possible. This happens because the E_{corr} values in this mixture did not have a noticeable drop below −330 mV. Finally, the E_{corr} values in mixture T1 remained between zones of 90% probability and severe corrosion after 400 days, with a slight tendency towards an uncertain corrosion zone.

Mixture T2 had E_{corr} values similar to mixture T1 from 0 to 1600 days. After that, the E_{corr} readings in mixture T2 were less negative (between 50 and 100 mV) than those E_{corr} values observed in mixture T1. In this case, the E_{corr} values remained low in the last 250 days. The t_{dp} for mixture T2 was 607 days. This indicates a positive effect of the combination of 20% FA plus 20% UtSCBA in increasing the depassivation period, similar to the effect observed in mixture T1.

The addition of UtSCBA clearly reduces the corrosion probability in mixtures T1 and T2 with respect to mixtures C and T0. The E_{corr} values are consistent with the other results where ternary mixtures showed the lowest chloride-ion diffusion at 28 and 90 days. The E_{corr} results corroborate the lower diffusion of species in mixtures T1 and T2 even at long-term ages.

3.5. Corrosion current densities and theoretical mass loss of the steel reinforcement

Fig. 7 shows the i_{corr} values in the reinforced concretes taken at 2500 days of testing. The horizontal dotted lines show the limits between corrosion rates proposed by Andrade and Alonso (2004) [44]. The i_{corr} values also show fluctuations due to the environmental changes in the testing room [40]. However, the fluctuations in the i_{corr} are less evident than those fluctuations observed in the E_{corr} readings. It is known that i_{corr} values may fluctuate in function

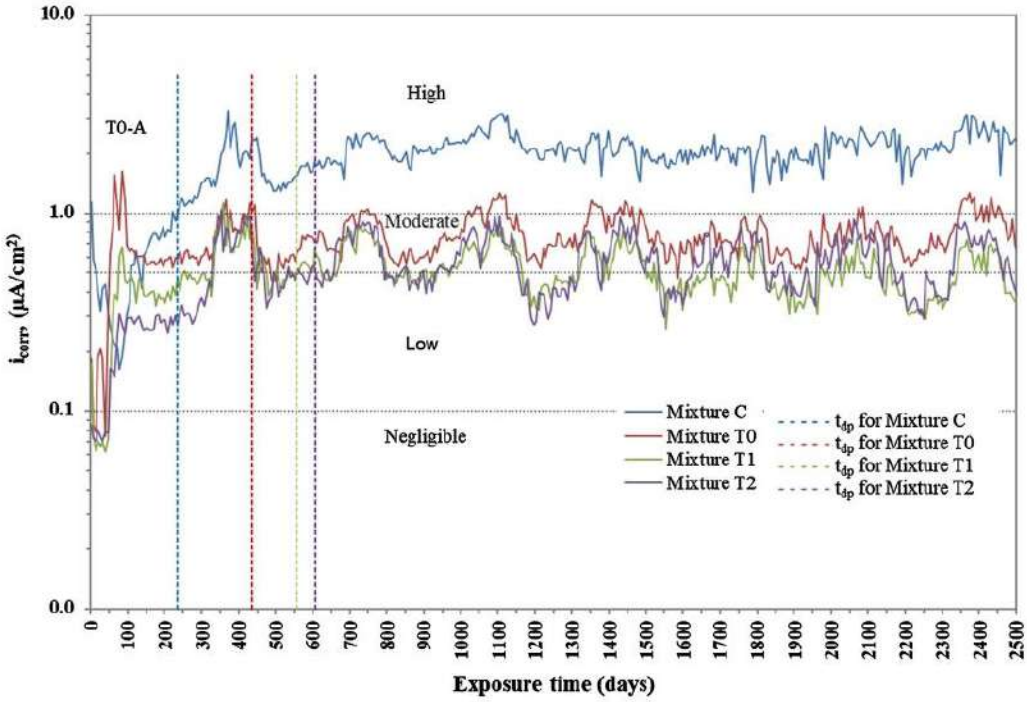

Fig. 7. Record of current densities of the concrete mixtures registered over the testing period.

Table 4
Theoretical mass loss of rebar embedded in concrete mixtures after 2500 days, %

Mixture	Specimen 1		Specimen 2		Specimen 3		Mean	S.D.	i_{corr}, μA/cm²	S.D.
	Rebar 1	Rebar 2	Rebar 1	Rebar 2	Rebar 1	Rebar 2				
C	1.08	1.79	0.98	0.84	1.30	2.09	1.35[A]	0.45	1.92	0.64
T0	0.52	0.51	0.59	0.48	0.49	0.57	0.53[B]	0.53	0.75	0.06
T1	0.39	0.32	0.35	0.38	0.37	0.36	0.36[C]	0.36	0.51	0.03
T2	0.36	0.45	0.38	0.40	0.33	0.36	0.38[C]	0.38	0.54	0.05

Note: Means that do not share letters are significantly different ($P < 0.05$).
S.D: standard deviation.

of the intrinsic corrosion process [44]. Results of mixture C show that its i_{corr} values remain in the low and moderate corrosion-rate condition from 0 to 220 days. After that, the i_{corr} values reach a high corrosion-rate condition over time. This event is close to t_{dp} of mixture C (233 days), which suggests that the rebars embedded in mixture C have been depassivated.

The results in the i_{corr} values show a beneficial effect on lowering the corrosion rate of concrete by the addition of FA (mixture T0). This coincides with that reported in the E_{corr} measurements. In this case, the mixture T0 had i_{corr} values in the negligible and low corrosion rate zones from 0 to 50 days. After that, the i_{corr} values continue in the moderate corrosion zone. Similar to that observed in the E_{corr} measurements, the fluctuation *T0-A* in the i_{corr} values was also observed in mixture T0. This suggests a corrosive activity in the rebar embedded in mixture T0. During that time, the pozzolanic reaction of the FA in the mixture T0 occurs [19]. It is well-known that the pozzolanic reaction reduces the pH value of concrete [45]; this reduction can release chlorides originally bound as Friedel's salts [46]. Accordingly, the dissolved chlorides in the cementitious matrix may cause a corrosive activity in the rebar embedded in mixture T0; however, the additional C-S-H compounds and alumina from FA bind physically and chemically Cl^-, reducing the corrosive activity in the rebar. The t_{dp} of mixture T0 was 435 days; at that time, the i_{corr} values suggest a moderate corrosion rate with a tendency towards a high corrosion rate. Although mixture T0 does not show a well-defined high corrosion rate, it is evident that this mixture has important corrosive activity after day 435.

Mixture T1 had a lower corrosion rate when compared to mixtures C and T0. This shows a positive effect on lowering the corrosive activity in reinforced UtSCBA-ternary concretes caused by the use of the combination of FA plus UtSCBA, as also observed in the results of E_{corr}.

Results show that the i_{corr} values of mixture T1 remain in the negligible corrosion-rate zone from 0 to 50 days. The i_{corr} values then increase rapidly, reaching the low corrosion zone and remain there for about 200 days. Finally, the i_{corr} values remain between the moderate and the low corrosion-rate zones until 2500 days, with a slight tendency towards the low corrosion zone.

Mixture T2 showed practically the same behavior as mixture T1. A small difference in the i_{corr} values between mixtures T1 and T2 was observed from 0 to 300 days. However, from day 301 until day 2500 the differences in the i_{corr} values are practically insignificant.

The t_{dps} of mixtures T1 and T2 were 556 and 607 days respectively; at these times i_{corr} values show that both mixtures are between a low corrosion-rate zone and moderate corrosion-rate zone. Despite the concrete mixtures not all showing the same corrosion condition when their estimated t_{dp} is reached, it is evident that all the mixtures present corrosive activity. The above suggests that depassivation must be considered as a period during which the process from initial pit formation until stable corrosion takes place, rather than an instantaneous event [47].

The i_{corr} results are consistent with other durability tests in which the addition of UtSCBA was shown to reduce the chloride-ion diffusion and the probability of corrosion of mixtures T1 and T2 with respect to mixtures C and T0. The best performance against chloride-induced corrosion was shown by mixtures T1 and T2 and can be supported with the results of SEM, XRD and percentage of voids.

The SEM images show that the addition of UtSCBA in concretes with FA produces a more complex cementitious matrix due to both the filler effect of the unreacted particles from the ashes and the additional C-S-H from the pozzolanic reaction. Moreover, it is known that the additional C-S-H can precipitate further away from the SCM particles, blocking the small spaces between the pores [43]. This additional C-S-H was identified in the XDR results.

A more complex cementitious matrix with less voids reduces chloride ingress into mixtures T1 and T2 with respect to C and T0, as shown in the chloride-ion diffusion results.

Other mechanisms can contribute to the better performance shown in mixtures T1 and T2. A first mechanism can be the physical and chemical chloride binding by the C-S-H from cement hydration and pozzolanic reaction, and from the alumina from the ashes, respectively [24]. A second mechanism can be that some carbon particles in the UtSCBA work as an absorbent media for chlorides [48], and the lower chloride ingress into UtSCBA-ternary concretes hinders the corrosion activity.

Table 4 shows the theoretical mass loss (T_{ms}) and i_{corr} average measurements at 2500 days for each embedded rebar in the concrete mixtures. The estimated values were compared against the obtained value for mixture C. The T_{ms} values in the reinforced ternary concretes are comparable to those values obtained by other researchers [49]. The reinforcing bars in mixture C had the highest T_{ms}, whereas those embedded in mixture T0 were 2.5 times lower, in mixture T1 were 3.75 times lower and in mixture T2 were 3.5 times lower, all with respect to mixture C. This demonstrates the positive effect of the combination of FA plus UtSCBA on lowering the corrosion of the steel reinforcement.

4. Conclusions

1. The use of 10% and 20% UtSCBA does not negatively affect the compressive strength of the ternary concretes at long-term ages.
2. The addition of 10% and 20% UtSCBA decreases the chloride-ion diffusion of the ternary concretes, which could be attributed to changes of the cementitious matrices caused by the pozzolanic reaction of UtSCBA.
3. The combination of 20% FA + 10% UtSCBA decreases the corrosion of ternary concretes at long-term ages when compared to the control mixture. This could be attributed to the decrease of chloride-ion diffusion. Furthermore, the combination of 20% FA + 20% UtSCBA produces concretes with a similar corrosion

resistance to those containing 20% FA + 10% UtSCBA. Therefore, the combination of FA + UtSCBA appears to be a suitable option against chloride-induced steel corrosion.

Conflict of interest

The authors declare no conflict of interest.

Acknowledgments

The authors are grateful to the Instituto Politécnico Nacional of Mexico (IPN) for the facilities and financial support provided for this research. Furthermore, the authors thank the Facultad de Ingeniería Civil of the Universidad Autónoma de Nuevo León in Mexico for the use of its facilities during the microstructural and mechanical characterization of the concretes. The authors are also grateful to Mexicós Consejo Nacional de Ciencia y Tecnología (CONACyT) for the doctoral scholarships granted to Víctor Alberto Franco-Luján and Marco Antonio Maldonado-García.

References

[1] E. Rakanta, T. Zafeiropoulou, G. Batis, Corrosion protection of steel with DMEA-based organic inhibitor, Constr. Build. Mater. 44 (2013) 507–513, https://doi.org/10.1016/j.conbuildmat.2013.03.030.
[2] M.M. Hossain, M.R. Karim, M. Hasan, M.K. Hossain, M.F.M. Zain, Durability of mortar and concrete made up of pozzolans as a partial replacement of cement: a review, Constr. Build. Mater. 116 (2016) 128–140, https://doi.org/10.1016/j.conbuildmat.2016.04.147.
[3] M. Ahmaruzzaman, A review on the utilization of fly ash, Prog. Energy Combust. Sci. 36 (2010) 327–363, https://doi.org/10.1016/j.pecs.2009.11.003.
[4] A.P. Gursel, H. Maryman, C. Ostertag, A life-cycle approach to environmental, mechanical, and durability properties of "green" concrete mixes with rice husk ash, J. Clean. Prod. 112 (2016) 112, https://doi.org/10.1016/j.jclepro.2015.06.029.
[5] J. Payá, J. Monzó, M.V. Borrachero, L. Díaz-Pinzón, L.M. Ordónez, Sugar-cane bagasse ash (SCBA): studies on its properties for reusing in concrete production, J. Chem. Technol. Biotechnol. 77 (2002) 321–325, https://doi.org/10.1002/jctb.549.
[6] K. Ganesan, K. Rajagopal, K. Thangavel, Evaluation of bagasse ash as supplementary cementitious material, Cem. Concr. Compos. 29 (2007) 515–524, https://doi.org/10.1016/j.cemconcomp.2007.03.001.
[7] A. Bahurudeen, M. Santhanam, Influence of different processing methods on the pozzolanic performance of sugarcane bagasse ash, Cem. Concr. Compos. 56 (2014) 32–45, https://doi.org/10.1016/j.cemconcomp.2014.11.002.
[8] C. Chandara, E. Sakai, K.A.M. Azizli, Z.A. Ahmad, S.F.S. Hashim, The effect of unburned carbon in palm oil fuel ash on fluidity of cement pastes containing superplasticizer, Constr. Build. Mater. 24 (2010) 1590–1593, https://doi.org/10.1016/j.conbuildmat.2010.02.036.
[9] N. Chusilp, C. Jaturapitakkul, K. Kiattikomol, Effects of LOI of ground bagasse ash on the compressive strength and sulfate resistance of mortars, Constr. Build. Mater. 23 (2009) 3523–3531, https://doi.org/10.1016/j.conbuildmat.2009.06.046.
[10] G.C. Cordeiro, R.D. Toledo Filho, L.M. Tavares, E. de M.R. Fairbairn,, Ultrafine grinding of sugar cane bagasse ash for application as pozzolanic admixture in concrete, Cem. Concr. Res. 39 (2009) 110–115, https://doi.org/10.1016/j.cemconres.2008.11.005.
[11] G.C. Cordeiro, L.M. Tavares, R.D.T. Filho, Improved pozzolanic activity of sugar cane bagasse ash by selective grinding and classification, Cem. Concr. Res. 89 (2016) 269–275, https://doi.org/10.1016/j.cemconres.2016.08.020.
[12] N. Amin, Use of Bagasse Ash in Concrete and Its Impact on the Strength and Chloride Resistivity, J. Mater. Civ. Eng. 23 (2011) 717–720, https://doi.org/10.1061/(ASCE)MT.1943-5533.0000227.
[13] R. Somna, C. Jaturapitakkul, P. Rattanachu, W. Chalee, Effect of ground bagasse ash on mechanical and durability properties of recycled aggregate concrete, Mater. Des. 36 (2012) 597–603, https://doi.org/10.1016/j.matdes.2011.11.065.
[14] G.C. Cordeiro, R.D. Toledo Filho, L.M. Tavares, E.M.R. Fairbairn, Experimental characterization of binary and ternary blended-cement concretes containing ultrafine residual rice husk and sugar cane bagasse ashes, Constr. Build. Mater. 29 (2012) 641–646, https://doi.org/10.1016/j.conbuildmat.2011.08.095
[15] S. Rukzon, P. Chindaprasirt, Utilization of bagasse ash in high-strength concrete, Mater. Des. 34 (2012) 45–50, https://doi.org/10.1016/j.matdes.2011.07.045.
[16] M.A. Maldonado-García, U.I. Hernández-Toledo, P. Montes-García, P.L. Valdez-Tamez, The influence of untreated sugarcane bagasse ash on the microstructural and mechanical properties of mortars, Mater. Constr. 68 (2018) 1–13, https://doi.org/10.3989/mc.2018.13716.
[17] J.C. Arenas-Piedrahita, P. Montes-García, J.M. Mendoza-Rangel, H.Z. López Calvo, P.L. Valdez-Tamez, J. Martínez-Reyes, Mechanical and durability properties of mortars prepared with untreated sugarcane bagasse ash and untreated fly ash, Constr. Build. Mater. 105 (2016) 69–81, https://doi.org/10.1016/j.conbuildmat.2015.12.047.
[18] V.G. Jiménez-Quero, F.M. León-Martínez, P. Montes-García, C. Gaona-Tiburcio, J.G. Chacón-Nava, Influence of sugar-cane bagasse ash and fly ash on the rheological behavior of cement pastes and mortars, Constr. Build. Mater. 40 (2013) 691–701, https://doi.org/10.1016/j.conbuildmat.2012.11.023.
[19] V. Ríos-Parada, V.G. Jiménez-Quero, P.L. Valdez-Tamez, P. Montes-García, Characterization and use of an untreated Mexican sugarcane bagasse ash as supplementary material for the preparation of ternary concretes, Constr. Build. Mater. 157 (2017) 83–95, https://doi.org/10.1016/j.conbuildmat.2017.09.060.
[20] H.F.W. Taylor, Cement chemistry, Thomas Telford Publishing, 1997.
[21] M. Nokken, A. Boddy, R.D. Hooton, M.D.A. Thomas, Time dependent diffusion in concrete—three laboratory studies, Cem. Concr. Res. 36 (2006) 200–207, https://doi.org/10.1016/j.cemconres.2004.03.030.
[22] C. Lu, W. Jin, R. Liu, Reinforcement corrosion-induced cover cracking and its time prediction for reinforced concrete structures, Corros. Sci. 53 (2011) 1337–1347, https://doi.org/10.1016/j.corsci.2010.12.026.
[23] F. Deschner, F. Winnefeld, B. Lothenbach, S. Seufert, P. Schwesig, S. Dittrich, F. Goetz-Neunhoeffer, J. Neubauer, Hydration of Portland cement with high replacement by siliceous fly ash, Cem. Concr. Res. 42 (2012) 1389–1400, https://doi.org/10.1016/j.cemconres.2012.06.009.
[24] M.D.A. Thomas, R.D. Hooton, A. Scott, H. Zibara, The effect of supplementary cementitious materials on chloride binding in hardened cement paste, Cem. Concr. Res. 42 (2012) 1–7, https://doi.org/10.1016/j.cemconres.2011.01.001.
[25] O.M. Jensen, P.F. Hansen, A.M. Coats, F.P. Glasser, Chloride ingress in cement paste and mortar, Cem. Concr. Res. 29 (1999) 1497–1504, https://doi.org/10.1016/S0008-8846(99)00131-3.
[26] Y.S. Choi, J.G. Kim, K.M. Lee, Corrosion behavior of steel bar embedded in fly ash concrete, Corros. Sci. 48 (2006) 1733–1745, https://doi.org/10.1016/j.corsci.2005.05.019.
[27] A. Arizzi, G. Cultrone, Aerial lime-based mortars blended with a pozzolanic additive and different admixtures: a mineralogical, textural and physical-mechanical study, Constr. Build. Mater. 31 (2012) 135–143, https://doi.org/10.1016/j.conbuildmat.2011.12.069.
[28] K. Sisomphon, L. Franke, Evaluation of calcium hydroxide contents in pozzolanic cement pastes by a chemical extraction method, Constr. Build. Mater. 25 (2011) 190–194. https://doi.org/10.1016/j.conbuildmat.2010.06.039.
[29] S.H. Kosmatka, B. Kerkhoff, W.C. Panarese, J. Tanesi, Design and Control of Concrete Mixtures, Portland Cement Association (PCA). EE. UU. (2004).
[30] A.M. Neville, Properties of concrete. Prentice Hall, London, 1995.
[31] G.C. Cordeiro, O.A. Paiva, R.D. Toledo Filho, E.M.R. Fairbairn, L.M. Tavares, Long-Term Compressive Behavior of Concretes with Sugarcane Bagasse Ash as a Supplementary Cementitious Material, J. Test. Eval. 46 (2018), https://doi.org/10.1520/JTE20160316.
[32] C. Lian, Y. Zhuge, S. Beecham, The relationship between porosity and strength for porous concrete, Constr. Build. Mater. 25 (2011) 4294–4298, https://doi.org/10.1016/j.conbuildmat.2011.05.005.
[33] X. Chen, S. Wu, J. Zhou, Influence of porosity on compressive and tensile strength of cement mortar, Constr. Build. Mater. 40 (2013) 869–874, https://doi.org/10.1016/j.conbuildmat.2012.11.072.
[34] G.C. Cordeiro, K.E. Kurtis, Effect of mechanical processing on sugar cane bagasse ash pozzolanicity, Cem. Concr. Res. 97 (2017) 41–49.
[35] E. Arift, M.W. Clark, N. Lake, Sugarcane bagasse ash from a high-efficiency co-generation boiler as filler in concrete, Constr. Build. Mater. 151 (2017) 692–703.
[36] S. Caré, Effect of temperature on porosity and on chloride diffusion in cement pastes, Constr. Build. Mater. 22 (2008) 1560–1573.
[37] J.P. Broomfield, Corrosion of steel in concrete, understanding, investigation and repair, E&FN Spon, London, U.K., 1997.
[38] M.F. Montemor, A.M.P. Simoes, M.M. Salta, Effect of fly ash on concrete reinforcement corrosion studied by EIS, Cem. Concr. Compos. 22 (2000) 175–185, https://doi.org/10.1016/S0958-9465(00)00003-2.
[39] W. López, J.A. González, Influence of the degree of pore saturation on the resistivity of concrete and the corrosion rate of steel reinforcement, Cem. Concr. Res. 23 (1993) 368–376, https://doi.org/10.1016/0008-8846(93)90102-F.
[40] S.K. Verma, S.S. Bhadauria, S. Akhtar, Monitoring Corrosion of Steel Bars in Reinforced Concrete Structures 2014 (2014), https://doi.org/10.1155/2014/957904.
[41] P. Ghods, O.B. Isgor, G.A. McRae, G.P. Gu, Electrochemical investigation of chloride-induced depassivation of black steel rebar under simulated service conditions, Corros. Sci. 52 (2010) 1649–1659, https://doi.org/10.1016/j.corsci.2010.02.016.
[42] J.O. Rivera-Corral, G. Fajardo, G. Arliguie, R. Orozco-Cruz, F. Deby, P. Valdez, Corrosion behavior of steel reinforcement bars embedded in concrete exposed to chlorides: effect of surface finish, Constr. Build. Mater. 147 (2017) 815–826, https://doi.org/10.1016/j.conbuildmat.2017.04.186.
[43] A.L.A. Fraay, J.M. Bijen, Y.M. de Haan, The reaction of fly ash in concrete: a critical examination, Cem. Concr. Res. 19 (1989) 235–246, https://doi.org/10.1016/0008-8846(89)90088-4.
[44] C. Andrade, C. Alonso, Test methods for on-site corrosion rate measurement of steel reinforcement in concrete by means of the polarization resistance method, Mater. Struct. 37 (2004), https://doi.org/10.1007/BF02483292.

[45] S. Diamond, Effects of two Danish fly ashes on alkali contents of pore solutions of cement-fly ash pastes, Cem. Concr. Res. 11 (1981) 383–394, https://doi.org/10.1016/0008-8846(81)90110-1.
[46] L. Bertolini, B. Elsener, P. Pedeferri, R. Polder, Corrosion of Steel in Concrete: prevention, diagnostic, repair. WILEY VCH (2004).
[47] U.M. Angst, B. Elsener, C.K. Larsen, Ø. Vennesland, Chloride-induced reinforcement corrosion: electrochemical monitoring of initiation stage and chloride threshold values, Corros. Sci. 53 (2011) 1451–1464, https://doi.org/10.1016/j.corsci.2011.01.025.
[48] V. Minkova, M. Razvigorova, E. Bjornbom, R. Zanzi, T. Budinova, N. Petrov, Effect of water vapour and biomass nature on the yield and quality of the pyrolysis products from biomass, Fuel Process. Technol. 70 (2001) 53–61, https://doi.org/10.1016/S0378-3820(00)00153-3.
[49] A. Alhozaimy, R.R. Hussain, R. Al-Zaid, A. Al-Negheimish, Coupled effect of ambient high relative humidity and varying temperature marine environment on corrosion of reinforced concrete, Constr. Build. Mater. 28 (2012) 670–679, https://doi.org/10.1016/j.conbuildmat.2011.10.008.

CHAPTER FIVE

Chloride-binding capacity of ternary concretes containing FA and UtSCBA

Víctor Alberto Franco-Luján, José Manuel Mendoza-Rangel, Victor Guillermo Jiménez-Quero, Pedro Montes-García.

2019.

Manuscript sent to Cement and Concrete Composites (JCR, Q1. IF=5.172)

Cement and Concrete Composites

Chloride-binding capacity of ternary concretes containing fly ash and untreated sugarcane bagasse ash

--Manuscript Draft--

Manuscript Number:	CCC-D-19-00023
Article Type:	Research Paper
Keywords:	Chloride conten; electrical resistivity; long-term durability; Supplementary cementing materials; untreated sugarcane bagasse ash
Corresponding Author:	Pedro Montes-Garcia, Ph.D. Instituto Politécnico Nacional Oaxaca, MEXICO
First Author:	Víctor A. Franco-Luján, M.Sc.
Order of Authors:	Víctor A. Franco-Luján, M.Sc.
	José M. Mendoza-Rangel
	Víctor G. Jiménez-Quero
	Pedro Montes-Garcia, Ph.D.
Abstract:	In order to understand the role of untreated sugarcane bagasse ash (UtSCBA) on the chloride binding of ternary concretes prepared with fly ash, an experimental program was carried out. Concrete specimens containing only cement, cement+fly ash and cement+fly ash+UtSCBA were manufactured. Specimens were exposed to a chloride solution for 3000 days. After exposure, a microstructural characterization using scanning electron microscopy and X-Ray diffraction was conducted. The percentage of voids, compressive strength, and electrical resistivity of the concretes were also obtained, while the chloride binding was obtained from the difference between total and free chlorides. Diffractograms showed that chlorides chemically reacted with the Afm and Aft phases of all concretes to form Friedel's salt, whereas compressive strength results corroborate that chlorides did not affect the strength of any tested concretes. In sum, ternary concretes containing UtSCBA showed the best performance against chloride ingress, the highest electrical resistivity, and the highest chloride-binding capacity.

Chloride-binding capacity of ternary concretes containing fly ash and untreated sugarcane bagasse ash

Víctor Alberto Franco-Luján [1], José Manuel Mendoza-Rangel [2], Víctor Guillermo Jiménez-Quero [3], Pedro Montes-García [3, *]

[1] PhD Student. Instituto Politécnico Nacional, CIIDIR-Oaxaca, Hornos 1003, Col. Noche Buena, Sta. Cruz Xoxocotlán C.P. 71230, México, francolujan_89@hotmail.com
[2] Universidad Autónoma de Nuevo León (UANL), FIC, Cd Universitaria S/N, San Nicolás de los Garza, Nuevo León C.P. 66451, México, jose.mendozarn@uanl.edu.mx
[3] Instituto Politécnico Nacional, CIIDIR-Oaxaca, Grupo de Materiales y Construcción, México, vgjimenez@hotmail.com, pmontesgarcia@gmail.com, pmontes@ipn.mx

* Corresponding author: pmontesgarcia@gmail.com, pmontes@ipn.mx (P. Montes-García)

Abstract

In order to understand the role of untreated sugarcane bagasse ash (UtSCBA) in chloride binding of ternary concretes prepared with fly ash, an experimental program was carried out. Concrete specimens containing only cement Portland (PC), PC+fly ash, and PC+fly ash+UtSCBA were manufactured. After curing these specimens were exposed to a chloride solution for 3000 days. After exposure, a microstructural characterization using scanning electron microscopy and X-Ray diffraction was conducted. The compressive strength, electrical resistivity of the concretes and percentage of voids, were also obtained, while information on chloride binding was obtained from the difference between the amount of total and free chlorides. Diffractograms showed that chlorides chemically reacted with the Afm and Aft phases of all concretes to form Friedel's salt, whereas compressive strength results corroborate that chlorides did not affect the strength of any of the tested concretes. In summary, ternary concretes containing UtSCBA showed the best performance against chloride ingress, the highest electrical resistivity, and the highest chloride-binding capacity.

Keywords: Chloride content; electrical resistivity; long-term durability; supplementary cementing materials; untreated sugarcane bagasse ash

1. Introduction

The durability of concrete structures regarding Cl^--induced corrosion of reinforcing steel is a vital issue which has been researched over many years. Corrosion prevention methods such as epoxy coatings or inhibitors have been proposed to avoid corrosion, however, the implementation of these methods has so far been unsuccessful [1-3]. The manufacturing of good-quality concrete by the addition of supplementary cementing materials (SCMs) appears to be a more comprehensive approach to prevent corrosion. Recently, industrial and agricultural wastes have been used as SCMs to develop sustainable, strong, and concrete with higher resistance against transport of external corrosive agents [4, 5].

The most commonly used SCM is fly ash (FA). Most FA particles are spherical, ranging in size between 10 and 100 μm and composed of silica and alumina in its amorphous state [6]. These features contribute to producing more workable, stronger and more durable mortars and concretes than those produced with only Portland cement (PC) [7, 8]. However, the availability of FA in countries like Brazil, Pakistan, India and Mexico is limited. Therefore, the use of agricultural wastes as SCM is considered a viable alternative.

In recent years, sugarcane bagasse ash (SCBA) has been characterized and used as a pozzolanic material [9, 10]. When the SCBA is post-treated, it produces mortars and concretes with superior mechanical properties than those made with only PC. Moreover, its use does not cause a reduction in the compressive strength (CS) to long-term [11, 12]. In this

context, it has also been reported that 10% to 30%PC replacement by SCBA subjected to various post-treatments (PtSCBA) significantly reduces both the permeability and the transport of chloride ions in PC-based materials [13-15]. Despite the higher mechanical and durability performance of mortars and concretes with PtSCBA, most post-treatments require a significant amount of energy, increasing the final cost and reducing the sustainability of these materials. In order to address this problem, a long-term research project on the effect of ‘‘practically as received” SCBA (UtSCBA) on the workability and the microstructural, mechanical and durability properties of mortars and concretes is being conducted. Some findings from that project indicate that the use of UtSCBA causes a significant reduction in the workability of mortars [16], however, it improves their microstructure, long-term CS, electrical resistivity (ER), and resistance to chloride ingress [17, 18]. Regarding the durability properties, Maldonado-Garcia et al. [19] investigated the long-term corrosion of steel reinforcement in mortar slabs containing UtSCBA. The authors found that the use of UtSCBA significantly decreased the chloride-ion diffusion coefficients (D_C), and less negative corrosion potentials (E_{corr}) of steel reinforcement embedded in these concretes were obtained when compared with the control mortar.

The reduction of workability in mortars caused by the addition of 10% and 20%UtSCBA can be overcome by the addition of 20%FA [16]. This combination seems adequate, as no negative effects on the microstructural and mechanical properties of UtSCBA-ternary concretes after 90 days of age have been reported [20]. Recently, it was found that the use of UtSCBA significantly decreased the D_Cs of UtSCBA-ternary concretes at 28 and 90 days of age. Furthermore, steel bars embedded in these concretes exposed to a 3.5%NaCl solution over 2,500 days experienced both less negative E_{corr} values and lower corrosion rates (I_{corr})

than those embedded in concretes with only PC and PC+FA [21]. In order to elucidate the apparently enhanced corrosion protection mechanism provided by UtSCBA, especially when added to a concrete containing FA, additional research should be carried out.

Several studies reported that a partial replacement of PC by 16% to 50%FA significantly increases the chloride-binding capacity (Pb) of pastes and concretes exposed to NaCl [22, 23]. This increase is attributed to the chemical interaction of chlorides (Cl^-) with the alumina from the FA in order to form Friedel´s salt. P_b by physical binding is another mechanism shown by FA [24, 25], where the Cl^- ions are caught on the surface of C-S-Hs produced during the pozzolanic reaction [26]. Surprisingly, no research about the influence of UtSCBA on the P_b of pastes, mortars or concretes has been reported in the literature. Therefore, studies on the P_b of UtSCBA to clarify the contribution of this ash on the improved durability properties of ternary concretes is highly needed.

This paper aims to investigate the P_b of concretes containing FA plus UtSCBA continually exposed to a simulated marine environment for 3000 days, i.e. for more than 8 years. For this purpose, a microstructural characterization by scanning electron microscopy (SEM) and X-ray diffraction (XRD) was carried out. Furthermore, the percentage of voids, CS, and ER were obtained. Finally, the total and free chloride contents were estimated in order to determinate the D_C and P_b of the ternary concretes.

2. Materials and Methods

2.1. Materials and mix design of the concrete mixtures

Portland cement (CPC-30R), UtSCBA, and Admix Tech® FA were used as cementitious materials for the concrete mixtures. The CPC fulfills the requirements established by the

Mexican standard NMX-C-414-ONNCCE-2004 standard [27]. The UtSCBA was sieved through a 75-µm ASTM mesh for four minutes. The FA is classified as class F in accordance with the ASTM C 618 standard. The chemical compositions of the materials are shown in Table 1. The sums of the major oxides (SiO_2, Al_2O_3 and Fe_2O_3) for the UtSCBA and FA were 88.28% and 89.55%, respectively. The LOI contents of the CPC and UtSCBA were higher than the limits established in the ASTM C 618-19 standard [28], which can be attributed to the presence of calcium carbonate ($CaCO_3$) and carbonaceous matter in the CPC and UtSCBA, respectively [29, 30]. In previous studies, neither the CPC nor the UtSCBA induced adverse effects on the fresh- and hardened-state properties of mortars and concretes prepared with these materials [16, 18, 20, 21].

Table 1. Chemical compositions of used cementitious materials (% by mass)

Material	Al_2O_3	CaO	Fe_2O_3	K_2O	MgO	MnO	Na_2O	P_2O_5	SiO_2	TiO_2	SO_3	LOI
CPC	4.87	60.03	3.57	0.85	1.50	0.08	0.52	0.19	20.67	0.58	4.95	8.40
UtSCBA	15.00	2.57	7.16	3.52	1.19	0.22	0.54	1.14	66.12	1.13	0.26	9.00
FA	20.01	4.00	5.42	0.96	0.63	0.10	0.19	0.38	64.12	1.12	0.86	2.60

LOI = Loss on ignition at 950ºC for the CPC and at 750ºC for the FA and UtSCBA.

River sand and calcareous crushed coarse aggregate were used to prepare the concrete mixtures. The volumetric weights, specific gravities, and adsorptions of the fine and coarse aggregates were 1596 kg/m^3, 2.78, and 1.74%, and 1624 kg/m^3, 2.66, and 0.47%, respectively. The fineness modulus of the sand was 2.97, and the maximum size of the coarse aggregate was 19 mm. Finally, bi-distilled water and a polycarboxylate-based superplasticizer (SP) Plastol 4000 ™, which fulfill the requirements of the ASTM C 194 standard, were used to prepare the concrete mixtures.

Four concrete mixtures containing either 100%CPC (C), 80%CPC+20%FA (T0), 70%CPC+20%FA+10%UtSCBA (T1) or 60%CPC+20%FA+20%UtSCBA (T2) were prepared. For all mixtures the total content of cementitious material, i.e. the sum of CPC, UtSCBA and FA, always amount to 410 kg/m^3 concrete. The concrete mixtures were designed in accordance with the absolute volume method from the ACI 211.1 [31]. All mixtures had a 0.5 water/cementitious material ratio (w/cm) and were designed to achieve a target slump of 75±20 mm (ASTM C 143). Mixture C was designed to achieve a CS target of 25±8 MPa at 28 days. Table 2 shows the proportions of the concrete mixtures and the CS values achieved.

Table 2. Proportions of the concrete mixtures (kg/m^3)

Mixture	CPC	FA	UtSCBA	Fine aggregate	Coarse aggregate	Water	SP	Slump	CS at 28 days
C	410	--	--	727	1015	205	2.7	78	31 ± 2.2
T0	328	82	--	727	1015	205	1.6	79	32 + 2.1
T1	287	82	41	727	1015	205	3.1	88	28 ± 2.3
T2	256	82	82	727	1015	205	4.9	90	23 ± 1.9

SP = Polycarboxylate-based superplasticizer (ml per kg of cementitious materials), slump is in mm, and CS in MPa.

A total of three prismatic specimens (100 x 150 x 300 mm^3) for each concrete mixture were cast. All specimens were demolded after 24 hours and thereupon cured in a Ca $(OH)_2$-saturated solution for 28 days. After that, the prisms were completely immersed in a 3.5% NaCl solution for 3000 days.

2.2 Electrical resistivity measurements

After 1000, 1500, 2000, 2500 and 3000 days of exposure to the NaCl solution, the electrical resistivities of the concrete mixtures were evaluated. Thus, the resistivities were measured on water-saturated concrete. The ER was measured using a Wenner probe Resipod model 38 mm device from Proceq®. The test was performed according to the recommendations from the AASTHO [32] (Standard Method of Test for Surface Resistivity Indication of Concrete's Ability to Resist Chloride-Ion Penetration). Ten readings under saturated surface-dry conditions were taken on the four faces of the prisms, and the average values of these ten measurements are reported. Fig. 1 indicates the position of the probe and test set-up. Finally, the ER results were corrected by the maximum size of aggregate, as proposed by Morris et al. [33].

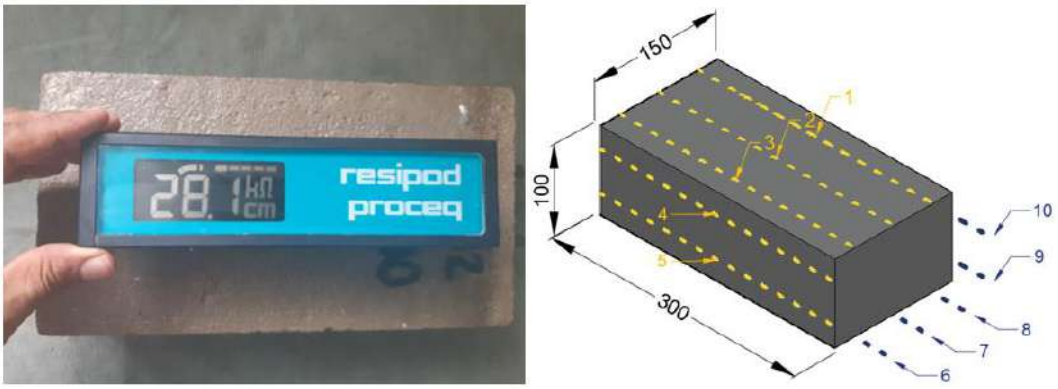

Fig. 1. a) Position of the probe and b) Schematic representation of the locations where the ER measurements were taken (mm)

2.3 Autopsy of the concretes

After 3000 days of continuous immersion in a Cl^- solution, an autopsy of one prismatic specimen for each concrete mixture was carried out. The visual inspection before and after the autopsy did not show visible damage, such as cracking and delamination of the concrete

(Figs. 2a and 2c). The autopsy procedure consisted of sectioning the original prism into smaller prism-shaped slices (Fig. 2b) using a CONTROLS® Model 55-C0210/DZ saw cutting machine. As a result, four sets of prismatic slices were obtained to carry out the different tests considered in this research (Fig. 2c). The first set comprised two slices, with dimensions of 35 x 100 x 180 mm^3 and 35 x 100 x 120 mm^3, labelled as CPA-1 and CPA-2, respectively, whereas the second set also had two slices, with the same dimensions as the first set, but were labelled as CPB-1 and CPB-2, respectively. The third and fourth sets comprised eight slices of 35 x 45 x 75 mm^3 each and these were labelled as CA-1 to CA-8 for the third set and CB-1 to CB-8 for the fourth set, respectively.

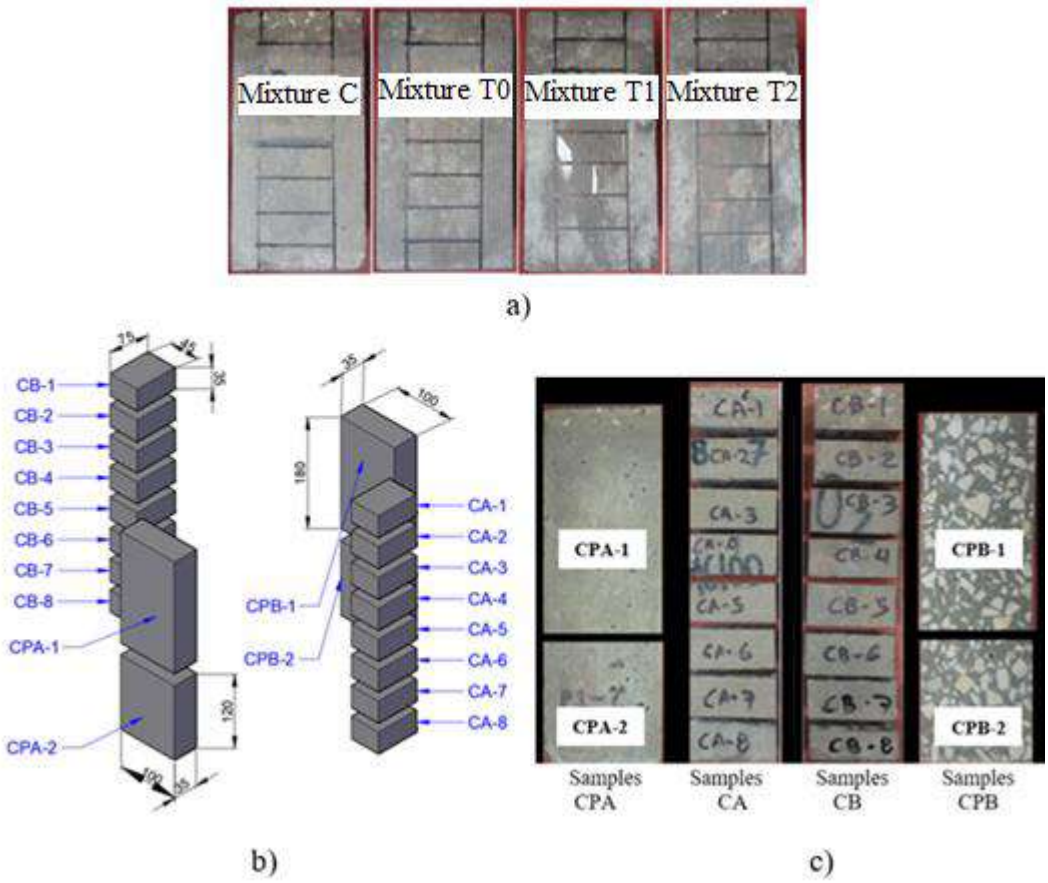

Fig 2. a) Selected prismatic specimens for the autopsy, b) Schematic representation of the slices (mm), and c) slices obtained for the control specimen

Table 3 shows a summary of the specific slices used for each of the tests carried out on all the concrete mixtures under investigation. For the sake of brevity only the tests carried out for the control mixture C are described in the following sections, as the same methodology was used for the specimens from the other concrete mixtures (T0, T1, and T2).

Table 3. Summary of the slices distribution for the different tests carried out in the present study.

Mixture	SEM	XRD	Bulk density	Absolute density	CS	D_c, P_b
C	CA-1 CB-1	CA-2 CA-3 CB-2 CB-3	CPA-2 CPB-2	CA-4 CA-5 CB-4 CB-5	CA-6 CA-7 CA-8 CB-6 CB-7 CB-8	CPA-1 CPB-1
T0	T0A-1 T0B-1	T0A-2 T0A-3 T0B-2 T0B-3	T0PA-2 T0PB-2	T0A-4 T0A-5 T0B-4 T0B-5	T0A-6 T0A-7 T0A-8 T0B-6 T0B-7 T0B-8	T0PA-1 T0PB-1
T1	T1A-1 T1B-1	T1A-2 T1A-3 T1B-2 T1B-3	T1PA-2 T1PB-2	T1A-4 T1A-5 T1B-4 T1B-5	T1A-6 T1A-7 T1A-8 T1B-6 T1B-7 T1B-8	T1PA-1 T1PB-1
T2	T2A-1 T2B-1	T2A-2 T2A-3 T2B-2 T2B-3	T2PA-2 T2PB-2	T2A-4 T2A-5 T2B-4 T2B-5	T2A-6 T2A-7 T2A-8 T2B-6 T2B-7 T2B-8	T2PA-1 T2PB-1

2.4 Microstructural and mineralogical evaluation

The morphology of mixture C was analyzed using a high vacuum scanning electron microscope (SEM) JEOL™ model JSM-6510LV equipped with an EDS microanalysis system from Oxford Instruments™. Two fragments of cementing paste (approximately 5 mm^3) were obtained from samples CA-1 and CB-1. The fragments were dried in an electric

oven at 40 °C for 10 minutes. These slices were then covered with a gold-palladium film using a Denton Vacuum Desk IV® equipment and taken to the microscope.

The mineralogical phases were identified by X-ray diffraction, using a diffractometer Empyrean® with a Cu anode. The diffractometer was operated with a voltage of 45 kV and a current of 40 mA. XRD tests were carried from 5 to 70º (2-Theta) at a scanning speed of 0.5 s and increments of 0.026º. For this purpose, cementing paste powders were obtained from slices CA-2, CA-3, CB-2, and CB-3 by crushing them and removing the large aggregate particles. Next, the fragments were manually ground and sieved through a 75-µm ASTM mesh. Finally, the mineral phases obtained by XRD were identified using the X´Pert HighScore Plus™ software.

2.5 Percentage of voids and compressive strength

The percentage of voids of mixture C was determined according to the ASTM C642-13 standard [34], considering both bulk (dry) and absolute densities. The bulk density was obtained from slices CPA-2 and CPB-2, whereas the absolute density was obtained from slices CA-4, CA-5, CB-4, and CB-5 using a multi-pycnometer Quantachrome Instruments™ in an inert media using nitrogen gas after the slices were dried in an electric oven at 110±5ºC 24 hours before the test.

The CS test was carried out using a hydraulic press Instron® model 600DX-B1-C3-G1A. For this purpose, six 33 x 33 x 33 mm^3 cubes labeled as CA-6, CA-7, CA-8, CB-6, CB-7, and CB-8 were used. The cubes were sand-smoothed to achieve flat parallel faces for the subsequent CS tests. The results were corrected by shape and size to compare them against

the results reported for the same concrete in previous research [20, 21], where Ø100 mm x 200 mm cylinders were used. For the shape correction the following Eq. 1 [35] was used:

$$CS_{ci\,\emptyset 150x300} = \frac{CS_{cu\ 33x33x33}}{\frac{1.17}{\sqrt{1+{}^{L_{cu\ 33x33x33}}/_{2.6}}}+0.62} \quad (1)$$

where $CS_{ci\emptyset 150x300}$ is the compressive strength of Ø150 mm x 300 mm cylinder (MPa), $CS_{cu33x33x33}$ is the compressive strength of a cube (MPa), and $L_{cu\ 33x33x33}$ is the size of the cube (cm); while for the size correction the following Eq. (2) [35] was used:

$$CS = CS_{ci\,\emptyset\ 100x200} = \frac{0.49CS_{ci\,\emptyset\ 150x300}}{\sqrt{1+{}^{d_{ci\,\emptyset\ 100x200}}/_{2.6}}} + 0.81CS_{ci\,\emptyset\ 150x300} \quad (2)$$

where CS is the compressive strength of a Ø100 mm x 200 mm cylinder in MPa, and the diameter of the cylinder ($d_{ci\ \emptyset 100x200}$) is in cm.

2.6 Chloride-ion diffusion coefficients and chloride-binding capacity

Concrete powders were obtained by drilling in increments of 3 mm through the depth of the specimens CPA-2 and CPB-2. The total chloride contents from the powders were measured by X-ray fluorescence according to the ASTM E1621-13 standard [36] using a spectrometer PANalytical™ Epsilon3-XL and chloride ingress profiles were established. Next, the total chloride concentration profiles were used to estimate the D_C of mixture C based on the so-called error function analytical solution to Fick's second law using the Table Curve 2D software version 5.01™.

The water-soluble chlorides concentration profile was obtained according to the procedure recommended by RILEM Technical Committee TC 178-TMC [37], using a potentiometric titrator Metrohm^{TM}. Finally, a linear regression analysis between the free and total chlorides concentration profiles was carried out to estimate the chloride-binding capacity (Pb) of mixture C in terms of percentage using the Eq. 3 as recommended by [25, 38]:

$$P_b = \frac{(C_t - C_f)\times 100}{C_t} \quad (3)$$

where C_t and C_f represent the total and free chloride contents, respectively.

As mentioned earlier, the same procedures were carried out to perform all the tests for the T0, T1 and T2 concrete mixtures.

3. Results and discussion

3.1 Microstructural and mineralogical analysis

Fig. 3 shows the micrographs of the concrete mixtures autopsied at 3000 days of exposure to the chloride solution. Mixture C shows a cementitious matrix with apparently fewer porous, with some pores interconnected by cracks (Fig 3a). The EDS analysis indicates that the cementitious compounds are mainly formed by Ca and Si (spectrum 1 and 2) and reveals that the analyzed sample has chlorine-containing compounds.

When FA replaces 20%PC in mixture T0, an apparent cementitious matrix with fewer pores than mixture C is observed (Fig. 3b). The EDS analysis shows cementitious compounds rich in Ca and O, probably portlandite due to the prismatic form characteristics of this compound

(spectrum 3) [39], and also shows other compounds rich in Si and Al (spectrum 4); and, similarly to mixture C, chlorine-containing compounds are observed.

The microstructure of mixture T1 appears to be more complex in nature and less porous than mixtures C and T0 (Fig. 3c). Nevertheless, some partially reacted FA particles were identified. In this mixture, the combination 20%FA+10%UtSCBA produced cementitious compounds with both high and low Ca/Si ratios; see spectrums 5 and spectrum 6, respectively. Cementitious compounds with a low Ca/Si ratio are due to the additional Si, provided by FA and UtSCBA [40, 41]. According to Fig 3c, the cementitious compounds appear blocked and divide the connections between pores. The addition of 20%FA+20%UtSCBA in T2 (Fig. 3d) created a cementitious matrix of similar complexity as mixture T1, with pores partially blocked by cementitious compounds rich in Si and Al, as well as rich in Ca and Al (spectrum 6).

According to the SEM micrographs, the addition of UtSCBA in mixtures with PC+FA produces concretes with a more complex microstructure. Similar microstructures have also been observed in mortars [18] and concretes [20] prepared with UtSCBA at 600 and 120 days of age, respectively.

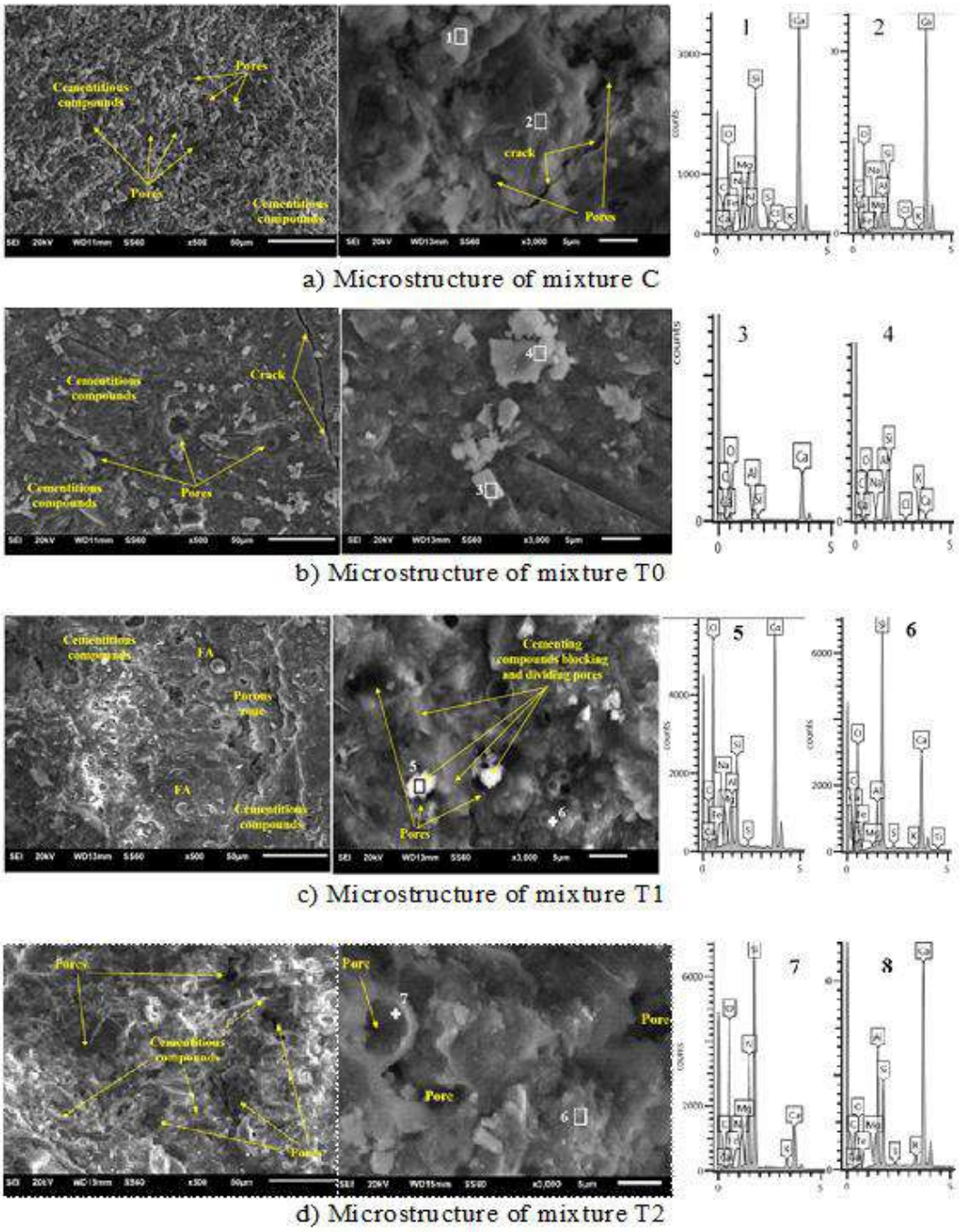

Fig 3. SEM micrographs and EDS analysis of the concrete mixtures exposed to the Cl^- solution for 3000 days

Fig. 4 shows the crystalline phases identified in the concrete mixtures. Phases of tobermorite (C-S-H), portlandite (CH) and ettringite (Aft) were identified as the main hydration products formed in mixture C (Fig 4a). Phases of quartz (Q) and anorthite (A) are attributed to the

sand, while calcite (C) is attributed to the $CaCO_3$ in the CPC [29]. Calcium chloro-aluminate, commonly known as Friedel's salt (Fs), was also identified, in 2θ range = 11.16-11.34° and 23.0-24.0° [42, 43]. This compound is attributed to the chemical interaction of the Cl^- with the Afm and Aft phases from the hydration of PC [44].

The XRD patterns of T0 show an increase in the intensity of C-S-H peaks (Fig. 4b) with respect to mixture C. This can be the result of a pozzolanic reaction between FA and CH in order to produce additional C-S-H; moreover, this reaction is corroborated by the decreased intensity of portlandite peaks compared with mixture C. The chemical interaction between chlorides with both Afm and Aft phases of T0 was corroborated by the identification of Fs peaks, with an intensity comparable with mixture C. In addition to Afm and Aft phases, the amorphous alumina from the FA can also chemically react with chloride ions in order to form Fs [23].

Figs. 4c and 4d show that the combination FA+UtSCBA in T1 and T2 produced concretes with a higher intensity of C-S-H peaks than mixtures C and slightly higher than T0. The above is due to the pozzolanic reaction between UtSCBA and CH, which is substantiated by the depletion of the CH phase. It seems reasonable to assume that additional C-S-H improved the microstructure of UtSCBA-ternary concretes as shown by the SEM results.

In the UtSCBA-ternary concretes the chemical interaction of Cl^- with their Afm and Aft phases was also identified, however, the intensities of the Fs peaks were lower compared to mixtures C and T0. The above does not necessarily indicate a lower quantity of bound chlorides in the concretes with UtSCBA. In this study, the concrete mixtures were exposed to an external source of chlorides. Hence, its content inside the concretes and its subsequent chemical interaction depend on properties such as the porosity and diffusivity of the same

concretes. Moreover, another binding mechanism, for example, the physical interaction between Cl^- and other cementitious compounds, cannot be elucidated with the use of XRD. In order to estimate the Pb of the UtSCBA-ternary concretes it is necessary to analyze and discuss results from porosity, diffusivity and ER, which will be carried out in the following sections.

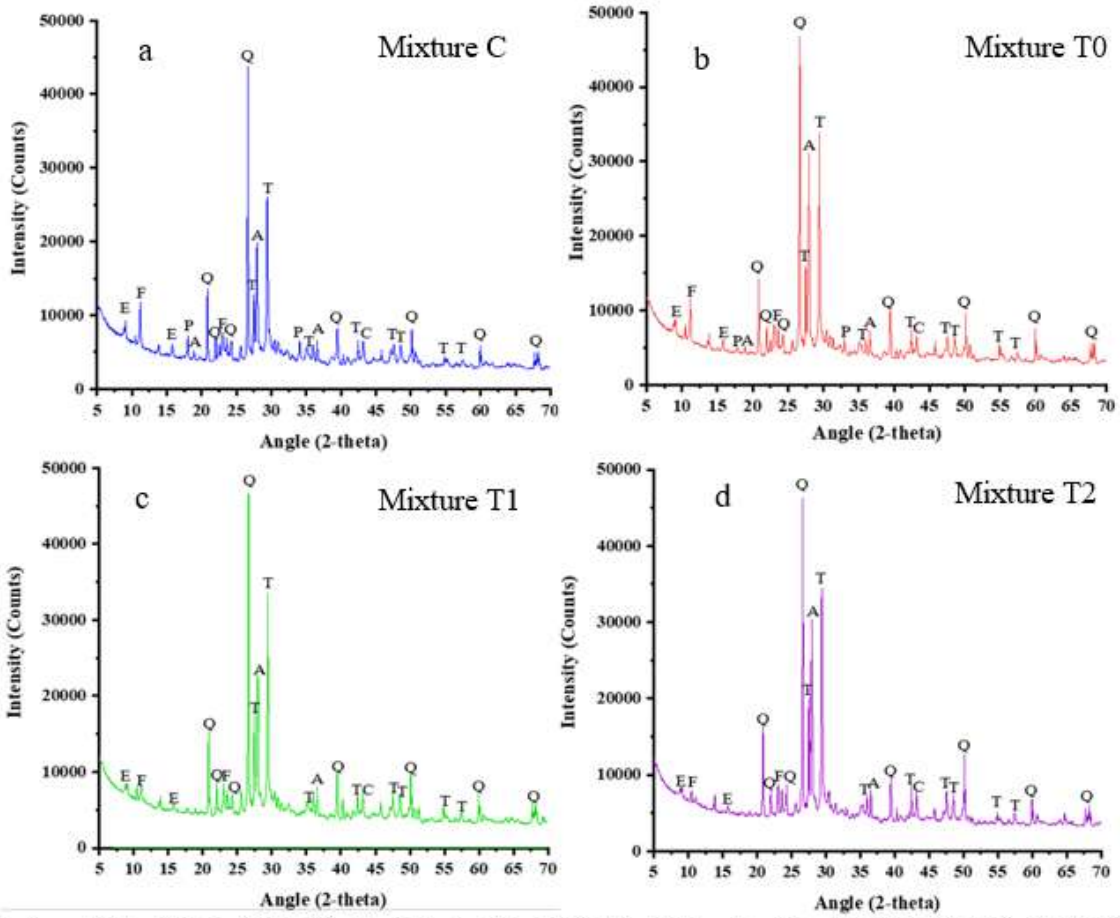

A=Anorthite ($Al_2Ca(SiO_4)_2$); C=Calcite ($CaCO_3$); E=Ettringite ($Ca_6Al_2(SO_4)_3(OH)_{12}26H_2O$); F= Friedel's salt ($3CaOAl_2O_3CaCl_210H_2O$); Q=Quartz ($SiO_2$); P= Portlandite ($Ca(OH)_2$); T=Tobermorite ($Ca_5(SiO_4)_2(OH)_2$)

Fig 4. XRD patterns of the concrete mixtures exposed to the Cl^- solution for 3000 days

3.2 Percentage of voids and compressive strength

Table 4 shows the PV of the concrete mixtures after exposure to the Cl^- solution for 3000 days. Mixture C presents the highest PV, however, when 20%FA was incorporated the PV in mixture T0 was significantly decreased ($p=0.001$). This beneficial effect can be explained by the additional C-S-H, which precipitates in the cementitious matrix of T0, reducing its pores and cracks, as shown in the SEM micrographs.

Similarly, the combination of 10%UtSCBA and 20%UtSCBA with 20%FA helped to significantly decrease the PV of mixtures T1 ($p<<0.05$) and T2 ($p<<0.05$) when compared to mixture C, however, the PVs of T1 ($p=0.605$) and T2 ($p=0.803$) were not significantly different than mixture T0. Again, the decrease in porosity can be attributed to the pozzolanic reaction between the UtSCBA added and CH from the hydration of the PC as such reactions produce secondary C-S-H. The presence of these compounds in the cementitious matrices of the UtSCBA-ternary concretes reduced the voids in their pore system. These changes in the microstructure can be observed in the micrographs of T1 and T2.

Porosity results are slightly lower but do not show significant difference ($p=0.065$) with previous results obtained from the same concretes exposed to a $Ca(OH)_2$ solution for 2500 days [21]. A comparison between the porosity results obtained from the two environments suggests reductions of 7, 9, 5 and 20% with time for concrete mixtures the C, T0, T1 and T2, respectively. This finding corroborates that the long-term exposure to water or seawater did not cause an increase in porosity due to the dissolution of $Ca(OH)_2$, as has been reported by some authors [45].

Table 4. Percentage of voids of the concrete mixtures exposed to the Cl^- solution for 3000 days.

Mixture	Bulk density, g/cm^3	Absolute density, g/cm^3	PV, %	Standard deviation
C	2.34	2.72	13.86^A	0.63
T0	2.29	2.54	9.72^B	0.33
T1	2.28	2.50	8.92^B	0.75
T2	2.26	2.47	8.38^B	0.18

PVs that do not share letters are significantly different (P<0.05)

The CS results of the concrete mixtures at 3000 days of exposure to the Cl^- solution corrected by shape and size are shown in Fig. 5a. All concretes had a greater CS than the design CS, however, mixture C showed the lowest CS. The partial replacement of PC by 20%FA slightly increased the CS of T0; however, this increase is not significantly different (p=0.553) when compared to the control. On the other hand, the additions of 10%UtSCBA and 20%UtSCBA to a concrete containing 20%FA caused significant increases in strengths of 16.00% (p=0.001) and 17.03%(p=0.001), respectively, when compared to C. The CS gain of the concretes containing UtSCBA can be attributed to the secondary C-S-H compounds produced in the pozzolanic reaction between the UtSCBA and CH. Furthermore, it is known that the large fibrous particles of UtSCBA covered with a layer of Si and O increase the specific surface area where the pozzolanic reaction can occur. Consequently, there is a gain in the CS when UtSCBA is added [18].

Some studies have reported that the long-term exposure to water or to a marine environment may dissolve the C-S-H. Therefore, a regression in the CS of mortars and concretes can occur [46]. Data on 2500-day compressive strengths of the same concretes used in the present research, but not exposed to Cl^- and previously reported in [21], are also shown in Fig 5. The statistical analysis did not show significant differences (p=0.844, p=0.975, p=0.202 and, p=0.172 for the mixtures C, T0, T1, and T2, respectively) between the CSs at 2500 days and

3000 days of each of the concrete mixtures. Therefore, it can be concluded that the long-term exposure to the Cl^- solution did not cause a negative effect in the CSs of the mixtures studied.

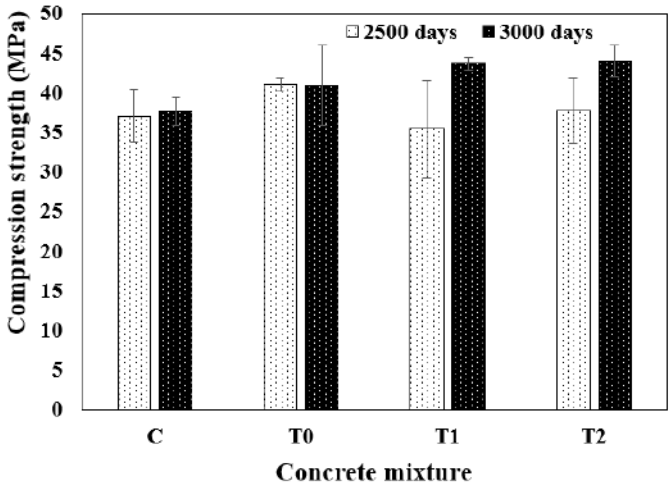

Fig. 5. CSs of concrete mixtures exposed to $Ca(OH)_2$ for 2500 days [21] and to the Cl^- solution for 3000 days

3.3 Electrical resistivity

The effects of the partial replacement of PC by FA and by FA+UtSCBA on the ER of concrete mixtures are shown in Fig. 6a. In general, the ER of all mixtures presented fluctuation throughout the entire exposure period. In the case of mixtures C, T0 and T2, their RE showed a significant increase (p=0.001, p=0.042 and p=0.035, respectively) between 1000 and 1500 days, but remained essentially constant until 3000 days, while the ER of T1 remained constant between 1000 and 2000 days, and did not significantly decrease (p=0.007) until 3000 days.

A more detailed analysis of the results shows that throughout the test period, mixture C presented the lowest ER, while the addition of 20%FA had a significant beneficial effect (p=0.000) on the ER of mixture T0 with respect to C. When the 10%UtSCBA and 20%UtSCBA were combined with 20%FA in T1 and T2, respectively, the performance of

ER of such concretes significantly increased with respect to mixtures C ($p<<0.05$ for both mixtures) and T0 ($p<<0.05$ and $p=0.009$ for T1 and T2, respectively). This behavior can be due to a lower Cl^- concentration [47] throughout the pore network of the UtSCBA-ternary concretes, consequence of a less porous microstructure [48] and hence with less spaces for the Cl^- penetration. This fact is confirmed in Fig 6b, which shows an inversely proportional relationship between the averages of the ER and PV of the concrete mixtures at 2500 and 3000 days. In other words, as the compactness of the microstructure increases, the ER of concretes will increase [49].

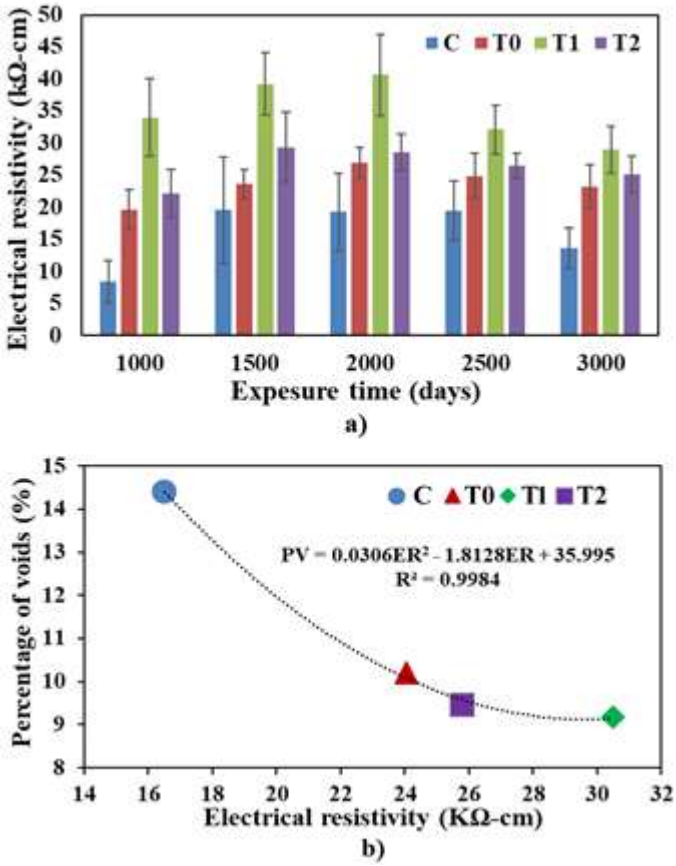

Fig. 6. (a) Electrical resistivities of the concrete mixtures exposed to the Cl^- solution and (b) Relationship between percentage of voids and electrical resistivity of the concrete mixtures studied

3.4 Diffusion coefficients and estimation of the chloride-binding capacity of concrete mixtures.

Fig. 7a shows the Dcs of the concrete mixtures exposed to the Cl^- solution for 3000 days. For comparison purposes, the Dcs at 28 and 90 days of age of the same mixtures, which have already been reported in [21], are also shown in this figure. The results confirmed that diffusivity of all concretes decreased with time. Regarding the 3000-days D_{CS}s, mixture C presented the highest diffusivity, while the addition of 20%FA in T0 contributed to reducing the D_c by approximately 58%. When 10% and 20%UtSCBA were combined with FA, the diffusivities of mixtures T1 and T2 were reduced by approximately 61% and 82%, respectively. The results also show that the high resistance of UtSCBA-ternary concretes against chloride ingress is maintained at long-term ages.

An explanation for the better performance of concretes with UtSCBA regarding resistance to chloride ingress is the improvement of their microstructure as a result of the C-S-H both from PC hydration and pozzolanic reaction. It is known that the C-S-H directly affects the microstructure of concretes, reducing their porosity [17, 50, 51] and consequently Cl^- penetration into the cementitious matrices is reduced.

In this study, the previous argument can be validated with information contained in Fig 7b, which shows that when UtSCBA is added, the PV of studied concretes is reduced. Consequently, the chloride diffusivity decreases and simultaneously the ER increases. Another explanation for results shown by the concretes with UtSCBA regarding chloride penetration can be their ability to bind Cl^-, which is discussed next.

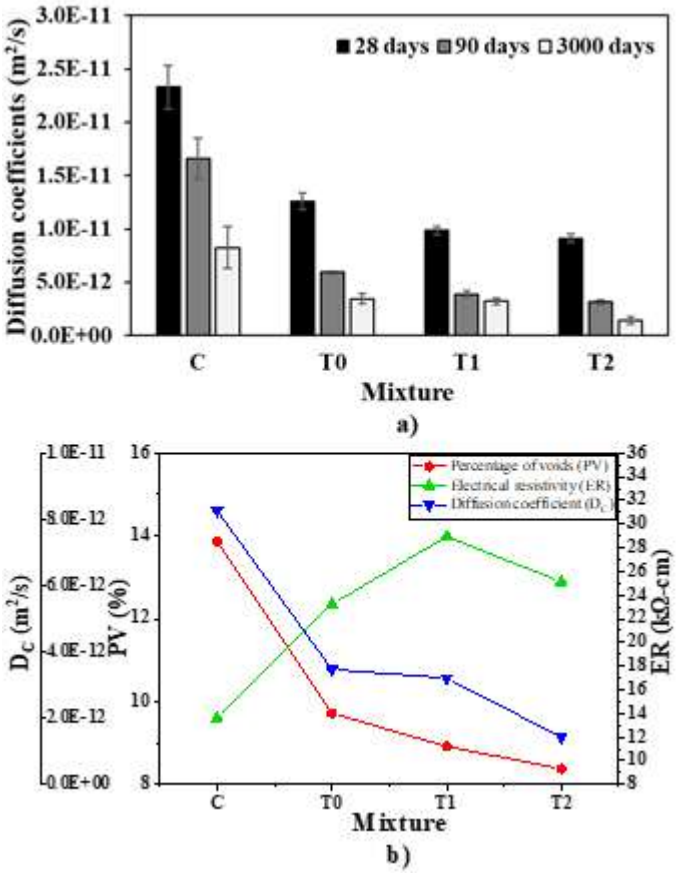

Fig. 7. a) Diffusion coefficients of concrete mixtures and b) PV, ER, and D_C of the concrete mixtures exposed to the Cl^- solution for 3000 days.

Fig 8a illustrates the regression analyses performed to obtain the relationships between the free (C_f) and total (C_t) chlorides of the concrete mixtures under study that were exposed to the Cl^- solution for 3000 days. In general, all concretes show a linear relationship between C_f and C_t with R^2 = 0.8016, 0.9696, 0.9246, and 0.8686 for C, T0, T1, and T2, respectively. Furthermore, two main effects can be observed with the incorporation of UtSCBA. First, the combination of 20%FA+10%UtSCBA and 20%FA+20%UtSCBA decreases the C_t content of mixtures T1 and T2 with respect to the control, which is a consequence of the lowest Cl^- diffusivity shown by the UtSCBA-ternary concretes during the 3000 days of exposure. Second, in terms of the C_t content, the C_f content decreases as the partial substitution of PC

increases [52]. In other words, the addition of UtSCBA not only produces concrete with a lower C_t content but also increases the chloride binding capacity. For example, in Fig. 8a the C*f* for mixture C correlates well to C*t* by the expression $C_f = (0.7438)Ct$, and by substituting this C_f in Eq. 3 the P_b of this mixture was estimated as 25.62%. Similarly, the Pb values of 28.99, 37.74 and 38.36% for T0, T1, and T2 were respectively estimated and are shown in Fig 8b. The results show that the P_bs of all the concretes are similar to the value of 24.65% found by Chalee et al. [38] for concretes with a 0.65 w/cm ratio, a substitution of PC by 50%FA, and exposure to seawater for seven years. Another study reported a P_b of 20% in concretes with a 0.65 w/cm ratio, 25%PC replacement by rice husk ash, and exposure for five years to seawater [25]. On the other hand, a value as high as 57% for P_b has been reported by Arya et al. [53] for pastes with a 0.5 w/cm ratio exposed to a 2.0% NaCl solution for 28 days. The reason for this large difference is that in this case a very short exposure time was considered, and the binding process needs time to be completely established.

In Section 3.1 the diffractograms showed that all concretes investigated in this research chemically bind Cl^-. Nonetheless, Fig 8b shows that the addition of 20%FA slightly increases the Pb of mixture T0 with respect to C, by 13%. On the other hand, the Pbs of mixtures T1 and T2 clearly show the beneficial effect of the addition of 10% and 20%UtSCBA in concretes with FA, increasing their Pbs to 47% and 49% when compared to mixture C.

It is known that the Pb of concrete depends on two main mechanisms: (I) chemical reactions and (II) physical adsorption [54]. As mentioned earlier, the Fs peaks identified in the XRD results corroborate the first binding mechanism in the UtSCBA-ternary concretes. The second mechanism involves the physical interaction of chlorides with the C-S-H, distinguishing three types of interaction: both electrostatic and Van der Waals forces, Cl^-

present in the C–S–H interlayer spaces, and Cl^- intimately bound in the C–S–H lattice [55]. Other researchers suggest that Cl^- ions are trapped inside the interlayer of the C-S-H particles to compensate the charge after adsorption of alkali ions [56]. In this respect, Fig. 8c illustrates the relationship between CS-Pbs of the concrete mixtures studied, indicating that the UtSCBA-ternary concretes present the highest CS which implies that there is more C-S-H in their cementitious matrix to physically bind Cl^-. Other compounds that can physically interact with Cl^- are the carbon particles in the UtSCBA. Such particles can work as an absorbent media for the Cl^- [57]. The interactions between the chemical and physical mechanisms previously mentioned explain the higher Pb shown by the concretes with UtSCBA with respect to mixture C.

The results of this paper show that the best performance regarding resistance against Cl^- penetration shown by the UtSCBA-ternary concretes is due to the improvement of their microstructure as a consequence of the pozzolanic reaction. Furthermore, the addition of UtSCBA produces concretes with a higher ability to bind Cl^-, indicating a lower free-Cl^- content in their cementitious matrix available to corrode the reinforcing steel.

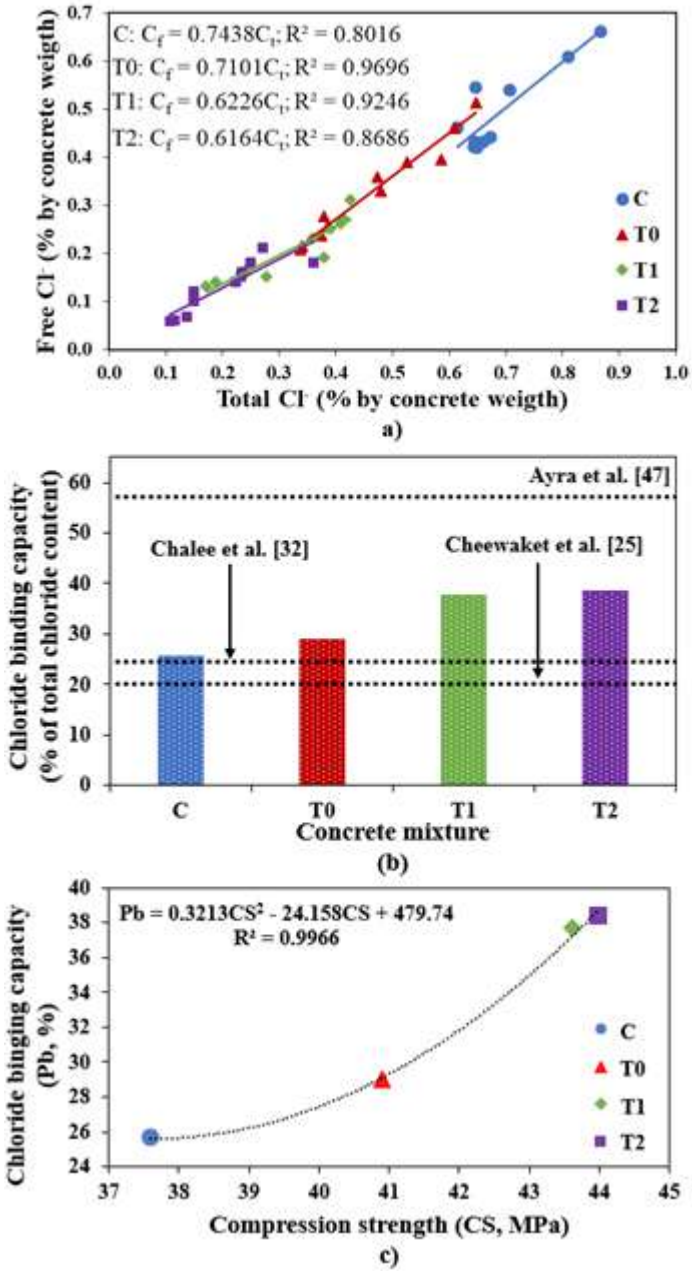

Fig 8. a) Relationship between the free and total Cl^- contents, b) Chloride binding capacity and, c) Relationship between Pb and CS of the concrete mixtures exposed to the Cl^- solution for 3000 days

Conclusions

Based on the analysis of the results obtained from this research, the following conclusions can be drawn:

1. The chlorides that entered through the cementitious matrices of all studied concrete mixtures chemically interacted with their Aft and Afm phases to form Friedel´s salt.
2. The long-term exposure to the Cl^- solution did not result into the phenomena of dissolution of $Ca(OH)_2$ and decalcification of C-S-H in the concretes studied.
3. The partial replacement of cement by the combinations of 20%FA+10%UtSCBA and by 20%FA+20%UtSCBA produces concretes with higher resistances against chloride ingress with respect to a control concrete with no additions. This beneficial effect is the result of the change to a more complex and less porous microstructure, as well as to a lower diffusivity of chlorides into the concrete. The latter, i.e. the lower diffusivity, is the logical result of a more tortuous (complex) microstructure.
4. Free and total chloride contents are linearly correlated in the studied concretes which were exposed to a Cl^- solution for 3000 days.
5. The chloride-binding capacity of concretes where cement was partially replaced by the combinations of 20%FA+10%UtSCBA and 20%FA+20%UtSCBA increases to approximately 12.12% and 12.74% when compared to the control concrete.

Conflict of interest

The authors declare no conflict of interest.

Acknowledgments

The authors are grateful to the Instituto Politécnico Nacional of Mexico (IPN) for the facilities and financial support provided for this research. Furthermore, the authors thank the Facultad de Ingeniería Civil of the Universidad Autónoma de Nuevo León in Mexico for the

use of its facilities during the characterization of the concretes. The authors are also grateful to Consejo Nacional de Ciencia y Tecnología (CONACyT) of Mexico for the doctoral scholarship granted to Víctor Alberto Franco-Luján.

References

[1] P. Montes, T.W. Bremner, I. Kondratova, Eighteen Year Performance of Epoxy Coated Rebar i n a Tunnel Structure Subjected to a Very Aggressive Chloride Contaminated Environment, CORROSION. 60 (2004).

[2] H.Z. López Calvo, P. Montes Garcia, I. Kondratova, T.W. Bremner, M.D.A. Thomas, Epoxy c oated bars as corrosion control in cracked reinforced concrete, Mater. Corros. 64 (2013) 59 9–608.

[3] P. Montes, T.W. Bremner, D.H. Lister, Influence of calcium nitrite inhibitor and crack width o n corrosion of steel in high performance concrete subjected to a simulated marine environ ment, Cem. Concr. Compos. 26 (2004) 243–253.

[4] tX. Shi, N. Xie, K. Fortune, J. Gong, Durability of steel reinforced concrete in chloride environ ments: An overview, Constr. Build. Mater. 30 (2012) 125 138. https://doi.org/10.1016/j.co nbuildmat.2011.12.038.

[5] M.M. Hossain, M.R. Karim, M. Hasan, M.K. Hossain, M.F.M. Zain, Durability of mortar and c oncrete made up of pozzolans as a partial replacement of cement: A review, Constr. Build. Mater. 116 (2016) 128–140.

[6] D.P. Mishra, S.K. Das, A studytof physicoy chemical and mineralogical properties of Talcher c oal fly ash for stowing in underground coal mines, Mater. Charact. 61 (2010) 1252–1259.

[7] Y.S. Choi, J.G. Kim, K.M. Lee, Corrosion behavior of steel bar embedded in fly ash concrete, Corros. Sci. 48 (2006) 1733–1745.

[8] N. Chousidis, E. Rakanta, I. Ioannou, G. Batis, Mechanical properties and durability performan ce of reinforced concrete containing fly ash, Constr. Build. Mater. 101 (2015) 810–817.

[9] M.M.N.S. de Soares, D.C.S. Garcia, R.B. Figueiredo, M.T.P. Aguilar, P.R. Cetlin, Comparing t he pozzolanic behavior of sugar cane bagasse ash to amorphous and crystalline SiO_2, Cem. Concr. Compos. 71 (2016) 20–25.

[10] G.C. Cordeiro, K.E. Kurtis, Effect of mechanical processing on sugar cane bagasse ash pozzol anicity, Cem. Concr. Res. 97 (2017) 41 49.

[11] S. Rukzon, P. Chindaprasirt, Utilization of bagasse ash in high strength concrete, Mater. Des. 34 (2012) 45–50.

[12] G.C. Cordeiro, O.A. Paiva, R.D. Toledo Filho, E.M.R. Fairbairn, L.M. Tavares, Long Term C ompressive Behavior of Concretes with Sugarcane Bagasse Ash as a Supplementary Ceme ntitious Material, J. Test. Eval. 46 (2018) 20160316.

[13] K. Ganesan, K. Rajagopal, K. Thangavel, Evaluation of bagasse ash as supplementary cementi tious material, Cem. Concr. Compos. 29 (2007) 515–524.

[14] N. Chusilp, C. Jaturapitakkul, K. Kiattikomol, Utilization of bagasse ash as a pozzolanic mate rial in concrete, Constr. Build. Mater. 23 (2009) 3352–3358.
[15] M.C. Chi, Effects of sugar cane bagasse ash as a cement replacement on properties of mortars, Sci. Eng. Compos. Mater. 19 (2012) 279–285.
[16] V.G. Jiménez Quero, F.M. León Martínez, P. Montes García, C. Gaona Tiburcio, J.G Chacón Nava, Influence of sugar cane bagasse ash and fly ash on the rheological behavior of ceme nt pastes and mortars, Constr. Build. Mater. 40 (2013) 691–701.
[17] J.C. Arenas Piedrahita, P. Montes García, J.M. Mendoza Rangel, H.Z. López Calvo, P.L. Vald ez Tamez, J. Martínez Reyes, Mechanical and durability properties of mortars prepared wit h untreated sugarcane bagasse ash and untreated fly ash, Constr. Build. Mater. 105 (2016).
[18] M.A. Maldonado-García, U.I. Hernández-Toledo, P. Montes-García, P.L. Valdez-Tamez, The influence of untreated sugarcane bagasse ash on the microstructural and mech anical properties of mortars, Mater. Constr. 68 (2018) 1–13.
[19] M. G.M. Antonio, H. T.U. Iván, M. G. Pedro, V. T.P. Leobardo, Long Term Corrosion Risk o f Thin Cement Composites Containing Untreated Sugarcane Bagasse Ash, J. Mater. Civ. E ng. 31 (2019) 4019020.
[20] V. Ríos Parada, V.G. Jiménez Quero, P.L. Valdez Tamez, P. Montes García, Characterization and use of an untreated Mexican sugarcane bagasse ash as supplementary material for the preparation of ternary concretes, Constr. Build. Mater. 157 (2017) 83–95.
[21] V.A. Franco Luján, M.A. Maldonado García, J.M. Mendoza Rangel, P. Montes García, Chlori de induced reinforcing steel corrosion in ternary concretes containing fly ash and untreated sugarcane bagasse ash, Constr. Build. Mater. 198 (2019) 608–618.
[22] R.K. Dhir, M.R. Jones, Development of chloride resisting concrete using fly ash, Fuel. 78 (19 99) 137–142.
[23] M.D.A. Thomas, R.D. Hooton, A. Scott, H. Zibara, The effect of supplementary cementitious materials on chloride binding in hardened cement paste, Cem. Concr. Res. 42 (2012) 1–7.
[24] H. Jensen, P.L. Prattt, The binding of chloride ions by pozzolanic product in fly ash cement bl ends, Adv. Cem. Res. 2 (1989) 121–129.
[25] T. Cheewaket, C. Jaturapitakkul, W. Chalee, Long term performance of chloride binding capa city in fly ash concrete in a marine environment, Constr. Build. Mater. 24 (2010) 1352–1357.
[26] H. Hirao, K. Yamada, H. Takahashi, H. Zibara, Chloride Binding of Cement Estimated by Bin ding Isotherms of Hydrates, J. Adv. Concr. Technol. 3 (2005) 77–84.
[27] NMX C 414 ONNCCE 2004. Industria de la construcción cementos hidráulicos especificacion es y métodos de prueba, normas mexicanas, organismo nacional de normalización y certifi cación de la construcción y edificación, S.C. p. 1–2 (in Spanish).
[28] ASTM C618 19, Standard Specification for Coal Fly Ash and Raw or Calcined Natural Pozzo lan for Use in Concrete, ASTM International, West Conshohocken, PA, 2019.
[29] H.F.W. Taylor, Cement chemistry, Thomas Telford Publishing, 1997.
[30] A. Bahurudeen, M. Santhanam, Influence of different processing methods on the pozzolanic p erformance of sugarcane bagasse ash, Cem. Concr. Compos. 56 (2014) 32–45.
[31] A.C.I.C. 211, Standard Practice for Selecting Proportions for Normal, Heavyweight, and Mass Concrete:(ACI 211.1-91), in: American Concrete Institute, 1991.

[32] A. TP95, Standard Method of Test for Surface Resistivity Indication of Concrete's Ability to Resist Chloride Ion Penetration, Am. Assoc. State Highw. Transp. Off. AASHTO, Washin gton, DC. (2011).
[33] W. Morris, E. Moreno, A.A. Sagües, Practical evaluation of resistivity of concrete in test cylin ders using a Wenner array probe, Cem. Concr. Res. 26 (1996) 1779–1787.
[34] ASTM C642 13, Standard Test Method for Density, Absorption, and Voids in Hardened Conc rete, ASTM International, West Conshohocken, PA, 2013.
[35] S.T. Yi, E.I. Yang, J.C. Choi, Effect of specimen sizes, specimen shapes, and placement direct ions on compressive strength of concrete, Nucl. Eng. Des. 236 (2006) 115–127.
[36] ASTM E1621 M13, Standard Guide for Elemental Analysis by Wavelength Dispersive X Ray Fluorescence Spectrometry, ASTM International, West Conshohocken, PA, 2013
[37] RILEM TC178, Analysis of water soluble chloride content in concrete, Mater. Struct. 35 (200 2) 586–588.
[38] W. Chalee, T. Sasakul, P. Suwanmaneechot, C. Jaturapitakkul, Utilization of rice husk bark as h to improve the corrosion resistance of concrete under 5 year exposure in a marine enviro nment, Cem. Concr. Compos. 37 (2013) 47–53.
[39] D. Stephan, S.N. Dikoundou, G. Raudaschl Sieber, Hydration characteristics and hydration pr oducts of tricalcium silicate doped with a combination of MgO, Al2O3 and Fe2O3, Therm ochim. Acta. 472 (2008) 64–73.
[40] J.J. Chen, J.J. Thomas, H.F.W. Taylor, H.M. Jennings, Solubility and structure of calcium sili cate hydrate, Cem. Concr. Res. 34 (2004) 1499–1519.
[41] A. V Girão, I.G. Richardson, R. Taylor, R.M.D. Brydson, Composition, morphology and nano structure of C S H in 70% white Portland cement 30% fly ash blends hydrated at 55°C., Ce m. Concr. Res. 40 (2010) 1350–1359.
[42] Talero, L. Trusilewicz, A. Delgado, C. Pedrajas, R. Lannegrand, V. Rahhal, R. Mejía, S. Delv asto, F.A. Ramírez, Comparative and semi quantitative XRD analysis of Friedel's salt origi nating from pozzolan and Portland cement, Constr. Build. Mater. 25 (2011) 2370–2380.
[43] M. Frias, S. Goñi, R. García, R. Vigil de La Villa, Seawater effect on durability of ternary ce ments. Synergy of chloride and sulphate ions, Compos. Part B Eng. 46 (2013) 173–178.
[44] M.V.A. Florea, H.J.H. Brouwers, Chloride binding related to hydration products Part I : Ordin ary Portland Cement, Cem. Concr. Res. 42 (2012) 282–290.
[45] H. Yang, L. Jiang, Y. Zhang, Q. Pu, Y. Xu, Predicting the calcium leaching behavior of ceme nt pastes in aggressive environments, Constr. Build. Mater. 29 (2012) 88–96.
[46] F.P. Glasser, J. Marchand, E. Samson, Durability of concrete Degradation phenomena involvi ng detrimental chemical reactions, Cem. Concr. Res. 38 (2008) 226–246.
[47] M. Sharfuddin Ahmed, O. Kayali, W. Anderson, Chloride penetration in binary and ternary bl ended cement concretes as measured by two different rapid methods, Cem. Concr. Compos . 30 (2008).
[48] R.A. Medeiros Junior, M.G. Lima, Electrical resistivity of unsaturated concrete using different types of cement, Constr. Build. Mater. 107 (2016) 11–16.
[49] A. Lübeck, A.L.G. Gastaldini, D.S. Barin, H.C. Siqueira, Compressive strength and electrical properties of concrete with white Portland cement and blast furnace slag, Cem. Concr. Co mpos. 34 (2012) 392–399.

[50] C.C. Yang, On the relationship between pore structure and chloride diffusivity from accelerate d chloride migration test in cement based materials, Cem. Concr. Res. 36 (2006) 1304–1311.
[51] G. Fajardo, P. Valdez, J. Pacheco, Corrosion of steel rebar embedded in natural pozzolan-based mortars exposed to chlorides, Constr. Build. Mater. 23 (2009) 768–774.
[52] T.U. Mohammed, H. Hamada, Relationship between free chloride and total chloride contents i n concrete, Cem. Concr. Res. 33 (2003) 1487-1490.
[53] C. Arya, N.R. Buenfeld, J.B. Newman, Factors influencing chloride binding in concrete, Cem. Concr. Res. 20 (1990) 291–300.
[54] R. Luo, Y. Cai, C. Wang, X. Huang, Study of chloride binding and diffusion in GGBS concret e, Cem. Concr. Res. 33 (2003) 1–7.
[55] V.S. Ramachandran, Possible states of chloride in the hydration of tricalcium silicate in the pr esence of calcium chloride, Matériaux Constr. 4 (1971) 3–12.
[56] G. Plusquellec, A. Nonat, Interactions between calcium silicate hydrate (C S H) and calcium c hloride, bromide and nitrate, Cem. Concr. Res. 90 (2016) 89–96.
[57] V. Minkova, M. Razvigorova, E. Bjornbom, R. Zanzi, T. Budinova, N. Petrov, Effect of water vapour and biomass nature on the yield and quality of the pyrolysis products from biomas s, Fuel Process. Technol. 70 (2001) 53–61.

CHAPTER SIX

Cl^- induced corrosion effect on the mechanical properties of steel reinforcement embedded in ternary-concretes containing FA and UtSCBA

Víctor Alberto Franco-Luján, José Manuel Mendoza-Rangel, Pedro Montes-García.

2020

Manuscript to be sent to Construction and Building Materials (JCR, Q1, IF=4.046)

Effect of Cl^--induced corrosion on the mechanical properties of reinforcing steel embedded in ternary-concretes containing FA and UtSCBA

Víctor Alberto Franco-Luján [1], José Manuel Mendoza-Rangel [2], Pedro Montes-García [3,*]

[1] PhD Student. Instituto Politécnico Nacional, CIIDIR-Oaxaca, Hornos 1003, Col. Noche Buena, Sta. Cruz Xoxocotlán C.P. 71230, México, francolujan_89@hotmail.com
[2] Universidad Autónoma de Nuevo León (UANL), FIC, Cd Universitaria S/N, San Nicolás de los Garza, Nuevo León C.P. 66451, México, jose.mendozarn@uanl.edu.mx
[3] Instituto Politécnico Nacional, CIIDIR-Oaxaca, Grupo de Materiales y Construcción, México, vgjimenez@hotmail.com, pmontesgarcia@gmail.com, pmontes@ipn.mx

* Corresponding author: pmontes@ipn.mx, pmontesgarcia@gmail.com (P. Montes-García)

Abstract

This paper investigates the effect of Cl^--induced corrosion on the mechanical properties of reinforcing steel embedded in ternary concretes with fly ash (FA) plus untreated sugarcane bagasse ash (UtSCBA). Concretes containing only Portland cement (PC), PC+FA, and CPC+FA+UtSCBA were manufactured and immersed in a chloride solution for 3000 days. The corrosion condition of the reinforced concretes was evaluated by corrosion potentials; then the rebars were extracted and their mass losses due to corrosion were determined. Next, elemental mapping of the concrete/reinforcement steel interface using scanning electron microscopy was conducted. Corrosion products were identified by X-Ray diffraction and infrared spectroscopy. Finally, rebars were subjected to tensile testing to evaluate their yield strengths, ultimate strengths, fracture loads, and ductilities. At the end of the exposure, corrosion potentials suggest high corrosion risk for all the rebars but one, and several had severe corrosion. Results indicate that rebars retrieved from concretes containing UtSCBA

experienced the lowest mass loss. Cl^--induced corrosion products as magnetite and akageneite were identified. The yield strengths of the rebars embedded in all concretes were not negatively affected, while the ultimate strengths, fracture loads and ductilities of rebars embedded in UtSCBA-ternary concretes were higher than those embedded in the control mixture.

Keywords: Corrosion products, ductility, supplementary cementing materials, ternary concretes, yield and ultimate stresses

1. Introduction

It is well known that the Cl^-induced steel corrosion is one of the main deterioration phenomena occurring in reinforced concrete structures (RCS). In addition to cracking, delamination and spalling of the concrete cover [1], the corrosion by Cl^- produces mass loss of the reinforcing steel (rebar) of RCS; consequently, their structural safety is jeopardized because the load-bearing capacity of reinforced concrete members is diminished [2].

In this perspective, the use of the supplementary cementitious materials (SCMs) as partial replacement of the Portland cement (PC) is a viable option to produce more corrosion-resistant concretes [3]. The use of Fly ash (FA) as SCM has contributed to lowering the permeability and Cl^- diffusion of mortars and concretes [4]. The enhancement of these properties reduces significantly the Cl^- ingress and, hence, the corrosion on the rebars [5-7]. Nowadays, the availability of FA is limited due to environmental regulations. For example, in the US, approximately 40% of coal-fired power plants have closed in the last five years, while the United Kingdom plans to retire all its coal-fired power plants by 2025 and the

Netherlands by 2030 [8]. Because of the demand for PC is constant and the availability of FA is declining, studies on the use of SCM such as sugarcane bagasse ash (SCBA) are highly needed,

In recent years, an on-going long-term research project has evaluated the use of ‘‘practically as received” SCBA, which was only sieved through the 75 μm sieve and has been named in the literature as UtSCBA. Workability, microstructural characteristics, mechanical properties and some durability aspects of mortars and concretes manufactured with the UtSCBA have been investigated. The results have shown that the PC replacement by 10 and 20% of UtSCBA reduces the workability of mortars [9]; however, it significantly improves the long-term microstructural, mechanical and durability properties of mortars [10-12]. As mentioned earlier, the use of 10 and 20% of UtSCBA reduces the workability in mortars; nonetheless, this problem can be surpassed with the addition of 20%FA [9]. This new combination of FA+UtSCBA produced concretes with similar long-term microstructural and mechanical properties than concretes elaborated with only PC [13]. Regarding the durability properties, the PC partial replacement by FA+UtSCBA significantly decreased the Cl^- diffusion; hence, UtSCBA-ternary reinforced concretes exposed to a NaCl solution over 2500 days presented both lower corrosion probability and lower corrosion densities than those reinforced concretes with only PC and PC+20%FA [14]. Although the results of UtSCBA-ternary concretes against corrosion by Cl^- are promising, they are based on non-destructive methods; therefore, the real condition of the rebars embedded in such concretes is a subject requiring to be investigated.

In the literature, several studies have reported the effect of corrosion induced by Cl^- on the mechanical properties of rebars embedded in concrete when is exposed to natural and

accelerated-simulated marine environments. It is worth notice that some of the studies are in conflict. For example, Du et al. [15] reported that corrosion significantly affected the flexural strength and changed the failure mode of reinforced concrete beams. Fernández et al. [16] and Ou et al. [17] also reported that the yield and ultimate strengths of rebars embedded in concrete were significantly affected when corrosion was induced by impressed current. In the same research, Ou et al. [17] found the same tendency but in Cl^--naturally induced corrosion of rebars. Other studies [18, 19] have reported that Cl^--induced corrosion moderately reduced the yield and ultimate strengths of reinforcing steels. On the contrary, Zhu and François [20] carried out mechanical tests to artificially and naturally corroded rebars and they found that in both cases the yield and ultimate strengths of rebars were not affected by corrosion when those are compared with an uncorroded bar.

Despite of the discrepancy observed about the corrosion effect on the yield and ultimate strengths, the ductility of rebars is indeed severely affected. All studies previously mentioned reported that the artificial and natural corrosion significantly reduces the ductility of corroded rebars. Likewise, Apostolopoulos et al. [21] and Zhu et al. [22] found that corrosion reduces the ductility of rebars, while their failure mode changes from ductile to brittle with the increase in the corrosion degree.

All in all, no research about the influence of UtSCBA on the mechanical properties of the reinforcing steel embedded in UtSCBA-mortars or concretes have been reported yet. In the light of this, studies on this subject are highly needed. The objective of this research was to investigate the mechanical properties of reinforcing steel embedded in concrete prisms containing FA plus UtSCBA, which were exposed to a NaCl solution over 3000 days. For this purpose, the corrosion conditions of the rebars were first evaluated using corrosion

potentials. Next, the concrete prisms were autopsied, and internal visual inspection and mass loss of the rebars embedded in the concretes were carried out. Elemental mapping of the concrete/steel reinforcing interface by scanning electron microscopy (SEM) was carried out to compare the presence of Fe, C, and Cl between rusted and rust-free zones. Furthermore, the corrosion products were identified by both X-ray diffraction (XRD) and Fourier transformation infrared spectroscopy (FTIR). Finally, the rebars were retrieved and subjected to tensile tests in order to determine their yield strengths, ultimate strengths, fracture loads, and ductilities.

2. Materials and Methods

2.1 Experimental design

To evaluate the influence of Cl^--induced corrosion on the real mass loss and mechanical properties of corroded rebars, a four-level factor with five-quantitative responses experimental design was considered (Table 1). The rebars were initially embedded in UtSCBA-ternary concrete prisms, exposed to a Cl^- solution for 3000 days, and retrieved after exposure for an in-depth meticulous evaluation.

Table 1. Details of the experimental design.

Factor	Levels	Description	Responses
Type of mixture	C	100%PC	Real mass loss (RML)
	T0	80%PC+20%FA	Yield stress (f_y)
	T1	70%PC+20%FA+10%UtSCBA	Ultimate stress (f_u)
	T2	60%PC+20%FA+20%UtSCBA	Fracture load (Fl)
			Ductility (μ)

2.2 Materials

Portland cement (CPC-30R), UtSCBA, and Admix Tech® FA were used as cementitious materials for the preparation of the concrete mixtures. The CPC fulfills the requirements established by the NMX-C-414-ONNCCE-2004 standard [23]. The UtSCBA was only sieved through a 75-μm ASTM mesh for four minutes. The FA is classified as Class F according to the ASTM C618 -19 standard [24]. The chemical compositions of the materials are shown in Table 2. The sums of the major oxides (SiO_2, Al_2O_3, and Fe_2O_3) for the UtSCBA and FA were higher to that recommended by the [24] to classify a material with high pozzolanic potential; however, the LOI contents of the CPC and UtSCBA were higher than that established by the same standard. This can be attributed to the presence of calcium carbonate ($CaCO_3$) in the CPC [25] and carbonaceous matter in the UtSCBA. In previous studies, neither the CPC nor the UtSCBA induced uncontrolled adverse effects on the fresh and hardened state properties of concretes prepared with these materials [9, 13, 14]; therefore, they were used for the concrete manufacture.

River sand and calcareous crushed coarse aggregate were used to prepare the concrete mixtures. The volumetric weights, specific gravities, and adsorptions of the fine and coarse aggregates were 1596 kg/cm^3, 2.78, and 1.74%, and 1624 kg/cm^3, 2.66, and 0.47%, respectively. The fineness modulus of the sand and the maximum size of the coarse aggregate, these were 2.97 and 19 mm, respectively. Finally, bi-distilled water and a polycarboxylate-based superplasticizer (SP) Plastol 4000^{TM} were used to prepare the concrete mixtures.

Table 2. Chemical compositions of used cementitious materials (% by mass) [13]

Material	Al_2O_3	CaO	Fe_2O_3	K_2O	MgO	MnO	Na_2O	P_2O_5	SiO_2	TiO_2	SO_3	LOI
CPC	4.87	60.03	3.57	0.85	1.50	0.08	0.52	0.19	20.67	0.58	4.95	8.40
UtSCBA	15.00	2.57	7.16	3.52	1.19	0.22	0.54	1.14	66.12	1.13	0.26	9.00
FA	20.01	4.00	5.42	0.96	0.63	0.10	0.19	0.38	64.12	1.12	0.86	2.60

LOI = Loss on ignition at 950 ºC for the CPC and at 750 ºC for the FA and UtSCBA.

2.3 Mixture design, casting of reinforced prisms and exposure conditions

The four concrete mixtures were designed under the procedure established by the absolute volume method from the ACI 211.1 [26]. All mixtures had a 0.5 water/cementitious materials ratio (w/cm) and were designed to achieve a slump target of 75 ± 20 mm [27]. Mixture C was designed to achieve a compressive strength (CS) target of 25±8 MPa at 28 days. Table 3 shows the mixture proportions and their corresponding 28-day CS values.

Table 3. Proportions of the concrete mixtures (kg/m^3) [13]

Mixture	CPC	FA	UtSCBA	Fine aggregate	Coarse aggregate	Water	SP	Slump	CS at 28 days
C	410	--	--	727	1015	205	2.7	78	31 ± 2.2
T0	328	82	--	727	1015	205	1.6	79	32 + 2.1
T1	287	82	41	727	1015	205	3.1	88	28 ± 2.3
T2	256	82	82	727	1015	205	4.9	90	23 ± 1.9

SP = Polycarboxylate-based superplasticizer (ml per kg of cementitious materials), slump is in mm, and CS in MPa.

Three prismatic specimens (100 mm x 150 mm x 300 mm) for each concrete mixture were cast and all the specimens were reinforced with two ∅ 9.5 mm steel bars. The thickness of the concrete cover was 45.5 mm (Fig. 1a). On each rebar a length of 260 mm was outlined in the middle section using an epoxy coating, which is equivalent to an original uncorroded surface (OUS) of 77.60 cm^2. Furthermore, 20 mm were left at the upper end of the rebar for corrosion testing. All rebars met the requirements of ASTM A 615/A615M standard Grade

60 [27]. After the casting, the reinforced concretes were cured for 28 days and then immersed in a 3.5% NaCl solution for 3000 days, leaving 30 mm of concrete cover above the NaCl solution level (Fig. 1b).

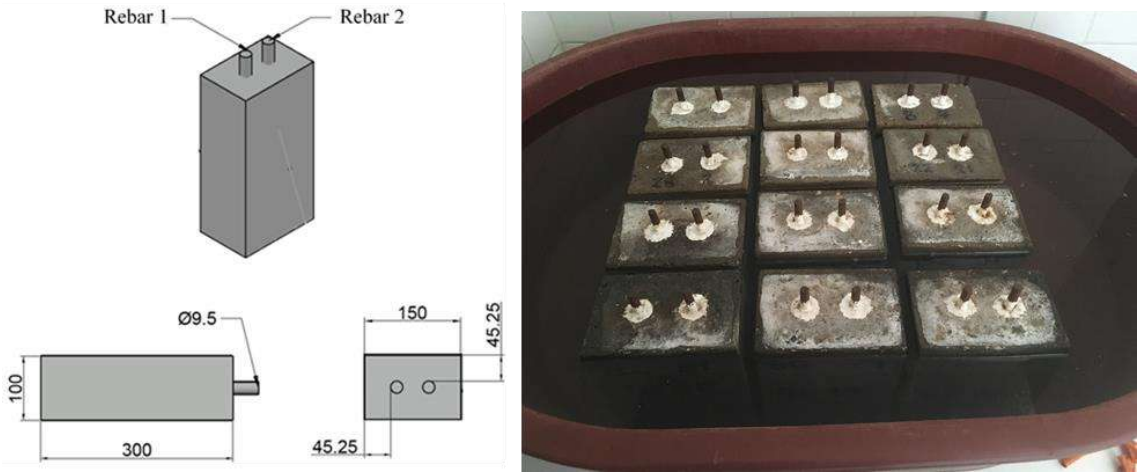

a) b)

Fig. 1. a) Schematic representation of reinforced prismatic specimens (mm) and b) exposure

2.4 Assessment of the corrosion condition of the reinforcing steel

The risk of corrosion of the steel bars embedded in the different concrete prisms exposed to the Cl^- solution was evaluated by corrosion potentials (E_{corr}) and corrosion current density (I_{corr}) in a weekly manner for 2500 days, and some of the results have been already presented in a previous paper [14]. After 3000 days of monitoring the specimen having the highest risk of corrosion from each mixture was selected. From here on, all the procedures and results correspond to these four selected reinforced concrete prisms.

A corrosion potential map for each one of the four selected concrete prisms was elaborated. To do this, the prisms were discretized, and a mesh containing 98 intersection points was drawn. E_{corr} measurements were then taken at each intersection of the mesh for each specimen following the procedures recommended by the ASTM C876-15 standard [29]. An Ag/AgCl

reference electrode and a high-impedance voltmeter Miller™ were used for this purpose. Significant differences between the E_{corr} values were analyzed by an ANOVA, and multiple comparisons between such values for all the mixtures were carried out using Tukey Post-Hoc tests.

2.5 Estimation of the theoretical mass loss (TML) of the reinforcing steel

The TML of all rebars embedded in the selected prisms from the previous section were estimated. For this purpose, the results from I_{corr} mentioned in the previous section were used. The I_{corr} values were obtained by the LPR technique using a potentiostat Gamry™ series G300, an Ag/AgCl reference electrode, and a stainless-steel bar as external counter. The working electrode was polarized to ±20 mV vs Rref at a scan rate of 0.075 mV/s. The LPR results were processed using the Gamry Echem Analyst™ version 5.1.3 software to obtain the corrosion current intensity (I_{corr}). After that, the total integrated corrosion (TIC) was estimated according to the ASTM G 109-07 standard [30]. Finally, the TML of the rebars embedded in the concrete mixtures was calculated using the Faraday´s law for electrolysis (Eq. 1), considering a valence (n) of 2 as recommended by Lu et al. [31].

$$TML = \frac{TIC \cdot M}{(F \cdot n)(Um)}\ x\ 100 \qquad \text{Eq. (1)}$$

where *TIC* is total integrated corrosion (C), *M* is the molar mass of Fe (55.847 g/mol), F is Faraday constant (96500 C/mol) and, Um is the uncorroded mass of rebar (g).

2.6 Extraction of the reinforcing steel, visual inspection and obtaining corrosion products

After the electrochemical monitoring ended, the selected prismatic concrete specimens were autopsied. The surrounding concrete to the reinforcement steel was removed using a CONTROLS^{TM} Model 55-C0210/DZ saw cutting machine (Fig. 2a). As a result, four prismatic samples of 20 x 70 x 300 mm^3 containing the reinforcing bars were obtained (Fig. 2b). The rebars were identified as No 7 and 8, 27 and 28, 33 and 34, and 77 and 78 for those embedded in the mixtures C, T0, T1 and, T2, respectively.

a)

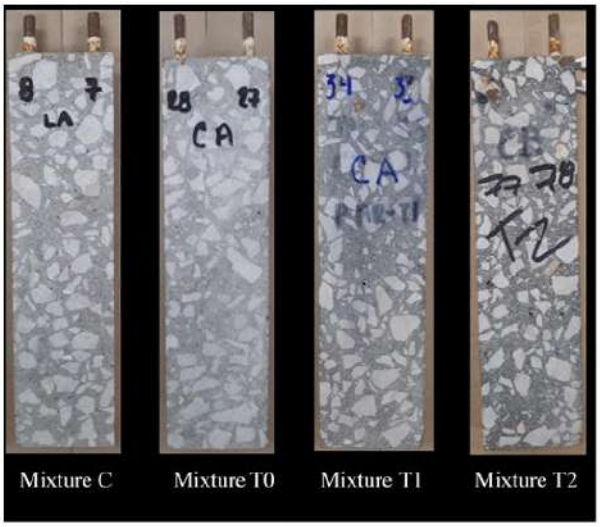

b)

Fig. 2. a) Photographs of the removal process of the surrounding concrete to the reinforcing steel and b) concrete samples obtained after removal

After labeling, the rebars were extracted and the condition of their surfaces was immediately inspected. The surface area of corrosion (SAC) for each rebar was estimated using a Mitutoyo™ Vernier to the measurement of length and width of the corroded zones. Next, the percentage of surface corrosion (PSC) was calculated using the following equation.

$$PSC = \frac{SAC}{OUS} x100\% \quad \text{Eq. (2)}$$

where *SAC* is the surface area of corrosion (cm^2) and *OUS* (cm^2) is original uncorroded surface of the rebars.

While the rebars were extracted, fragments of concrete from the concrete/reinforcement steel interface containing rust and rust-free were also visually inspected for the corrosion products identification. Elemental mapping was carried out for the same fragments using SEM as described later in section 2.7. Moreover, powdered samples were collected with a plastic scraper from the same fragments for corrosion products identification. The powdered samples were split in two for the posterior analyses using XRD and FTIR, as described later in section 2.8.

2.7 Elemental mapping of the concrete/reinforcing steel interface

Concrete fragments taken from the rusted and rust-free zones were selected to carry out elemental mapping by scanning electron microscopy (SEM). The elemental mapping was used to compare the presence of Fe, C, and Cl between both zones. Such elements are of interest in this research due to their main role in the corrosion process. The elemental

mapping was carried out using a high vacuum scanning electron microscope, (SEM) JEOL ™ model JSM-6510LV, equipped with an EDS microanalysis system from Oxford Instruments™. Before the test, the concrete fragments were vacuum dried at room temperature using a vacuum dryer Bachiller™.

2.8 Identification of corrosion products

The first portion of the powdered samples was analyzed by X-ray diffraction (XRD). The XRD tests were carried out using an Empyrean™ diffractometer, equipped with a Cu anode, and operated to a voltage of 45 kV with a current of 40 mA. The XRD data were collected from 5° to 70° (2-Theta) at a scanning speed of 0.5 s and increments of 0.026°. Finally, the crystalline phases from XRD patterns were identified using the X´Pert HighScore Plus™ software. The second portion of the powdered samples was finely ground and then pressed (in a vacuum) in the form of a disc using spectroscopically pure dry K Br. Next, the disc sample was analyzed by FTIR using a NICOLET™ iN10 MX spectrometer. The FTIR tests were performed over the wavenumber range from 2500 to 500 cm^{-1} and the spectral resolution was set to 4 cm^{-1}. Finally, FTIR spectra were identified according to the literature [32-40].

2.8 Estimation of the real mass loss (RML) of the corroded reinforcing steel

The corroded rebars were cleaning using a hydrochloric acid solution as recommended by the ASTM G1-03 Standard [41]. During the procedure uncorroded control rebar was used to register the mass loss due to exposure to the hydrochloric acid solution. Next, the rebars were retired of the solution, and their masses after the exposure to Cl^- (Cm) was registered using

an OHAUS™ analytical balance. The RML due to corrosion of the rebars was determined using the following equation

$$RML = \frac{Um - Cm}{Um} \times 100\% \quad (3)$$

where *Um* is the uncorroded mass of rebars (g) and *Cm* is the mass of the rebar after the exposure to Cl^- (g).

2.9 Tensile tests of the reinforcing steel

After the mass losses of the corroded steel reinforcement were estimated, the rebars were subjected to displacement-controlled tensile testing, in accordance with the ASTM E8/E8-16 standard [42], using an Instron™ universal testing machine. During testing, the loads were measured by a load cell of the testing machine and the linear elongation of the reinforcement by an electrical transducer. The data were processed in the software MATLAB™ to calculate the yield and ultimate strengths and identify the fracture load. Finally, the ductilities of the corroded rebars were estimated using the Eq. 4, as proposed by [43].

$$\mu = \frac{\varepsilon_f}{\varepsilon_Y} \quad (4)$$

where μ is the ductility of the rebar, while ε_f and ε_Y are the fracture and yield strains, respectively.

3. Results and discussion

3.1 Corrosion condition of the reinforcing steel

The means of the E_{corr} obtained from the mapping (Fig. 3) suggest that the steel rebars embedded in the concrete mixtures T0 and T1 had a high risk of corrosion. Results also indicate that bars embedded in the C and T2 underwent severe corrosion as a result of the exposure condition. The ANOVA results indicate that there are significant differences ($p<<0.05$) between the E_{corr} values of the rebars extracted from all the concretes, and the Post-Hoc tests (Table 4) reveal that there are inclusive significant differences between the two rebars extracted from the same concrete mixture. The highest corrosion probability occurred in rebars embedded in mixtures C and T2, while lesser corrosion probability occurred in rebars embedded in the concretesT0 and T1, respectively.

Previous research [14] showed that the same reinforced concretes exposed a NaCl solution by 2500 days had a severe corrosion probability for mixtures C and T0; while the mixtures with UtSCBA presented high corrosion risk. Other studies have also shown that the use of UtSCBA does not negatively affect the corrosion risk of reinforced mortar slabs exposed at Cl^- by 900 days [12]. Since the E_{corr} values were more negative than -246 mV, it seems reasonable to assume that the corrosion in the steel reinforcement took place; therefore, comparisons between the effectiveness of the studied concretes to protect the steel rebars become meaningful.

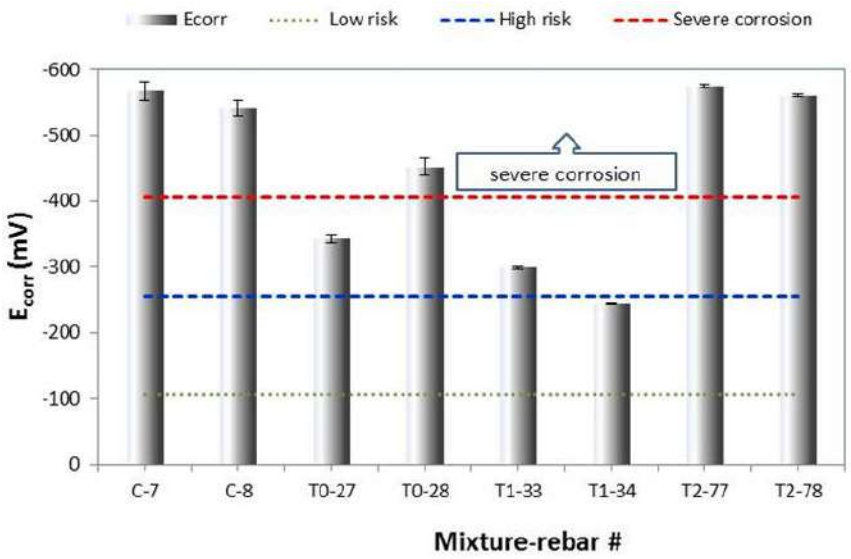

Fig. 3. Summary of the corrosion potentials means for each rebar

Table 4. Results from the Post-Hoc comparison tests (mV)

Rebar #	N	Subgroups							
		1	**2**	**3**	**4**	**5**	**6**	**7**	**8**
T2-77	98	-574.79							
C-7	98		-567.65						
T2-78	98			-560.79					
C-8	98				-540.68				
T0-28	98					-451.49			
T0-27	98						-342.96		
T1-33	98							-299.19	
T1-34	98								-243.42
Sig.		1.00	1.00	1.00	1.00	1.000	1.00	1.00	1.00

For comparison purposes results of the TML are presented in the RML section. In that section, the reliability of the TML estimations based on the results from the LPR technique is going to be evaluated.

3.2 Visual inspection of the corroded reinforcing steel and of the corrosion products

Fig. 4 shows the rebars retrieved from the concrete specimens. In general, all rebars show evidence of corrosion due to the long-term exposition to Cl^-, which agrees with the results from the E_{corr} measurements. A more detailed analysis shows that the rebars embedded in the

ternary concretes containing 10% of UtSCBA (rebars 33 and 34) and 20% UtSCBA (77 and 78) experienced much less corrosion than rebars embedded in both the concretes with only PC (rebars 7 and 8) and with CPC+20%FA (rebars 27 and 28). Table 5 shows the SAC of the rebars after exposure and the PSC of each rebar extracted from the concrete prisms. It can be observed that the rebars of the mixture C presented the highest SAC. The rebars embedded in concretes with 80%CPC+20%FA presented a slightly lower SAC when compared to those rebars embedded in concretes with only PC, but the rebars embedded in concretes containing 10% and 20% of UtSCBA exhibited the lowest SAC.

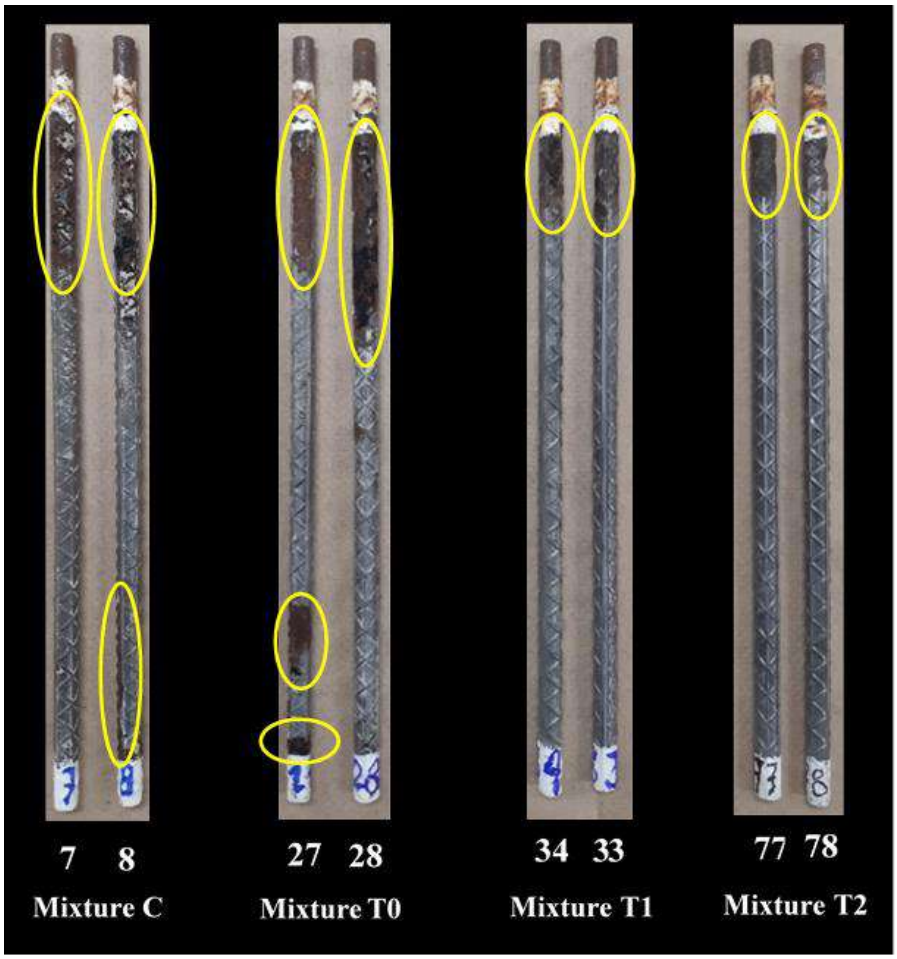

Fig. 4. Corrosion damage of the rebars extracted from the concrete prisms after exposure to Cl^- for 3000 days (Mixture C = 100%PC, Mixture T0 = 80%PC+20%FA, T1= 70%PC+20%FA+10%UtSCBA, and T2 = 60%PC+20%FA+20%UtSCBA)

Table 5. Results of the estimated SAC of rebars.

Surface area	Mixture-rebar#							
	C		T0		T1		T1	
	7	8	27	28	33	34	77	78
OUS, cm^2	77.60	77.60	77.60	77.60	77.60	77.60	77.60	77.60
SAC, cm^2	20.53	19.06	14.79	20.00	12.89	9.37	11.58	10.18
Avg. of the PSC, %	25.51 ± 1.35		22.42 ± 4.75		14.35 ± 3.31		14.02 ± 1.28	

Fig. 5 shows photographs of the corrosion products located at the concrete/ reinforcing steel interface during the extraction of the rebars. Corrosion products can be visually identified by their characteristic colors in order to approximately know the rust composition [44, 45]. Schwertmann [46], Coey et al. [47], and Marcotte and Hansson [48] have reported that the characteristic color of several corrosion products are useful to infer their chemical composition. In accordance with these hints in the present research, the reddish yellow (7.5YR6/6) rust in the concrete/reinforcing steel interface can be associated to akageneite (Fig. 5a), greyish black rust or black iron associated to magnetite (Fig. 5b) and yellow (10YR) and reddish yellow (5YR 6/8) associated to bernalite (Fig. 5c) and lepidocrocite (Fig. 5d), respectively. Also, dark red (10R 3/6) and reddish-brown (2.5YR 3/4) are characteristic of feroxyhyte (Fig. 5e) and maghemite (Fig. 5f), respectively.

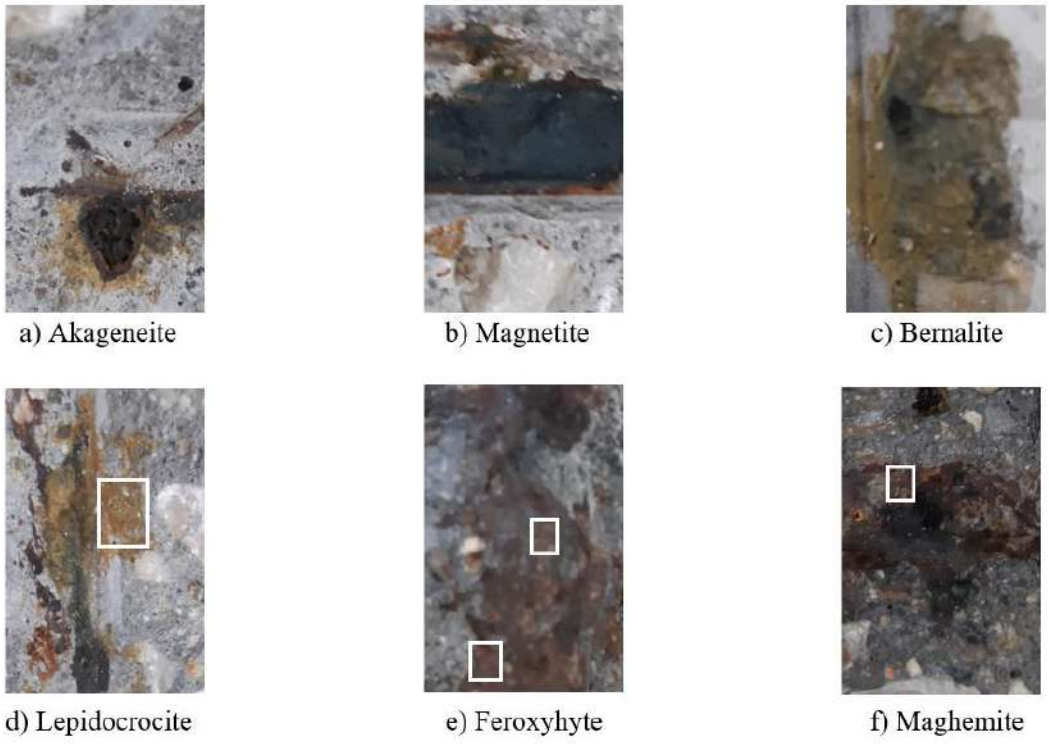

a) Akageneite - *mixture C*, b) Magnetite - *mixture T0*, c) Bernalite - *mixture T1*, d) Lepidocrocite - *mixture T2*, e) Feroxyhyte - *mixture T1*, and f) Maghemite - *mixture T2*.
Fig 5. Photographic record of the corrosion products localized at the concrete/reinforcing steel interface of the mixtures concrete

3.3 Elemental mapping of the concrete/reinforcing steel interface of the mixtures

Figs. 6 to 9 show selected photographs of the concrete/ reinforcing steel interfaces the C, T0, T1, and T2 concrete specimens, respectively. Figures also show micrographs from rusted and rust-free zones at the same concrete/reinforcing steel interface and elemental maps obtained from the latter. Elemental maps display the distribution of certain elements of interest in the sample. The contrast between two elemental maps helps to differentiate specific characteristics of two different composites or the change of characteristics of the same composite after the occurrence of a specific phenomenon. For example, the contrast of Iron, Chlorine and Carbon maps obtained from rusted and rust-free zones evidence the presence

of corrosion products, the Cl^- diffusion might be the indication of the presence of a binding element or an indicator of the different nature of the concretes.

Elemental maps for C, taken from the rust-free zones explain the presence of $CaCO_3$ from the CPC used to manufacture the concrete mixtures. For the maps taken from the rusted zone also might explain the presence of the typical carbon particles coming from the UtSCBA [49]. Certain carbon particles can work as an absorbent media for Cl^- ions [50]; this effect may contribute, in a way, to the low corrosion of the rebars embedded in the mixtures T1 and T2.

Elemental maps for Cl from the rust zones show a higher presence of chlorine with respect to the free-rust zones, which suggests that in these zones higher concentrations of Cl^- can be the cause of the corrosion of the rebars. Elemental maps for Fe show the presence of Fe cementitious compounds of the concrete itself. Furthermore, maps from both rusted and rust-free evidence the existence of a higher concentration of Fe indicating the presence of the corrosion products, as a result of the occurrence of Cl^--induced corrosion.

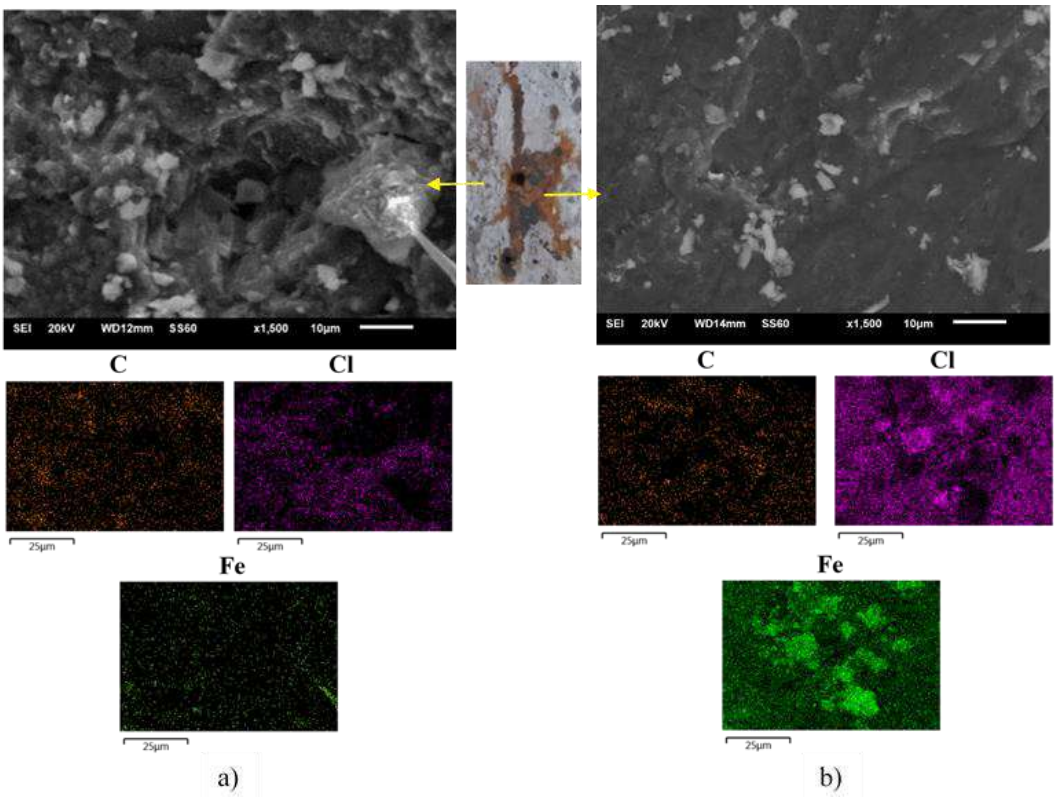

Fig. 6. Elemental mapping of concrete/reinforcing steel interface of the mixture C

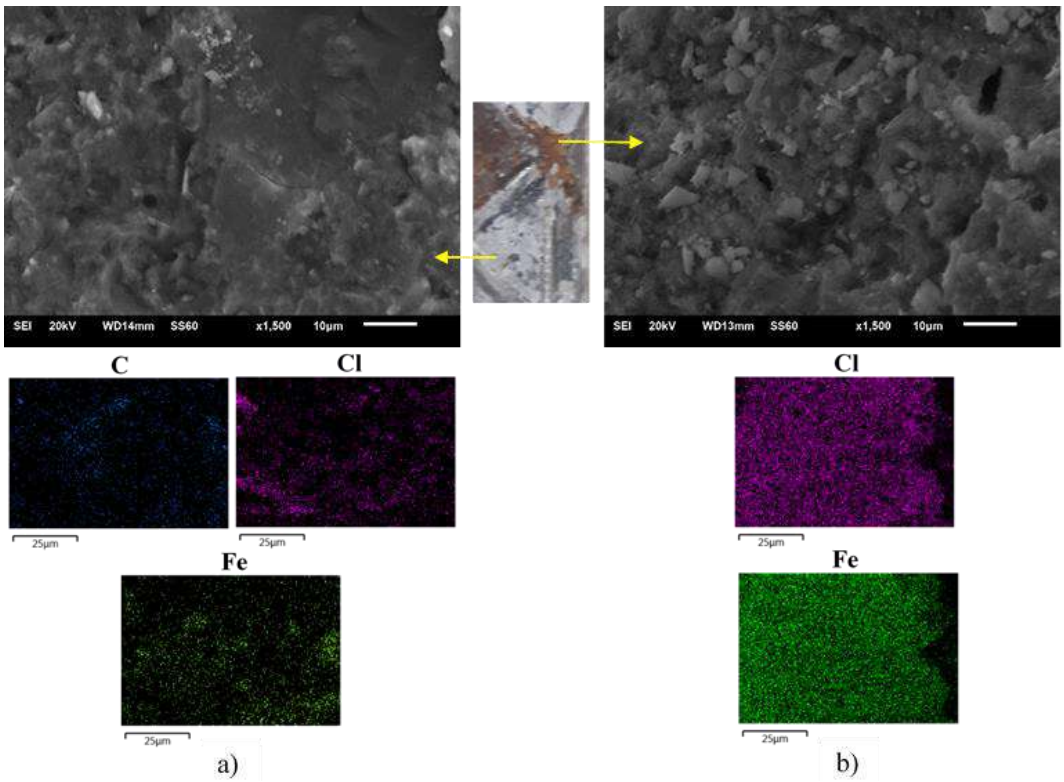

Fig. 7. Elemental mapping of concrete/reinforcing steel interface of the mixture T0

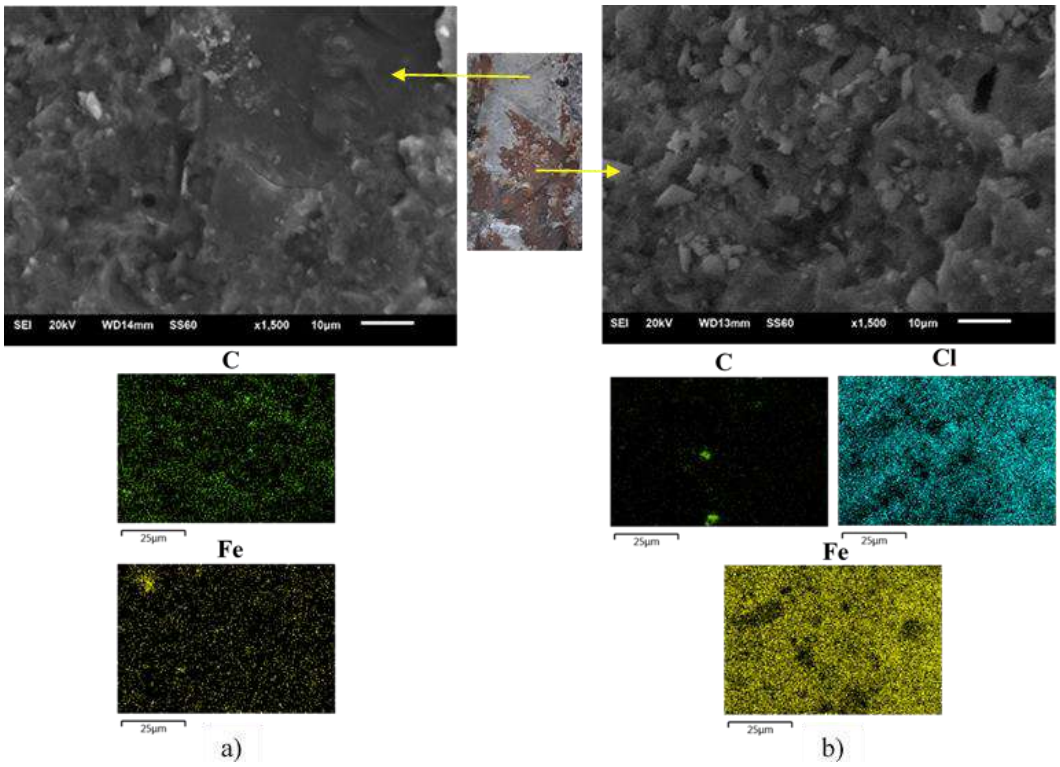

Fig. 8. Elemental mapping of concrete/reinforcing steel interface of the mixture T1

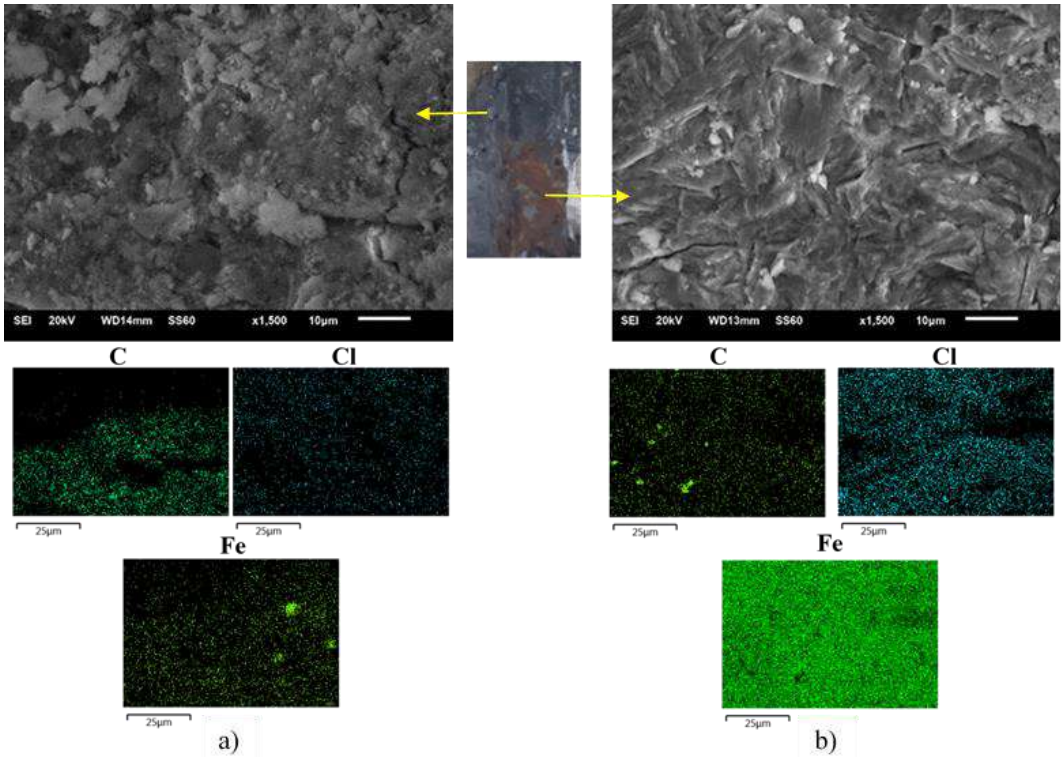

Fig. 9. Elemental mapping of concrete/reinforcing steel interface of the mixture T2

3.4 Identification of the corrosion products

Fig. 10 illustrates the XRD and FTIR spectra of the corrosion products extracted of the reinforcing steel embedded in the studied concrete mixtures. First, the XRD spectra show that the rust produced during the long-term exposition of the reinforced concretes to the NaCl solution is composed of akageneite (β-FeOOH), bernalite ($Fe(OH)_3$), lepidocrocite (γ-FeOOH), goethite (α-FeOOH), wustite (FeO), magnetite (Fe_3O_4), maghemite (γ-Fe_2O_3), and β-$Fe(OH)_3Cl$. This last phase has been identified as an intermediate phase to form akageneite [51]. In the case of wustite, its identification can be explained by its initial presence in the metallic substrate as inclusions [52]. In the case of magnetite and maghemite, both show the same XRD patron since these have a similar spinel structure and very close lattice constants [33].

The XRD analysis is consistent with that reported in the literature, where several studies about the reinforcing steel corrosion have demonstrated that the rust is mainly composed of lepidocrocite, goethite, and maghemite [53, 54]. In the particular case of reinforcement concretes exposed to a marine environment, studies report that it is common to find magnetite [55], while akageneite is a characteristic phase of chloride ions presented in the corrosion process [56]. In this perspective, both corrosion products were also identified in the XRD spectra as a result of Cl^--induced corrosion of the reinforcing steel embedded in the studied concretes.

The FTIR spectra of the corrosion products from the reinforcing steel embedded in the studied concretes are illustrated in Fig. 10b. It is known that the absorption peaks from the FTIR spectra of iron oxides present a high wavenumber region due to OH stretching and bending and at lower wavenumber as a result of Fe-O and Fe-O-H lattice vibrations [32,38].

In this respect, Fig. 9b shows the characteristic absorption peak of the OH stretching of akageneite at 1615 cm^{-1} [35], and an absorption peak at 1020 cm^{-1} for the OH bending of lepidocrocite [37]. The absorption peaks due to O-H bending occur at 1400 cm^{-1} and 1000 cm^{-1} for goethite (a-FeOOH) [33]. Unlike the XRD diagram, the FTIR analysis allows identifying to magnetite and maghemite. The IR spectra of magnetite show absorption peaks of iron oxyhydroxide for the Fe-O-H and Fe–O vibrations at 580 cm^{-1} and 566 cm^{-1} [39], while maghemite shows absorption peaks at 630 cm^{-1} and 550 cm^{-1} [33, 38]. The analysis of the FT-IR spectra is consistent with the results from XRD, specifically in the case of corrosion products associated with Cl^--induced corrosion such as akageneite and magnetite [53].

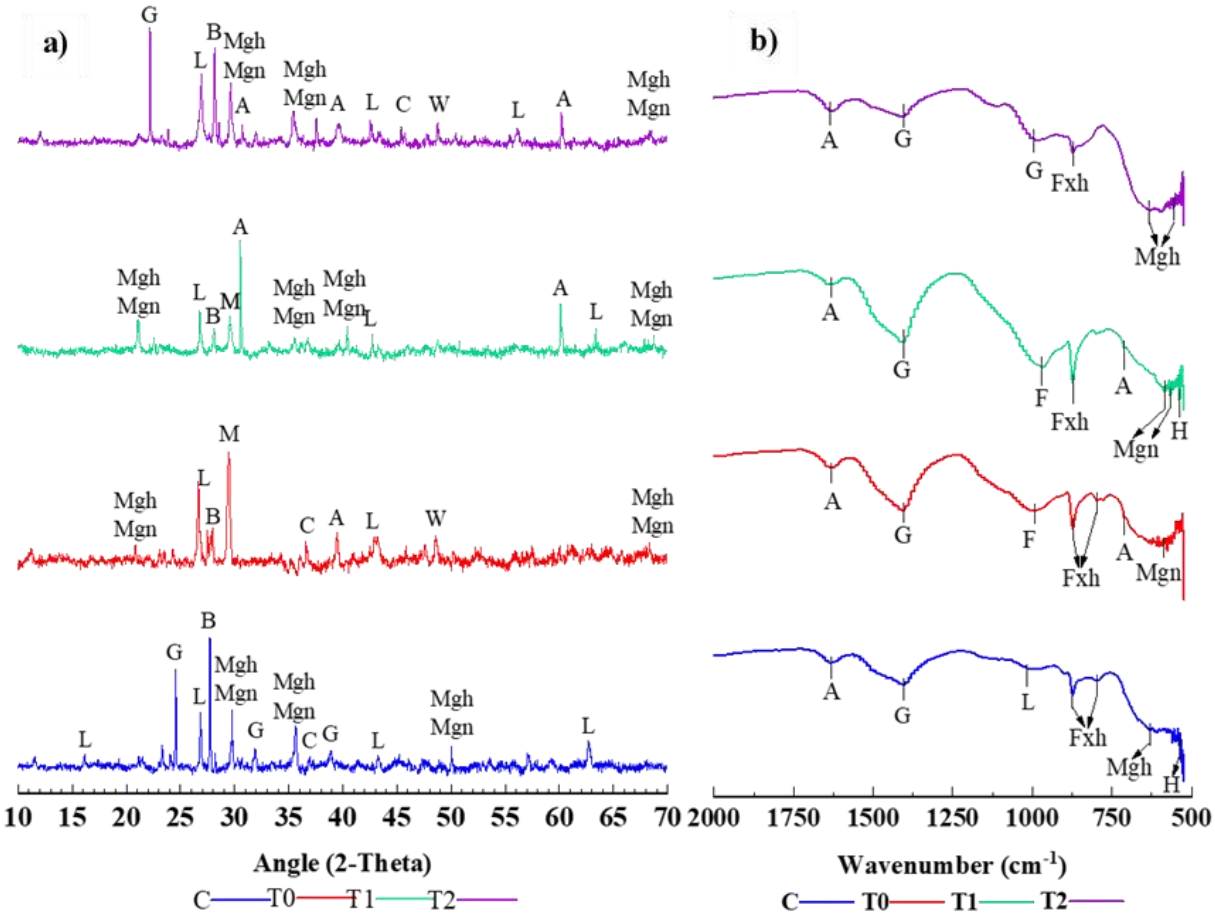

A: Akageneite (β-FeOOH); B: Bernalite ($Fe(OH)_3$); F: Ferrihydrite ($Fe_2O_3{\cdot}4{-}5H_2O$)
Fxh: Feroxyhyte (δ-FeOOH) L:Lepidocrocite (γ-FeOOH); G: Goethite (α-FeOOH);
Mgn: Magnetite (Fe_3O_4); Mgh: Maghemite (γ-Fe_2O_3); C: β-$Fe(OH)_3Cl$; W: Wuestite (FeO)

Fig 10. a) XRD patterns and b) FTIR spectra of the corrosion products recollected from concrete/reinforcing steel interface of the concrete mixtures

It is to be noted that the FTIR spectra showed corrosion products that could not be identified from the XRD results. Several investigations have reported that feroxyhyte (δ-FeOOH) shows absorption peaks between 1602 cm^{-1} and 750 cm^{-1} [33, 36]. In this research, absorption peaks at 880 cm^{-1} and 798 cm^{-1}, assigned to the OH bending, were identified for feroxyhyte. Another corrosion product identified by FTIR is haematite (α-Fe_2O_3), which has a key absorption peak at 539 cm^{-1} assigned to the Fe-O stretching [40]. In the case of ferrihydrite ($Fe_2O_3{\cdot}4{-}5H_2O$), its identified absorption peaks were at 975 cm^{-1} and 989 cm^{-1} [34].

3.5 RML and TML of the reinforcing steel extracted from the concretes

Table 6 shows the RML of the rebars caused by corrosion. The results indicate that the rebars extracted of the mixture C had the highest mass loss followed by those extracted from mixture T0. On the contrary, rebars extracted from T1 y T2 experienced lower mass losses than the rebars from both mixture C and T0. Results from the SAC suggest that the damage of rebars extracted from concretes C and T0 are similar; however, the RML estimations evidence the beneficial effect of the addition of 20%FA. This fact can be explained by the pozzolanic reaction between the FA and the $Ca(OH)_2$ generated from the hydration of the Portland cement [13, 57]. This reaction produces secondary C-S-H, which creates a more complex and less permeable microstructure with respect to concretes with only PC. In consequence, the ingress of chlorides, which is the driving force for corrosion to occur, is diminished [14]. Rebars extracted from mixtures T1 and T2 had lower RML than those extracted in concretes manufactured with only PC and PC+FA. This fact indicates that the combinations of 20%FA with 10%UtSCBA and 20%UtSCBA produce concretes with higher protection against Cl^--induced corrosion. This beneficial effect is the result of the improvement of several microstructural properties: (a) a significant reduction of the percentage of voids, (b) a more complex cementitious matrix, and (c) a lower diffusivity of Cl^- [14]. These improvements are a consequence of the pozzolanic reaction between the amorphous silica and alumina of the UtSCBA with the Portlandite from the CPC hydration [11, 13]. Another explanation by the best performance of the UtSCBA-ternary concretes against Cl^--induced corrosion is their chloride binding capacity as was shown in the previous chapter. The above reduces the amount of available free Cl^- to corrode their rebars.

Table 6 also shows the TML of the rebars under study. The close values between RML and TML indicate that the results are consistent with each other; where the rebars embedded in the UtSCBA-ternary concretes were those who showed the lowest RML and the lowest TML. Results from the RML estimations are consistent with results from corrosion potentials and SAC.

Table 6. Summary of RML and TML of rebars embedded in the concretes estimated after 3000 days of exposure to Cl^-.

Mixture	Rebar	Uncorroded rebars mass (g)	Corroded rebars mass (g)	RML (%)	Avg. RML (%)	TML loss (%)	Avg. TML (%)	Difference between RML and TML (%)
C	**7**	171.31	168.20	1.82	2.19 ± 0.38	1.70	2.27 ± 0.58	3.65
	8	169.48	165.12	2.57		2.84		
T0	**27**	171.07	169.64	0.84	0.93 ± 0.10	0.80	0.87 ± 0.07	6.45
	28	171.30	169.53	1.03		0.93		
T1	**33**	170.05	169.01	0.61	0.62 ± 0.01	0.59	0.60 ± 0.01	3.22
	34	169.46	168.38	0.64		0.62		
T2	**77**	172.02	170.98	0.60	0.68 ± 0.08	0.61	0.66 ± 0.06	2.94
	78	170.16	168.86	0.76		0.72		

Notes: standard deviations of the Avg. real and theoretical mass losses were obtained using only the two measurements

3.6 Mechanical properties of the reinforcing steel extracted

Fig. 11 shows the stress-strain diagrams of the corroded rebars. All rebars show the typical behavior of a steel bar subjected to tensile stress. The rebars exhibited a linear elastic behavior with no significant difference (p=0.489) between their elasticity modulus (EM) compared to 210000 MPa from the literature [58]. The yield strains from the rebars were similar to 0.002 (p=0.470), which is in accordance with [42].

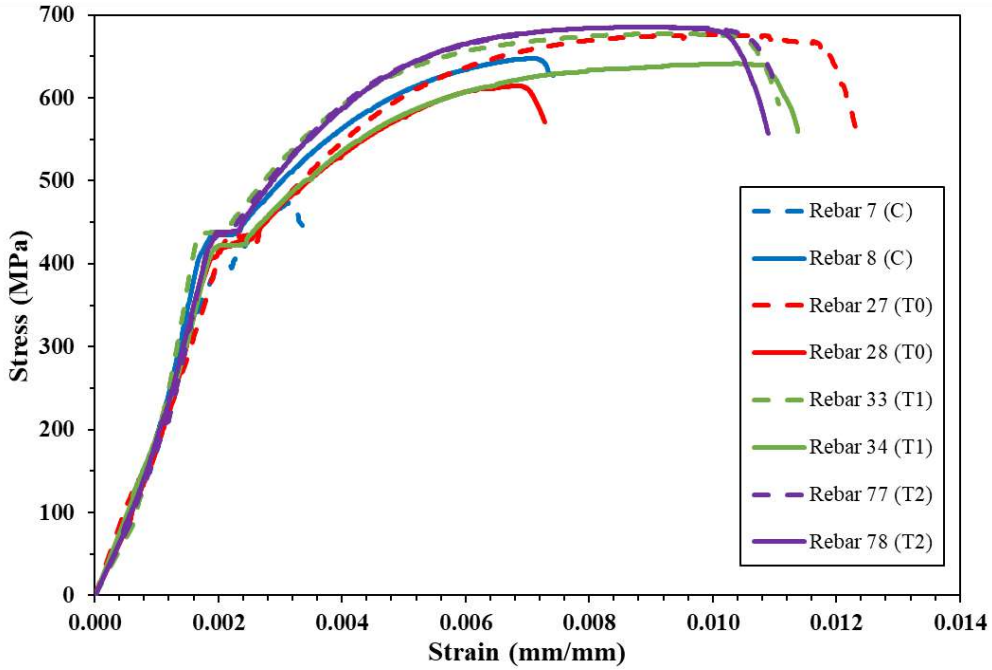

Fig. 11. Stress-strain curves of the corroded rebars embedded in the studied concrete mixtures

There was also no significant difference between the yield stresses (f_Y) of the rebars ($p=0.279$) and the value 420 MPa reported for this type of steel; however, significant differences ($p=0.013$, $p<<0.05$, and $p<<0.05$) between the ultimate stress (f_U), the fracture load (Fl) and the elongations (e) were found when these values were compared to 720 MPa, 48 kN and 10% [59], respectively.

Next, the effects of RML on the tensile parameters of the corroded rebars are analyzed. Fig. 12a clearly shows that the corrosion damage practically does not affect the yield strenths of the rebars. On the contrary, Fig. 12b shows that the damage caused by corrosion negatively affects the ultimate strengths of the steel reinforcement. In this case, when the corrosion damage increases, the average ultimate strength decreases. This behavior is evident for rebars extracted from the mixture C. A similar pattern like the one seen in the ultimate strength can be observed for the Fl, which is shown in Fig. 12c. Again, specimens with higher corrosion damage failed to lower loads. Fracture loads for rebars embedded in T0 mixture were 12%

and 18% higher than those embedded in the mixture C; while ultimate loads for T1 and T2 were 20% and 18%, and 22% and 15% higher than the mixture C, respectively.

The results shows that the RML due to corrosion by Cl^- did not affect the EM and f_Y of all studied rebars; however, their f_U and F_l are negatively affected by damage due to Cl^-. The non-negative effect of the corrosion by Cl^- on the ME and f_Y of all rebars can be owing to that these parameters depend on the chemical composition and manufacture of the reinforcing steel [60]. Corrosion removes iron ions only from the corroded surface area and does not change the nature and composition of the remaining rebar.

Different effects of the corrosion on the f_Y and f_U have been reported in the literature. Almusallam, [18] found that an RML about 11.6% slightly reduced the f_Y and f_U of rebars grade 60 corroded by an impressed current. On the other hand, Du et al. [60] reported that the f_Y and f_U of corroded bars up to 16% by impressed current were not significative affected with respect to uncorroded bars.

The effect of the RML on the ductilities of the rebars is illustrated in Fig 12d. In this figure is evident that the rebars with the highest RML presented the lowest ductility values. Average values (square markers) demonstrate a clear beneficial effect when 20% of CPC is replaced by FA (mixture T0). This beneficial effect is magnified when 10%CPC is replaced by UtSCBA (mixture T1). The results also indicate that no additional beneficial effect is experienced when CPC is replaced by 20% of UtSCBA. In spite of the limited amount of data, this trend can be represented by the linear relationship $\mu = -2.1274\ RML + 6.9765$ with a coefficient of correlation $R=0.96$.

In general, a comparison between Figs. 12b against 12c and 12d corroborates that the deleterious effect of RML on μ is much more significant than on f_U and Fl. This effect is the result of the ductility affected by both the morphology and distribution of the corrosion [22]. The results of the ductility obtained in this research agree with other studies about its effect on the ductility of reinforcing steel. Almusallam [18] found that an RML of 1% reduced the ductility of the corroded rebars by impressed current with respect to non-corroded rebars. From that research was reported that an RML higher than 12.6%, the corroded rebars exhibited a fragile behavior. Furthermore, Du et al. [19] reported that RML of 10% reduced the ductility of corroded rebar by impressed current, much more than the yield and ultimate strengths.

From the performance showed by the corroded rebars extracted from UtSCBA-ternary concretes when tested in tension, it can be affirmed that the use of UtSCBA, in order to produce ecological concretes, is a viable option. A previous study on the same concretes showed that the combination of FA+UtSCBA did not negatively affect the long-term mechanical properties of these ternary-concretes [13]. Moreover, this combination produces concretes with better microstructural properties and lower diffusivity than concretes with only PC. The above reduced the probability and corrosion rate of the rebars embedded in the UtSCBA-ternary concretes [14]. The results of this paper show clear evidence of the superior long-term performance of the UtSCBA-ternary concretes against Cl^--induced corrosion. Moreover; mechanical properties of the rebars embedded in the concretes with UtSCBA were affected to a less degree by corrosion than to the rebars from concretes with CPC+FA only CPC.

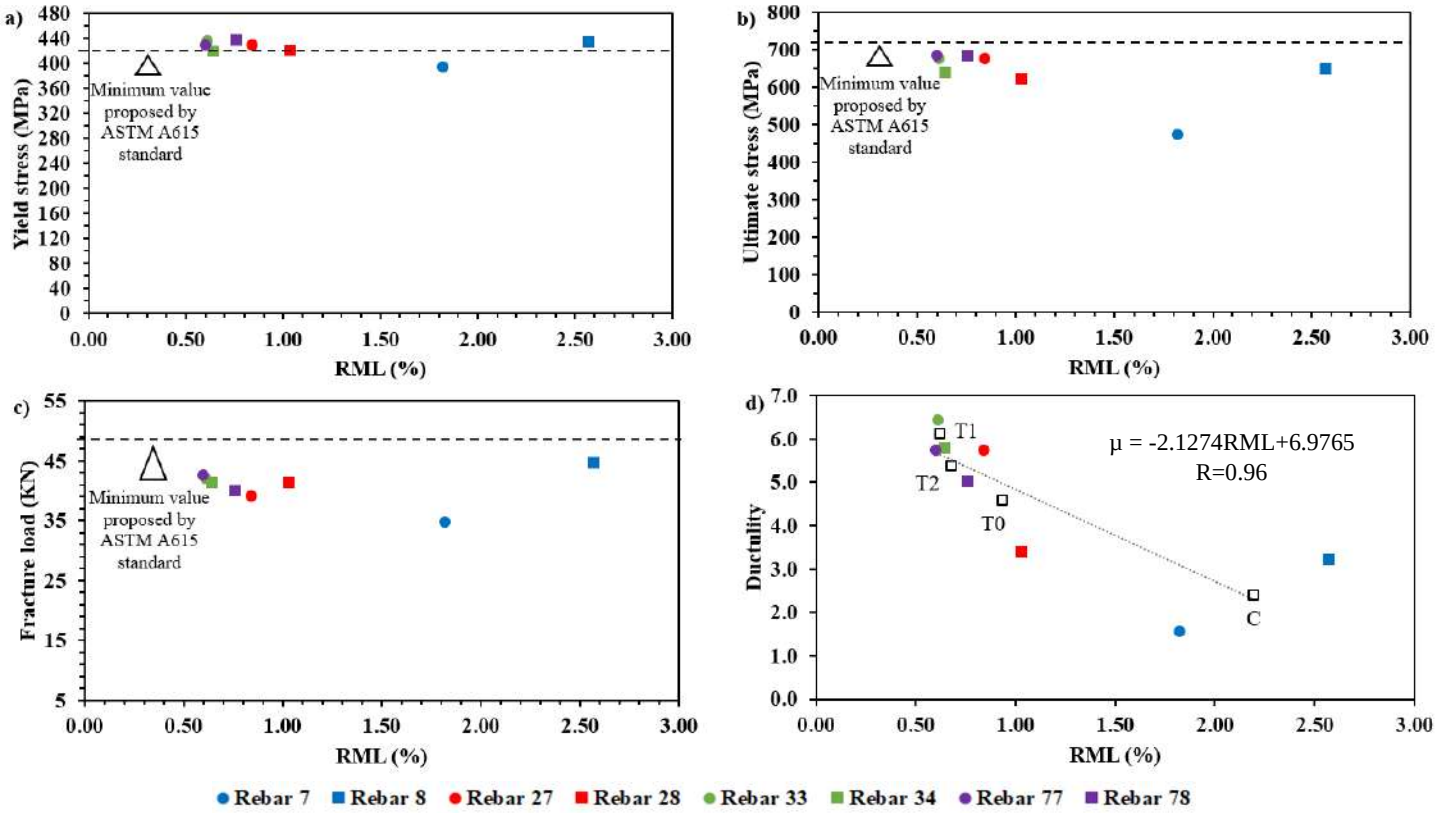

Fig. 12. Effect of the RML on the mechanical properties of the rebars extracted from the concrete mixtures.

Conclusions

In accordance with the results obtained under the conditions in this research, the following conclusions can be drawn:

1. The addition of 10%UtSCBA and 20%UtSCBA to concretes with 20%FA caused lower surface corrosion and lower mass loss on the reinforcing steel when compared to both concrete containing only PC and PC+20%FA.
2. The linear polarization resistance is a reliable technique to predict the mass loss of steel reinforcement embedded in concrete exposed to a Cl^- contaminated environment.

3. Yield strength of steel reinforcement embedded in the concretes under investigation was not significantly affected by the mass losses estimated in this research, which ranged from 0.6 and 2.57%.
4. Ultimate strengths and fracture loads of reinforcing steel extracted from concrete prisms exposed for 3000 days to a Cl^- solution were negatively affected by corrosion. Reductions until 34 and 28% for ultimate stress and fracture load, respectively, were experienced when these values are compared to those indicated by the ASTM A615/A615M-16 standard.
5. Ductility of the reinforcing steel was significantly affected by corrosion. Ductilities of rebars embedded in concretes containing 10% of UtSCBA were 2.56 and 1.34 times higher than ductilities of bars from concretes that containing only CPC and CPC+20%FA, respectivaley. Similarly, ductilities of rebars embedded in concretes containing 20% of UtSCBA were 2.25 and 1.18 times higher, respectively.

Conflict of interest

The authors declare no conflict of interest.

Acknowledgments

The authors are grateful to the Instituto Politécnico Nacional of Mexico (IPN) for the facilities and financial support provided for this research. Furthermore, the authors thank the Facultad de Ingeniería Civil of the Universidad Autónoma de Nuevo León in Mexico for the

use of its facilities and equipment for the extraction of the rebars and characterization of the corrosion products. The authors are also grateful to Mexico´s Consejo Nacional de Ciencia y Tecnología (CONACyT) for the doctoral scholarship granted to Víctor Alberto Franco-Luján.

References

[1] B. Šavija, E. Schlangen, Chloride ingress in cracked concrete a literature review BT Advances in Modeling Concrete Service Life, in: C. Andrade, J. Gulikers (Eds.), Springer Netherlands, Dordrecht, 2012: pp. 133–142.

[2] Y.G. Du, L.A. Clark, A.H.C. Chan, Residual capacity of corroded reinforcing bars, Mag. Concr . Res. 57 (2005) 135–147.

[3] M.C.G. Juenger, R. Siddique, Recent advances in understanding the role of supplementary cem entitious materials in concrete, Cem. Concr. Res. 78 (2015) 71–80.

[4] N. Chousidis, E. Rakanta, I. Ioannou, G. Batis, Mechanical properties and durability performan ce of reinforced concrete containing fly ash, Constr. Build. Mater. 101 (2015) 810–817.

[5] H.Z. Lopez Calvo, P. Montes Garcia, E.M. Alonso Guzmán, W. Martinez Molina, T.W. Bremn er, M.D.A. Thomas, Effects of corrosion inhibiting admixtures and supplementary cementiti ous materials combinations on the strength and certain durability properties of HPC, Can. J. Civ. Eng. 44 (2017) 918–926.

[6] A.G. Lekatou, S. Tsouli, C. Nikolaidis, S. Kleftakis, I.K. Tragazikis, T.E. Matikas, Effect of fly ash on the corrosion performance and structural integrity of stainless steel concrete rebars in acid rain and saline environments, Frat. Ed Integrita Strutt. 13 (2019) 423–437.

[7] M.A. Baltazar Zamora, D.M. Bastidas, G. Santiago Hurtado, J.M. Mendoza Rangel, C. Gaona Tiburcio, J.M. Bastidas, F. Almeraya Calderón, Effect of silica fume and fly ash admixtures on the corrosion behavior of AISI 304 embedded in concrete exposed in 3.5% NaCl solution , Materials (Basel). 12 (2019).

[8] M.J. McCarthy, T. Robl, L.J. Csetenyi, 14 Recovery, processing, and usage of wet stored fly as h, in: T. Robl, A. Oberlink, R.B.T. C.C.P. (CCP's) Jones (Eds.), Woodhead Publishing, 201 7: pp. 343–367.

[9] V.G. Jiménez Quero, F.M. León Martínez, P. Montes García, C. Gaona Tiburcio, J.G. Chacón Nava, Influence of sugar cane bagasse ash and fly ash on the rheological behavior of cement pastes and mortars, Constr. Build. Mater. 40 (2013) 691–701.

[10] J.C. Arenas Piedrahita, P. Montes García, J.M. Mendoza Rangel, H.Z. López Calvo, P.L. Vald ez Tamez, J. Martínez Reyes, Mechanical and durability properties of mortars prepared with untreated sugarcane bagasse ash and untreated fly ash, Constr. Build. Mater. 105 (2016) 69–81.

[11] M.A. Maldonado García, U.I. Hernández Toledo, P. Montes García, P.L. Valdez Tamez, The influence of untreated sugarcane bagasse ash on the microstructural and mechanical properties of mortars, Mater. Constr. 68 (2018) 1–13.
[12] M.A. Maldonado García, U.I. Hernández Toledo, P. Montes García, P.L. Valdez Tamez, Long term corrosion risk of thin cement composites containing untreated sugarcane bagasse ash, J. Mater. Civ. Eng. 31 (2019) 1–13.
[13] V. Ríos Parada, V.G. Jiménez Quero, P.L. Valdez Tamez, P. Montes García, Characterization and use of an untreated Mexican sugarcane bagasse ash as supplementary material for the preparation of ternary concretes, Constr. Build. Mater. 157 (2017) 83–95.
[14] V.A. Franco Luján, M.A. Maldonado García, J.M. Mendoza Rangel, P. Montes García, Chloride induced reinforcing steel corrosion in ternary concretes containing fly ash and untreated sugarcane bagasse ash, Constr. Build. Mater. 198 (2019) 608–618.
[15] Y. Du, L.A. Clark, A.H.C. Chan, Impact of reinforcement corrosion on ductile behavior of reinforced concrete beams, ACI Struct. J. 104 (2007)
[16] I. Fernandez, J.M. Bairán, A.R. Marí, Corrosion effects on the mechanical properties of reinforcing steel bars. Fatigue and σ-ε behavior, Constr. Build. Mater. 101 (2015) 772–783.
[17] Y.C. Ou, Y.T.T. Susanto, H. Roh, Tensile behavior of naturally and artificially corroded steel bars, Constr. Build. Mater. 103 (2016) 93–104.
[18] A.A. Almusallam, Effect of degree of corrosion on the properties of reinforcing steel bars, Constr. Build. Mater. 15 (2001) 361–368.
[19] Y.G. Du, L.A. Clark, A.H.C. Chan, Residual capacity of corroded reinforcing bars, Mag. Concr. Res. 57 (2005) 135–147.
[20] W. Zhu, R. François, Experimental investigation of the relationships between residual cross section shapes and the ductility of corroded bars, Constr. Build. Mater. 69 (2014) 335–345.
[21] C.A. Apostolopoulos, V.G. Papadakis, Consequences of steel corrosion on the ductility properties of reinforcement bar, Constr. Build. Mater. 22 (2008) 2316–2324.
[22] W. Zhu, R. François, C.S. Poon, J.G. Dai, Influences of corrosion degree and corrosion morphology on the ductility of steel reinforcement, Constr. Build. Mater. 148 (2017) 297–306.
[23] NMX C 414 ONNCCE 2004. Industria de la construcción cementos hidráulicos especificaciones y métodos de prueba, normas mexicanas, organismo nacional de normalización y certificación de la construcción y edificación, S.C. p. 1–2 (in Spanish).
[24] ASTM C618 19, Standard Specification for Coal Fly Ash and Raw or Calcined Natural Pozzolan for Use in Concrete, ASTM International, West Conshohocken, PA, 2019.
[25] H.F.W. Taylor, Cement chemistry, Thomas Telford Publishing, 1997.
[26] A.C.I.C. 211, Standard Practice for Selecting Proportions for Normal, Heavyweight, and Mass Concrete:(ACI 211.1-91), in: American Concrete Institute, 1991.
[27] ASTM C143/C143M15a, Standard Test Method for Slump of Hydraulic Cement Concrete, ASTM International, West Conshohocken, PA, 2015.
[28] ASTM A615/A615M20, Standard Specification for Deformed and Plain Carbon Steel Bars for Concrete Reinforcement, ASTM International, West Conshohocken, PA, 2020.
[29] ASTM C876 M15, Standard Test Method for Corrosion Potentials of Uncoated Reinforcing Steel in Concrete, ASTM International, West Conshohocken, PA, 2015.

[30] ASTM G109 M07, Standard Test Method for Determining Effects of Chemical Admixtures o n Corrosion of Embedded Steel Reinforcement in Concrete Exposed to Chloride Environme nts, ASTM International, West Conshohocken, PA, 2013.
[31] C. Lu, W. Jin, R. Liu, Reinforcement corrosion induced cover cracking and its time prediction for reinforced concrete structures, Corros. Sci. 53 (2011) 1337–1347.
[32] G. Nauer, P. Strecha, N. Brinda Konopik, G. Liptay, Spectroscopic and thermoanalytical char acterization of standard substances for the identification of reaction products on iron electrod es, J. Therm. Anal. 30 (1985) 813–830.
[33] A. Raman, B. Kuban, A. Razvan, The application of infrared spectroscopy to the study of atm ospheric rust systems I. Standard spectra and illustrative applications to identify rust phases i n natural atmospheric corrosion products, Corros. Sci. 32 (1991) 1295–1306.
[34] S. Musić, M. Gotić, S. Popović, X ray diffraction and Fourier transform infrared analysis of th e rust formed by corrosion of steel in aqueous solutions, J. Mater. Sci. 28 (1993) 5744–5752.
[35] B. Weckler, H.D. Lutz, Lattice vibration spectra. Part XCV. Infrared spectroscopic studies on the iron oxide hydroxides goethite (α), akaganéite (β), lepidocrocite (γ), and feroxyhite (δ), Eur. J. Solid State Inorg. Chem. 35 (1998) 531–544.
[36] R. Balasubramaniam, A. V Ramesh Kumar, Characterization of Delhi iron pillar rust by X ray diffraction, Fourier transform infrared spectroscopy and Mössbauer spectroscopy, Corros. S ci. 42 (2000) 2085–2101.
[37] R.K. A.V., N. R.K., M. S.S., M. G.N., Effect of inhibitors on the nature of corrosion products of mild steel by Mossbauer and FTIR spectroscopy, Anti Corrosion Methods Mater. 49 (200 2).
[38] H. Namduri, S. Nasrazadani, Quantitative analysis of iron oxides using Fourier transform infra red spectrophotometry, Corros. Sci. 50 (2008) 2493–2497.
[39] S.A. Kahani, M. Jafari, A new method for preparation of magnetite from iron oxyhydroxide o r iron oxide and ferrous salt in aqueous solution, J. Magn. Magn. Mater. 321 (2009) 1951–1954.
[40] E. Darezereshki, One step synthesis of hematite (α Fe_2O_3) nano particles by direct thermal dec omposition of maghemite, Mater. Lett. 65 (2011) 642–645.
[41] ASTM G1 03(2017)e1, Standard Practice for Preparing, Cleaning, and Evaluating Corrosion Test Specimens, ASTM International, West Conshohocken, PA, 2017.
[42] ASTM E8 / E8M 16ae1, Standard Test Methods for Tension Testing of Metallic Materials, A STM International, West Conshohocken, PA, 2016.
[43] M. Bruneau, C. M. Uang, R. Sabelli, Ductilite Desing of Steel Structures, Second, McGrawHi ll, 2011.
[44] A.C. Scheinost, U. Schwertmann, Color Identification of Iron Oxides and Hydroxysulfates, So il Sci. Soc. Am. J. 63 (1999) 1463–1471.
[45] R. O'Donovan, B.D. O'Rourke, K.D. Ruane, J.J. Murphy, Anaerobic Corrosion of Reinforce ment, Key Eng. Mater. 569–570 (2013) 1124–1131.
[46] U. Schwertmann, Relations Between Iron Oxides, Soil Color, and Soil Formation, in: Soil Col or, Soil Science Society of America, Madison, WI, 1993: pp. 51–69.
[47] J.M.D. Coey, I. V Shvets, R. Wiesendanger, H. Güntherodt, Charge freezing and surface aniso tropy on magnetite (100), J. Appl. Phys. 73 (1993) 6742–6744.

[48] T.D. Marcotte, C.M. Hansson, The influence of silica fume on the corrosion resistance of steel in high performance concrete exposed to simulated sea water, J. Mater. Sci. 38 (2003) 4765 –4776.
[49] A. Bahurudeen, K. Wani, M.A. Basit, M. Santhanam, Assesment of pozzolanic performance o f sugarcane bagasse ash, J. Mater. Civ. Eng. 28 (2016) 1–11.
[50] V. Minkova, M. Razvigorova, E. Bjornbom, R. Zanzi, T. Budinova, N. Petrov, Effect of water vapour and biomass nature on the yield and quality of the pyrolysis products from biomass, Fuel Process. Technol. 70 (2001) 53–61.
[51] S. Reguer, P. Dillmann, F. Mirambet, J. Susini, P. Lagarde, Investigation of Cl corrosion prod ucts of iron archaeological artefacts using micro focused synchrotron X ray absorption spect roscopy, Appl. Phys. A. 83 (2006) 189–193.
[52] W.J. Chitty, P. Dillmann, V. L'Hostis, C. Lombard, Long term corrosion resistance of metalli c reinforcements in concrete A study of corrosion mechanisms based on archaeological artef acts, Corros. Sci. 47 (2005) 1555–1581.
[53] T.D. Marcotte, C.M. Hansson, Corrosion products that form on steel within cement paste, Mat er. Struct. 40 (2007) 325–340.
[54] J.G. Castaño, C.A. Botero, A.H. Restrepo, E.A. Agudelo, E. Correa, F. Echeverría, Atmospher ic corrosion of carbon steel in Colombia, Corros. Sci. 52 (2010) 216–223.
[55] K. Asami, M. Kikuchi, In depth distribution of rusts on a plain carbon steel and weathering st eels exposed to coastal industrial atmosphere for 17 years, Corros. Sci. 45 (2003) 2671– 2688.
[56] O. Poupard, V. L'Hostis, S. Catinaud, I. Petre Lazar, Corrosion damage diagnosis of a reinfor ced concrete beam after 40 years natural exposure in marine environment, Cem. Concr. Res. 36 (2006) 504–520.
[57] G.C. Cordeiro, R.D. Toledo Filho, L.M. Tavares, E.M.R. Fairbairn, Pozzolanic activity and fil ler effect of sugar cane bagasse ash in Portland cement and lime mortars, Cem. Concr. Com pos. 30 (2008) 410–418.
[58] D. Gross, W. Hauger, J. Schröder, W.A. Wall, J. Bonet, Engineering Mechanics 2 Mechanics of Materials, Springer, 2014.
[59] ASTM A615 / A615M-
20, Standard Specification for Deformed and Plain Carbon Steel Bars for Concrete Reinforc ement, ASTM International, West Conshohocken, PA, 2020.
[60] Y.G. Du, L.A. Clarkt, A.H.C. Chan, Effect of corrosion on ductility of reinforcing bars, Mag. Concr. Res. 57 (2005) 407–419.

DISCUSSION

This doctoral thesis aimed to study the effect of long-term Cl^--induced corrosion on the mechanical properties of reinforcing steel bars embedded in ternary concretes. Two ternaries concretes were manufactured when 10% and 20% of PC was replaced by UtSCBA in a binary concrete containing 80%PC+20% of FA (mixtures T1 and T2, respectively). The properties and performances of these ternary concretes were contrasted against those corresponding to concretes manufactured with 100%PC (mixture C) and that containing 80%PC+20%FA (mixture T0).

The analysis of results showed that the addition of 10 and 20% of UtSCBA significantly reduced the percentages of voids (PV) of mixtures T1 and T2. It also showed that the combination FA+UtSCBA did not negatively affect the long-term compressive strength (CS at 2500 days)) of the ternary concretes. This finding indicates that the mechanical properties of the ternary concretes reported by Rios-Parada et al. [1] at an early age are maintained up to a long-term age. Surprisingly, the PV and CS of the ternary concretes from the present research do not correlate well as has been reported by others [2]. This contradiction indicates than the matrices of the ternary concretes are less porous but with similar CSs than those from mixtures C and T0. A possible explanation for this behavior can be that the addition of UtSCBA in the ternary concretes contributes to creating more complex concrete matrices. The complexity of such matrices can be corroborated by the combination of the following ultrasonic parameters: ultrasonic pulse velocity from the P-wave, and spatial attenuation, temporal attenuation, and energetic content from the S-wave.

Results indicate that the addition of UtSCBA significantly decreased the Cl^- diffusion into the ternary concretes. Similar results have also reported in the literature [3, 4]. The low Cl^- diffusivity was the result of the low porosity and more complex microstructures of the ternary concrete mixtures, as it was earlier stated. The above was a consequence of the secondary C-S-H produced by the pozzolanic reaction and the unreacted particles and carbon particles from the UtSCBA. The lower diffusivity of the ternary concretes reduced the Cl^- penetration and the rebars embedded in these concretes experienced fewer negative values of

corrosion potential and lower corrosion current densities than those embedded in concretes with only PC after 2500 days of exposition at Cl^- [5].

Results obtained at 3000 days of age corroborate that the porosity of the ternary concretes was significantly reduced; moreover, the long-term exposure to Cl^- did not cause the phenomenon of C-S-H decalcification [6]; hence, the CSs of the ternary concretes were not significantly affected with respect to mixture C. Furthermore, the results demonstrated that certain amount of Cl^- diffused through the cementitious matrices of the studied concretes chemically reacted with the Afm and Aft phases to form Friedel´s salt. It was corroborated that the concrete with 80%PC+20%FA effectively bound chlorides as reported in the literature [7, 8]; however, the combination FA+UtSCBA produced ternary concretes with higher chloride binding capacities. This finding is relevant because the chloride binding capacity of concretes containing SCBA or UtSCBA has not been previously reported elsewhere in the literature. The results at this point indicate than the apparent higher resistance against Cl^--induced corrosion of the rebars embedded in the ternary concretes is owed by their microstructural changes leading to the following: (I) less porosity, (II) more complexity, (III) less diffusivity, and (IV) higher chloride binding capacity.

Results from the last phase of this research deal with the analysis of the effect of Cl^--induced corrosion on the mechanical properties of the rebars embedded in the ternary concretes. It was corroborated that when 10% and 20% of UtSCBA was added to the 80%PC+20%FA concrete mixture considerable reductions in the steel surface corrosion and mass loss (RML) of the rebars were experienced. Regarding the influence of corrosion on the mechanical properties of the steel reinforcement, the following general effects are presented next. There is a non-significant effect of corrosion on the yield stresses (f_Y) of all the tested rebars, which is in accordance with previous studies [9, 10]. On the contrary, the ultimate stresses (f_U), fracture loads (Fl), and ductilities of all tested rebars were significantly affected by corrosion. The negative effect of corrosion on these parameters is directly correlated with the RML of the rebars because the decrease in the cross-sectional area of the rebar induces stress-concentration which leads to quicker brittle failure of the material [11]. Nevertheless, rebars embedded in the ternary concretes were affected to a less degree. All in all, rebars embedded

in the ternary concretes had higher f_U, higher Fl, and higher ductilities. The mechanism to slow corrosion of the rebars in the ternary concretes relies on the beneficial influence of the improved concrete matrix resulting from the addition of UtSCBA.

References

[1] V. Ríos Parada, V.G. Jiménez Quero, P.L. Valdez Tamez, P. Montes García, Characterization a nd use of an untreated Mexican sugarcane bagasse ash as supplementary material for the pre paration of ternary concretes, Constr. Build. Mater. 157 (2017) 83–95.

[2] C. Lian, Y. Zhuge, S. Beecham, The relationship between porosity and strength for porous con crete, Constr. Build. Mater. 25 (2011) 4294–4298.

[3] N.U. Amin, Use of bagasse ash in concrete and its impact on the strength and chloride resistivit y, J. Mater. Civ. Eng. 23 (2011) 717–720.

[4] M.A. Maldonado García, U.I. Hernández Toledo, P. Montes García, P.L. Valdez Tamez, Long term corrosion risk of thin cement composites containing untreated sugarcane bagasse ash, J. Mater. Civ. Eng. 31 (2019) 1–13.

[5] V.A. Franco Luján, M.A. Maldonado García, J.M. Mendoza Rangel, P. Montes García, Chlorid e induced reinforcing steel corrosion in ternary concretes containing fly ash and untreated su garcane bagasse ash, Constr. Build. Mater. 198 (2019) 608–618.

[6] T. Sugiyama, W. Ritthichauy, Y. Tsuji, Simultaneous Transport of Chloride and Calcium Ions i n Hydrated Cement Systems, J. Adv. Concr. Technol. 1 (2003) 127–138.

[7] T. Cheewaket, C. Jaturapitakkul, W. Chalee, Long term performance of chloride binding capaci ty in fly ash concrete in a marine environment, Constr. Build. Mater. 24 (2010) 1352–1357.

[8] W. Chalee, T. Sasakul, P. Suwanmaneechot, C. Jaturapitakkul, Utilization of rice husk bark ash to improve the corrosion resistance of concrete under 5 year exposure in a marine environ ment, Cem. Concr. Compos. 37 (2013) 47–53.

[9] W. Zhu, R. François, C.S. Poon, J.G. Dai, Influences of corrosion degree and corrosion morpho logy on the ductility of steel reinforcement, Constr. Build. Mater. 148 (2017) 297–306.

[10] Y.G. Du, L.A. Clarkt, A.H.C. Chan, Effect of corrosion on ductility of reinforcing bars, Mag. Concr. Res. 57 (2005) 407–419.

[11] C.A. Apostolopoulos, S. Demis, V.G. Papadakis, Chloride induced corrosion of steel reinforce ment Mechanical performance and pit depth analysis, Constr. Build. Mater. 38 (2013) 139–146.

CONCLUSIONS

The results obtained from this doctoral thesis and reported in a series of manuscripts allow withdrawing the following conclusions:

1. The additions of 10% and 20% of UtSCBA to a concrete containing 20%FA produce ternary concretes with less porous but more complex microstructures. The compressive strengths of these ternary concretes are maintained at long-term ages.
2. The complex nature of the studied ternary concretes cannot be characterized by the ultrasonic pulse velocity (V_P) calculated from only the P-wave, but other ultrasonic parameters from the S-wave, such as spatial attenuation (α_{ss}), temporal attenuation (α_{ts}), and energy ($\mathcal{E}_S$), are necessary to detect significant differences when they are compared to concretes containing 20%FA or only PC.
3. The addition of 10%UtSCBA to a concrete containing 20%FA produces a ternary concrete with 22% and 58% lower 28-day Cl^--diffusivity than concretes containing only 20%FA and only PC, respectively. The 90-day Cl^- diffusivity is also lowered by 34% and 77%, respectively.
4. The addition of 20%UtSCBA to a concrete containing 20%FA produces a ternary concrete with 28% and 61% lower 28-day Cl^--diffusivity than concretes containing only 20%FA and only PC, respectively. The 90-day Cl^- diffusivity is also lowered by 47% and 81%, respectively.
5. The addition of 10%UtSCBA to a reinforced concrete containing 20%FA produces a ternary concrete with lower corrosion probability (E_{corr}) than concretes containing only 20% of FA and only PC. After 2500 days of immersion in a Cl^- solution the ternary concrete has a mean E_{corr} of -260 mV, whereas, the 20%FA and only PC concretes have means of -420 and -470 mV, respectively.
6. The addition of 20%UtSCBA to a reinforced concrete containing 20%FA produces a ternary concrete with a lower E_{corr} than concretes containing only 20%FA and only PC. After 2500 days of immersion in a Cl^- solution the ternary concrete has a mean

E_{corr} of -300 mV, whereas, E_{corr}s of -420 and -470 mV were measured for the 20%FA and only PC concretes, respectively.

7. The additions of 10 and 20% of UtSCBA to a reinforced concrete containing 20%FA produce ternary concretes with lower corrosion densities (i_{corr}) than concretes containing only 20%FA and only PC. After 2500 days of immersed in a Cl^- solution the ternary concretes have i_{corr} values lower than 0.5 $\mu A/cm^2$; whereas, I_{corr}s of 0.7 and 2.0 $\mu A/cm^2$ are measured for only 20%FA and only PC concretes, respectively.
8. The long-term immersion in a chloride solution does not negatively affect the compressive strength of the ternary concretes.
9. The addition of 10% of UtSCBA to a concrete containing 20%FA produces a ternary concrete with improved chloride binding capacity in 13 and 18% when it is compared to a concrete added with 20%FA and only PC, respectively; where as, the addition of 20%UtSCBA increses 19 and 25% its chloride binding capacity, respectively.
10. The addition 10% UtSCBA to a concrete with 20%FA contribute to decrease 1.5 and 3.5 the mass loss of the reinforcing steel caused by corrosion in a ternary concrete compared to those embedded in mixtures containing 20%FA and only PC; whereas, the addition of 20%UtSCBA, decreases the mass loss 1.4 and 3.2 times, respectively.
11. The addition of 10%UtSCBA to a concrete with 20%FA produces a ternary concrete which contributes to decrease the deleterious effect of corrosion on the mechanical properties of rebars embedded in it. The ultimate strength, the fracture load and ductility are 1.01, 2.07 and 1.34 times higher when they are compared to concrete added with only 20%FA, and 1.77, 2.09 and 2.62 times higher when compared to the concrete with only PC.
12. Similarly, the addition of 20% of UtSCBA to a concrete with 20%FA produces a ternary concrete which also contributes to decrease the detrimental effect of corrosion on the mechanical properties of the rebars embedded in it. The ultimate strength, the fracture load and ductility are 1.05, 2.05 and 1.18 times higher when they are compared to the concrete added with only 20%FA, and 1.22, 2.07 and 2.25 times higher when compared to the concrete with only PC.
13. All in all, ternary concretes manufactured with 70%PC+20%FA+10%UtSCBA and 60%PC+20%FA+20%UtSCBA outperformed concretes prepared with

80%PC+20%FA and 100%PC regarding the long-term compressive strengths, chloride diffusivities, electrical resistivities, and chloride binding capacities of their concrete matrices. Results obtained from the non-destructive testing were validated with results from destructive testing. The improvement of these properties contributed to enhance the corrosion protection of the steel reinforcing bars embedded in the ternary concretes. The involved protection mechanism is upon the interaction of a higher resistance to chloride ingress, a higher chloride-threshold level for corrosion to start, and a lower corrosion rate after the steel depassivation; being the dominant factor the increase in the chloride threshold level.

RECOMMENDATIONS

The findings reported in this research project make important contributions to the body of knowledge on the determination of the properties of ternary concretes manufactured with the triplet Portland cement+FA+UtSCBA. Undoubtedly, the most important contribution is the evaluation of durability performance of the ternary concretes, which completes previous studies on their workability, microstructure and mechanical properties.

The results showed than UtSCBA-ternary concretes CS is maintained a long-term age; however, these results do not correlate with their PV as has been reported in the literature [1]. Therefore, the influence of the UtSCBA in the pore structure of PC-based materials have to be researched by techniques that provide more data and information, for example, traditional mercury intrusion porosimetry, constant-rate-controlled mercury porosimetry, and NMR spectral analysis [2]. The ultrasonic parameters of UPV from the P-wave, and α_S, α_t, and ε from the S-wave are useful to determine the influence of UtSCBA in the physical and mechanical properties of ternary concretes. In this perspective, studies on such ultrasonic parameters to build non-linear experimental models in order to predict certain properties of the ternary concretes are required.

Electrochemical monitoring by E_{corr} and i_{corr} during 2500 days of reinforced concretes with UtSCBA shown lower corrosive activity than those with only PC and PC+FA. In like manner, data of ER during 3000 days of the same concretes indicates a lower ionic concentration in their pore solution available for inducing corrosion. The large amount of data from E_{corr} and i_{corr} can be processed using signal analysis to identify important events that occurred in the porous system of the concrete matrix or important features during the corrosion process of the reinforcing steel as have been reported in the literature [3]. Regarding data from ER, those can be useful to identify the effect of the cast direction and the wall-effect on the mechanical properties of concrete. Another interesting subject can be the evaluation of segregation of the coarse aggregate using the generated data of the ER test.

The addition of UtSCBA demonstrated to increase the chloride binding capacity (Pb) of the concrete manufactured with the PC+FA+UtSCBA compared to those manufactured with only PC or PC+FA. The following two mechanisms of binding have been reported in the literature [4]: chemical reactions and physical adsorption. Based on that, another interesting subject to address in the UtSCBA-ternary concretes is the elucidation of the predominant binding mechanism (chemical or physical). Research on the role of the carbon particles from the UtSCBA in the Pb of the studied concretes is also interesting, since it has been reported that such particles can work as an absorbent media for the Cl^- [5].

Research projects on different levels of partial replacement of PC by UtSCBA to manufacture concretes, various w/cm ratios, and other deterioration conditions are a must. The combination of UtSCBA as a supplementary cementitious material with other eco-friendly materials are topics scarcely investigated in the literature [6], and they have to be evaluated to expand scientific knowledge about the use of the UtSCBA as supplementary cementitious material.

Reference

[1] C. Lian, Y. Zhuge, S. Beecham, The relationship between porosity and strength for porous con crete, Constr. Build. Mater. 25 (2011) 4294–4298.

[2] Y. Yao, D. Liu, Comparison of low field NMR and mercury intrusion porosimetry in characteri zing pore size distributions of coals, Fuel. 95 (2012) 152–158.

[3] P. Montes García, F. Castellanos, J.A. Vásquez Feijoo, Assessing corrosion risk in reinforced concrete using wavelets, Corros. Sci. 52 (2010) 555–561.

[4] Z. Yang, S. Sui, L. Wang, T. Feng, Y. Gao, S. Mu, L. Tang, J. Jiang, Improving the chloride bi nding capacity of cement paste by adding nanoAl_2O_3: The cases of blended cement pastes, Constr. Build. Mater. 232 (2020) 117219.

[5] V. Minkova, M. Razvigorova, E. Bjornbom, R. Zanzi, T. Budinova, N. Petrov, Effect of water vapourtand biomass nature on the yield and quality of the pyrolysis products from biomass, Fuel Process. Technol. 70 (2001) 53–61.

[6] M.C.G. Juenger, R. Snellings, S.A. Bernal, Supplementary cementitious materials: New source s, characterization, and performance insights, Cem. Concr. Res. 122 (2019) 257–273.

VITA

M. Sc. Víctor Alberto Franco Luján

Education

Bachelor degreetin Mechanical Engineer from Instituto Politécnico Nacional of Mexico. December 2011.

Master in Science in Conservation and Managemen of Natural Resources. Instituto Politécnico Nacional. CIIDIR Oaxaca Unit. Mexico. July 2015.

Referred research articles

V.A. Franco-Luján, M.A. Maldonado-García, J.M. Mendoza-Rangel, P.tMontes-García, Chloride-induced reinforcing Steel corrosión in ternary concretes containing fly ash and untreated sugarcane bagasse ash, Constr. Build. Mater. 198 (2019) 608–618. https://doi.org/10.1016/j.conbuildmat.2018.12.004.

V.A. Franco-Luján, V.G. Jiménez-Quero, J.M. Mendoza-Rangel, P. Montes-García, Chloride-binding capacity of ternary concretes containing fly ash and untreated sugarcane bagasse ash, Manuscript sent to *Cement and Concrete Composite*.

Conferences

V.A. Franco-Luján, P. Montes-García. "Availability and viability of sugarcane bagasse ash for the production of sustainable concrete". 4° Congreso Internacional Sustentabilidad: Hegemonía y Visiones Alternas en el Contexto Actual, Universidad Autónoma del Estado de México, Mexico. October 18-20, 2017.

V.A. Franco-Luján, P. Montes-García. "Influence of chloride ions on the cementitious matrix of ternary concrete exposed to a marine environment". XII Jornadas Politécnicas en Ciencia y Tecnología 2019. CIIDIR Oaxaca Unit. May 16-17, 2019.

Research projects

Assessment of the durability of ternary bricks prepared with clay and industrial waste. SIP-20180589. Instituto Politécnico Nacional - CIIDIR Oaxaca Unit, México. 2018.

Study of the amorphicity of two ashes with and without post-treatment to be used as supplementary cementing materials. SIP-20190199. Instituto Politécnico Nacional - CIIDIR Oaxaca Unit, México. 2019.

The electrical resistivity technique for the characterization of ternary concretes. SIP-20200390. Instituto Politécnico Nacional-CIIDIR Oaxaca Unit, México. 2020.

Research stays at:

Civil Engineering Faculty of Universidad Autónoma de Nuevo León. Mexico. From February 09th to 15th. 2018.

Civil Engineering Faculty of Universidad Autónoma de Nuevo León. Mexico. From August 06th to December 21th. 2018.

Civil Engineering Faculty of Universidad Autónoma de Nuevo León. Mexico. From March 14th to 26th. 2019.